Materials Advances

REVIEW

View Article Online
View Journal | View Issue

Cite this: *Mater. Adv.*, 2023, 4, 5050

Recent advances in Zn-MOFs and their derivatives for cancer therapeutic applications

Minmin Li,†[ab] Zhixin Zhang,†[b] Yamei Yu,†[b] Hui Yuan,*[c] Alireza Nezamzadeh-Ejhieh,[d] Jianqiang Liu,*[ab] Ying Pan[ab] and Qian Lan*[a]

Received 14th August 2023,
Accepted 24th September 2023

DOI: 10.1039/d3ma00545c

rsc.li/materials-advances

Researchers have developed dozens of cancer treatment strategies to address the high proportion of cancer deaths in total deaths. However, the treatment of cancer inevitably has various drawbacks and sequelae. Drug delivery systems (DDSs) provide hope for addressing issues such as early release in cancer treatment, as they have active ingredients with controllable doses and delivery kinetics (AI). Metal organic frameworks (MOFs) offer various possibilities for constructing drug delivery systems: organic ligands serve as carriers, metal ions serve as attachment sites, and self-assemble through ligand binding to adaptive structures, exhibiting excellent biocompatibility, biodegradability, high cancer cell toxicity, and low normal cell toxicity. Zinc-based MOFs are some of the MOFs. It is very important to choose zinc-based MOFs that have good inhibitory and diagnostic effects on cancer as drug delivery carriers. Although numerous studies and reviews have explored the application of zinc-based MOFs in drug delivery, they typically only cover one aspect. In contrast, we hope to focus on the application of zinc-based MOFs in various cancer treatments, including: (1) chemotherapy, (2) photodynamic therapy, (3) photothermal therapy, (4) chemical kinetics therapy, (5) sonodynamic therapy, (6) immunotherapy, (7) gene therapy, (8) hunger therapy, and (9) two or more combination therapies. This paper summarizes the application of zinc-based MOFs in cancer treatment and discusses their advantages, disadvantages and application prospects. At the same time, a review was conducted on the synthesis of typical Zn-MOFs, with the expectation of better in-depth research on Zn-MOFs.

1. Introduction

Today, malignant tumours are one of the most common causes of death in humans. To address this challenge, researchers have developed more than a dozen cancer treatment strategies in recent decades, such as surgical resection, chemotherapy, and light therapy, among others. As medical research technology continues to advance, the development of new anti-tumour drugs has increased, improving the treatment of many tumours and their efficacy. At the same time, with the deepening of people's understanding of tumours, related anti-tumour drugs have been constantly developed, and the variety of drugs used has become increasingly rich. Therefore, anti-tumour drugs have very promising development prospects in oncology medicine. However, there are still some limitations to improving oncology treatment with drugs, such as resistance to chemotherapeutic agents,[1] inefficient drug delivery to solid tumours,[2] and the efficacy of photodynamic therapy (PDT) being limited by hypoxic tumour parenchyma, to name a few. Therefore, it is crucial to develop a variety of new strategies to address the impediments to cancer therapy.

Nanomaterial-based modification strategies represent a way to improve the limitations of various cancer treatments. Among them, metal–organic frameworks (MOFs) are a new class of nanoporous coordination polymers self-assembled by coordination bonding with organic ligands as supports and metal ions as connectors. They are a good choice as a carrier for the delivery of substances such as drugs, photosensitisers and contrast agents. They are also widely used in sensing,[3] catalysis,[4] magnetism,[5] and gas storage.[6] In addition, metal–organic frameworks (MOFs) have been tremendously used in cancer therapeutic applications. In recent years, researchers have published many reviews on different types of MOFs in cancer therapy.[7] However, there are few reviews reporting the use of zinc-based MOFs for various types of cancer therapy, which limits the progress of research in

[a] *The First Dongguan Affiliated Hospital, Guangdong Medical University, Dongguan, 523700, China. E-mail: jianqiangliu8@gdmu.edu.cn, lanqianmimi@126.com*
[b] *Guangdong Provincial Key Laboratory of Research and Development of Natural Drugs, and School of Pharmacy, Guangdong Medical University, Guangdong Medical University Key Laboratory of Research and Development of New Medical Materials, Dongguan, 523808, China*
[c] *Department of Gastroenterology, Huizhou Municipal Central Hospital, Huizhou, Guangdong 516001, China. E-mail: yuanhui2017@hotmail.com*
[d] *Chemistry department, Shahreza Branch, Islamic Azad University, Shahreza, Isfahan, Iran*
† These authors contributed equally to this work.

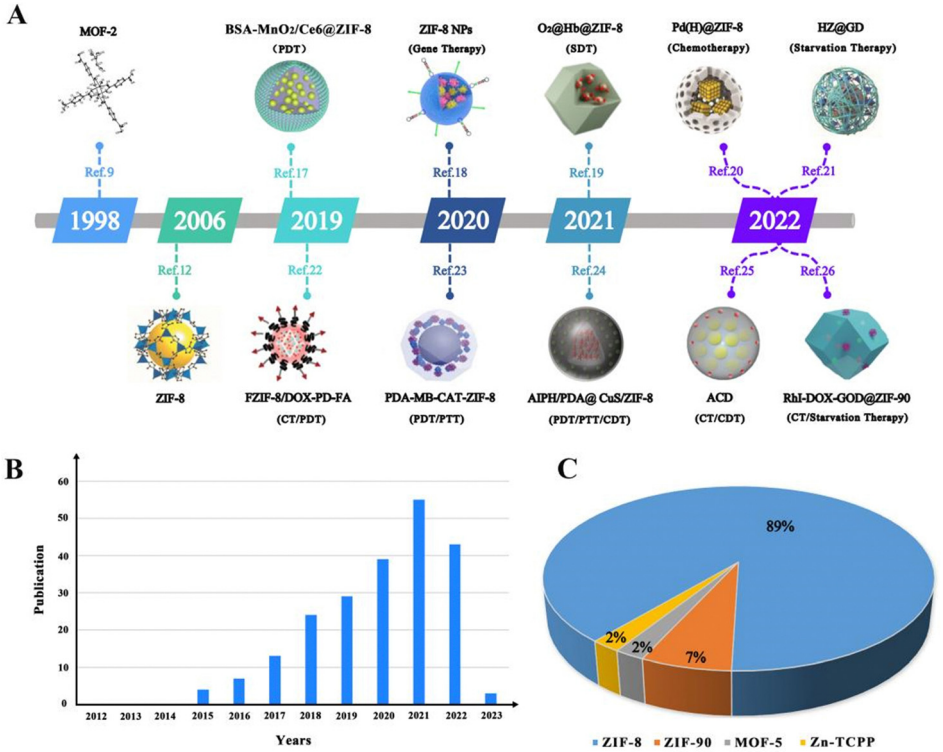

Fig. 1 (A) Research history of Zn-MOFs in cancer treatment. (B) Publications and citation frequencies of articles retrieved from international academic databases on the use of ZIF-8 for oncology treatment from 2012 to 2023. (C) The pie chart shows the percentage of the various Zn-MOFs in the literature.

cancer therapy. Zinc is widely used in dermatology for its anti-dandruff, astringent, anti-inflammatory and antibacterial properties.[7] Also, zinc with low toxicity is an ideal candidate for the preparation of zinc-based MOFs for use in biological systems, especially for use as drug carriers.[8] Since the first zinc-based MOF (*i.e.*, MOF-2, as shown in Fig. 1A) was reported by Yaghi's group in JACS in 1998,[9] the research on zinc-containing MOFs has developed rapidly in the following decades. During these decades, MOF-74,[10] MOF-5,[11] ZIF-8,[12] and ZIF-11,[12] among others, were successively reported. In the last decade, one Zn-MOF after another has been synthesised and published, and Zn-MOF derivatives applied in cancer therapy have been gradually enriched (*e.g.*, Fig. 1A). To this end, we have listed in chronological order the following representative Zn-MOF derivatives used in cancer therapy in the last four years: BSA-MnO_2/Ce6@ZIF-8,[17] ZIF-8 NPs,[18] O_2@Hb@ZIF-8,[19] Pd(H)@ZIF -8@AP,[20] HZ@GD,[21] FZIF-8/DOX-PD-FA,[22] PDA-MB-CAT-ZIF-8,[23] AIPH/PDA@CuS/ZIF-8,[24] ACD,[25] and RhI-DOX-GOD@ZIF-90.[26] Among them, ZIF-8, a Zn-MOF, has made the most rapid progress in cancer therapeutic applications (*e.g.*, see Fig. 1B and C).

Compared with other metal–organic frameworks (MOFs), the unique features of Zn-based MOFs for cancer therapy are as follows: (1) Zn-MOFs with low toxicity and easy biodegradability have little effect on the human body.[13] (2) Most of the Zn-MOFs have excellent pH-responsive controlled drug release properties and can release drugs with single or multiple stimulus responses, which is helpful to overcome the limitations of cancer therapy such as releasing too much drug too quickly.[13] (3) Some Zn-MOFs can prevent the aggregation and self-destruction of PSs and ROS, which makes them ideal nanomaterials for effective loading of PSs (photosensitisers) or used as PSs.[14] (4) The chemical structure of Zn-MOFs allows them to be embedded in a wide range of biomolecules used for therapeutic purposes, such as enzymes, DNA, proteins and other biological macromolecules used for cancer therapy through simple synthesis. Also Zn-MOFs can combine single/multiple cancer therapies with imaging techniques (*e.g.* magnetic resonance imaging) to achieve the integration of cancer diagnosis and treatment, which greatly improves the accuracy and effectiveness of tumour treatment. For this purpose, we have also compiled the anticancer activities of Zn-MOFs with other metal–organic frameworks (Fe-MOFs, Cu-MOFs, and Hf-MOFs) in Table 1, in the hope that it will be easier for the readers to understand.

Among the reviews on Zn-MOFs published in the last five years, a systematic review summarising single/multiple stimulation of Zn-based MOF drug carriers from the perspective of pH response reported in the last 20 years was conducted by Liu *et al.*[15] whereas Rashda Safdar Ali *et al.* reviewed and summarised the methods of fabricating different Zn-MOF-based sensors and their applications in early cancer diagnosis and treatment.[16] Unlike them, this review concentrates on exploring the synthesis of Zn-MOFs and their advances in cancer chemotherapy (CT), phototherapy, chemodynamic therapy (CDT), sonodynamic therapy (SDT), immunotherapy, gene therapy,

Table 1 Typical examples of the anticancer activity of Zn-MOFs *versus* other MOFs containing different metal ions

Metal-based MOFs	MOF composite	Type of therapy	Anticancer efficacy	Ref.
Zn-MOFs	BSA-MnO_2/Ce6@ZIF-8	PDT	79% inhibitory effect on HeLa cells	17
	RhI-DOX-GOD@ZIF-90	CT/starvation therapy	Cancer cells (4T1 cells and HCT116 cells) showed less than 20% cell viability, optimal anti-tumor effects in tumor-bearing mice after 14 days	26
	CMC/5-FU@MOF-5	CT	More than 90% cytotoxicity at 0.156 μg mL^{-1} in 24 hours	29
	Au@ZIF-8/DOX	CT/PTT	82% MCF-7 cytotoxicity at 50 ppm Au@ZIF-8/DOX+NIR	87
Fe-MOFs	MOF-MB-DHA@PLA@PEG (MMDPP)	CT/PDT	The tumor inhibition rate was 96%, and the activity of cancer cells decreased to 17.6%	131
	Fe_3O_4@Bio-MOF-FC	CT	The cell viability of NIH-3T3 and MDA-MB-231 were 66% and 62% at 24 h and 48 h, respectively	132
	MOF-S-S-OVA@CpG	Immunotherapy	Causing approximately 67% of the E.G7-OVA cell death	133
	Au@$Fe(BTC)_3(H_2O)_6$	CT/PTT	More than 80% of the exposed cells died after 10 h of culture and less than 10% survived after 4 min of irradiation	134
Cu-MOFs	Cu-MOF/MTX@GM	CT	MTX encapsulation amount was 68%, and survival rate of MCF-7 cells was only about 23% after 48 hours	135
	H_2S-activated HKUST-1	CDT/PTT	79% death of HeLa cells at 50 mg mL 1 HKUST-1, 83% of tumor inhibition ratios, and thermal conversion efficiency of up to 45.7%	136
	PS@MOF-199 NPs	PDT	The tumour shrinkage rates of TPAAQ- and Ce6-containing MOF-199 NPs were 45% and >60%, respectively, higher than those of 27% and 37% for bare Ce6 and TPAAQ	137
Hf-MOFs	DBBC-UiO	PDT	At 750 nm, 94% of MCF-7 cells died and the tumour volume in nude mice almost completely disappeared at 15 days	138
	Hf-DBP MOFs/MOLs	PDT	Hf-DBP *n*MOL showed 80% higher cure rate, 49.1% higher inhibition rate, and 16.3-fold lower metastatic potential than Hf-DBP *n*MOF on tumours in mice with breast cancer	139
	Hf-UiO-AM@POP-PEG	PDT/PTT	41% photothermal conversion efficiency; intra-tumour injection tumour inhibition rate 88.4%; and intravenous tumour inhibition rate 69.7%	140
	TPZ/Hf-TCPP/PEG	PDT/CT	Induces TPZ activation; dead HeLa, 4T1 cells ratio of 32.8% and the lowest viability of 59.2%	141

starvation therapy, or the combination of two and more of the above therapies. Tables 2 and 3 summarize the recent findings of nano-formulations of Zn-MOFs for oncology therapy. At the end of the article, in order to further promote the progress of Zn-MOF research in biomedicine, we also provide an outlook for future research in this field.

2. Chemical synthesis and preparation of Zn-MOFs

The method of MOF synthesis is usually determined by the type of metal, organic linker and or targeting agent. Several methods have been used to synthesize excellent and novel MOF materials, such as hydrothermal/solvent-thermal synthesis, room temperature synthesis, microwave heating, and electrochemical methods.[129] In this review, the synthesis methods of Zn-MOFs are discussed, namely, solvent-heated, room temperature synthesis, one-pot methods, ultrasonic synthesis methods, *etc.* The physical and chemical structures of Zn-MOFs synthesised by the above methods are relatively stable and the synthesis methods are also relatively simple, which is also conducive to the application of Zn-MOFs in cancer therapy.

2.1 Solvothermal methods

Solvothermal methods are some of the commonly used methods for the synthesis of Zn-MOFs, and have the advantages of low cost, high reaction efficiency, easy scalability and high thermal stability. There are a number of materials synthesised using these methods, which are reviewed in this paper, and *N*,*N*-dimethylformamide (DMF) is a commonly used solvent.

Hang *et al.* prepared a 2D Zn-TCPP-MOF as a photosensitiser for the first time (Fig. 2), and TCPP and PVP (polyvinylpyrrolidone) were homogeneously mixed in DMF, after which an aqueous solution of zinc nitrate was added to the former, stirred and heated at 150 °C for 1 h. The product was then modified using PVP and flakes with a size of 90 ± 25 nm were obtained after washing with ethanol and deionised water. The product was able to maintain stability in FBS for 24 h under 660 nm laser light. And it gradually collapsed in acidic solution with controllable photodynamic properties.[39] Javanbakht *et al.* mixed zinc nitrate hexahydrate and BDC (terephthalic acid) in DMF, followed by heat treatment at 120 °C for 25 h. Finally, MOF-5 was obtained by washing with DMF and $CHCl_3$. The BET surface area of MOF-5 encapsulated with 5-FU was 106.4 m^2 g^{-1}, which may be due to encapsulation of the drug to reduce its uptake of N_2, indicating that the structure of MOF-5 is not damaged by the encapsulation of the drug.[29] In PDT, Yang *et al.* also prepared hairpin probe-photomimetic MOFs (PMOFs) using a solvothermal method. The loading efficiency of the hairpin probe on PMOFs was as high as 92.3%, which was only 1.8% lower than that on HPMOFs without ZIF-8 coating, and its average size and positive ζ-potential were higher than those of HPMOFs. The PMOFs were also able to keep their structure unchanged under PBS incubation for 24 h and it was also demonstrated that they would not be degraded by nuclease in gel electrophoresis experiments.[45] Zhu *et al.* synthesized 2D Zn-TCPP nanosheets (TEM about 200 nm) using a solvothermal method, which not only effectively adsorbed about 66.8% of the immunoadjuvant CpG (a single-stranded DNA) through noncovalent interactions, but also exhibited enhanced acoustic kinetic therapeutic effects by enhanced electron conduction and reduced self-burst.[62]

Table 2 Some recently published works based on the application of Zn-MOFs in cancer monotherapy

Zn-MOF composite	Particle size (nm)	Type of therapy	Anticancer efficacy	Ref.
CEC@ZIF-8NP	—	GT	Enhanced intracellular, interstitial accumulation and toxicity	18
BSA@ZIF-8 NPs	87 ± 6.8	GT	Cell viability of incubated HeLa cells and MCF-7 were significantly reduced	18
O_2@Hb@ZIF-8	—	SDT	Inhibits tumor growth and achieve SDT at different depths	19
Pd (H)@ZIF-8@AP	190	CT	90% survival rate within 5 days	20
HZ@GD	—	Starvation therapy	Effective for melanoma starvation efficacy	21
BSA-Gem@ZIF-8/Dopa/GA and BSA-Gem-Amy@ZIF-8/Dopa/GA	400–500	CT	62%, 55% cell death, 76%, 78% Dopa/GA release	27
RGD@CPT@ZIF-8	100	CT	75% of CPT was released	28
2-ME/TK/CPT@ZIF-90	100	CT	Approx. 93.1% cell viability, approx. 69.6% anti-tumor ability, and 100% drug release rate within 5 minutes	30
ZIF@GOx/GQDs and free GOx	—	CT	About 100% tumor inhibition	31
BA-NBA-IPA@ZIF-8	248.0 ± 1.3	CT	The drug release rate within 24 hours was 100%	32
PEG-DSF-Cu/ZIF-8	208.3	CT	83.6% cell killing at 15 mg mL^{-1} concentration	33
aZIF-8/5-FU	140	CT	100% survival rate within 50 days	34
CpG/ZANPs	80	CT	High antigenic load of 30.6%	35
Au@Ag $NRs^{4\text{-}ATP}$@ZIF-8/FA	—	CT	High drug loading of 60.31 mg DOX/100 mg Au@Ag $NRs^{4\text{-}ATP}$@ZIF-8/FA	36
AP-ZIF-90@DOX	104.7 ± 6.3	CT	80% survival rate within 40 days	37
iRGD/AVO-hemin@ZIF-90	72.4 ± 11.3	CT	The cell viability was over 90%	38
2D Zn-TCPP MOF	104.6	PDT	Generates high $^1O_2$ levels at a 660 nm laser	39
ZnPc@ZIF-8	—	PDT	The power density of the cell surface is about 3.3 mW cm^{-2}	40
CaO_2@ZIF-8@THPP	—	PDT	86.5% apoptosis rate and necrosis rate	41
TBD@ZIF-8-PMMA-S-S-mPEG	200	PDT	Almost 100% tumor growth inhibition	42
l-CHA@l-His ZIF-8 NPs	—	PDT	Over 68% cell killing power	43
DF-BODIPY@ZIF-8	250	PDT	A single linear state oxygen quantum yield of 18.07%, 90% cell killing	44
HPMOF@ZIF-8	—	PDT	HeLa cell inhibitory power about 80%	45
Zn(II)-PPIX/G-quadruplex VEGF aptamer-tetrahedra nanostructures	200–300	PDT	The formation of ROS products was enhanced by about 2.5-fold and 70% of MDA-MB-231 cells died	46
ZrMOF@MnO_2	—	PDT	Manganese release reached 84% and U87MG apoptosis rate reached 80%	47
UCNPs-g-C_3N_4-CD@ZIF-8	—	PDT	Super 80% inhibition of HeLa cells	48
PDA-PCM@ZIF-8/DOX	130	PTT	78% drug release rate, 87% tumor inhibition rate	49
IM@ZP	82.29	PTT	About 67% reduction in tumor growth	50
Cy@ZIF-8	118.7 ± 1.3	PTT	Super 80% inhibition of HeLa cells	51
ICG@ZIF-8	190	PTT	Cell viability inhibitory power about 70%	52
GBZ	100	PTT	The photothermal conversion rate of 24.4%, toxicity to Huh-7 cells about 90%	53
PSMCA	—	PTT	Thermal transformation efficiency of 63% and the survival rate of HeLa cells less than 40%	54
CLALN	145.76 ± 1.28	PTT	Apoptosis rate of tumor cells: 77.48%	55
Au@ZIF-8	115	PTT	Apoptosis rate of tumor cells: 77.48%	56
Pdop@ase@aZIF-8	—	PTT	100% cancer cell elimination rate	57
CNP-NO@RBCs	—	PTT	Photothermal conversion rate reached 54.1% and CT26 cell killing rate was 77.6%	58
GOx@Pd@ZIF-8	—	CDT	Inhibits cancer cell growth and promotes apoptosis	59
GOx@MPN	—	CDT	Maintains the conformational freedom of the enzyme	60
ZIF-8 NCs	180	SDT	The tumor inhibition rate was 84.6%	61
Zn TCPP/CpG	—	SDT	About 25% of $CD8^+$ T cells accumulate in tumors	62
ZIF-8@$mSiO_2$	180–190	SDT	Critical decreased cell at a lower concentration (6.25 mg mL@1)	63
mCG@ZIF	—	Starvation therapy	The highest apoptotic cell% in tumor tissues by MCG@ZIF group	64
Met/GOx@His/ZIF-8 ~ RGD	142.4	Starvation therapy	The survival rate of cancer cells is only 30.4% and only 22.3% of cells remain alive under low glucose conditions	65
GOx & Hb@ZIF-8	400 ± 50	Starvation therapy	The decreased survival rates for HeLa and MCF-7 cells: 64% and 39%	66
CHC/GOx@ZIF-8	—	Starvation therapy	CHC/GOx@ZIF-8 therapy showed more effective tumor growth inhibition than GOx@ZIF-8	67
DOX@EGCG/Fe NC	347.8	GT	The highest tumor growth inhibition (84.2%) by high-dose of DOX@EGCG/Fe 33	68
BEFORE	—	GT	The tumor volume in BEFORE group was about 1/20 of that in saline treatment	69
Cet@protein@ZIF-8N	—	GT	It showed >50% inhibition on A431 cells	70
CEC@ZIF-8	100–150	GT	Increases toxicity of cancer cells	71

Table 2 (*continued*)

Zn-MOF composite	Particle size (nm)	Type of therapy	Anticancer efficacy	Ref.
Vir-ZM@TD	160	Immunotherapy	Resulting in complete regression of about 68% tumors.	72
mEHGZ	133.92 ± 2.93	Immunotherapy	The tumor growth inhibition rate was 82.02%	73
KN046@^{19}F-ZIF-8	112.4 ± 4.7	Immunotherapy	KN046@^{19}F-ZIF-8 group's areas of tumor necrosis was larger and the highest necrosis percentage was found	74
CUR-BMS1166@ZIF-8@PEG-FA(CBZP)	200	Immunotherapy	A critical tumor size decrease for mice receiving CBZP	75
Gd-MOF-5	130	Immunotherapy	The toxicity of Gd-MOF-5 to 4T1 cells was 62%	76
(M+H)@ZIF/HA	176.3 ± 1.6	Immunotherapy	Stronger tumor growth inhibition ability of (M+H)@ZIF/HA group than that of control group	77

The solvothermal method can also be combined with other methods to synthesise desirable products. Yang *et al.* reported that ZIF-8, on the other hand, was prepared by direct mixing of 2-methylimidazole (2-MIM) in different molar ratios with zinc nitrate hexahydrate in methanol at 40 °C for 2 h. The product is a mixture of 2-methylimidazole (2-MIM) and zinc nitrate hexahydrate (their TEM diameters were about 60, 110 and 20 nm, respectively). They found that, again by simple direct pyrolysis of the above ZIF-8 nanoparticles, the obtained ZIF-8-derived carbon nanoparticles (ZCNs) not only retained a similar morphology to the ZIF-8 nanoparticles, but also retained a higher internal porosity than that of ZIF-8.[89] Solvothermal methods in recent years have tended to be more flexible and versatile synthesis methods to obtain Zn-MOFs with different particle size distributions to achieve better cancer therapeutic effects.

2.2 Room temperature synthesis

In room temperature synthesis, MOF crystals were prepared by physically stirring a reaction mixture in organic solvents such as water or methanol at room temperature, which has the advantages of simple operation, low energy consumption, and small loss of materials. There are few materials synthesised using this method according to this review paper.

Kulkarni *et al.* found that the size of ZIF-8 made from different solvents was different, so they prepared ZIF-8 using water and methanol, respectively. After synthesis, using a zetameter, they came up with ZIF-8 with a size of 226.5 nm and a PDI of 0.281 synthesised using methanol as a solvent, whereas the data for water were even smaller, with a particle size of 98.4 nm and a PDI of 0.06.[103] Siboro *et al.* prepared modified ZIF-8 by adding PVP (polyvinylpyrrolidone) in a conventional room temperature synthesis as shown in Fig. 3. SEM and transmission electron microscopy (TEM) showed that this modified ZIF-8 has a cubic shape with a particle size of 201.1 ± 2.1 nm, a ζ-potential of 20.1 ± 0.5 mV, hollow cavities and a high specific surface area,[32] which make it an ideal carrier for a drug delivery system. Qian *et al.* on the other hand had controlled the particle size of ZIF-8 NPs by using polyethylene glycol (PEG) as a mineralising agent. The synthesis process is shown in Fig. 4A, and finally, to remove the ZIF-8 template, protein-loaded MPN capsules were obtained for cancer therapy by centrifugation and after washing the precipitate three times with ethylenediaminetetraacetic acid (EDTA) solution. We can infer the successful synthesis of GOx@MPN capsules by the change in ζ potential from the positive to negative charge of ZIF-8 NPs (30.4 mV), GOx@ZIF-8 NPs (−8.9 mV), GOx@ZIF-8@MPN NPs (−26.6 mV), and GOx@MPN capsules (−42.3 mV).[60]

In addition, most of the literature studies described in this paper have achieved good synthetic results by either compositing Zn-MOFs with other nanomaterials or functionalising them under room temperature synthesis conditions. Liu *et al.* synthesized a clickable ligand (norbornene-modified imidazole (MIM-Nor)) by introducing an imidazole ligand partially into norbornene and embedding it into ZIF-8 during particle formation, which was then attached to the surface of cetuximab (Cet) to obtain Cet@POI@ZIF-8N, providing a way for other targeting ligands to be able to more readily modify the surface of the surface of ZIF-8N.70 Jiang *et al.* used polyvinylpyrrolidone (PVP) to surface modify KN046 prior to formulation. Subsequently, the modified KN046 was encapsulated in fluorine-containing ZIF-8 nanoshells using a modified ZIF-8 synthesis technique. Scanning electron microscopy (SEM) and transmission electron microscopy (TEM) showed (*e.g.*, Fig. 4C and D) that the KN046-loaded 19F-ZIF-8 was hexagonal, with regular shape and uniform size. Meanwhile, KN046@19F-ZIF8 showed good dispersion stability in water. These results suggest that KN046@19F-ZIF-8 can respond to the tumour microenvironment and can control the release of KN046.74. Wang *et al.* effectively controlled the OH-mediated etch-decomposition process of the cores of ZIF-8 NCs by appropriately adjusting the volume ratio of CH_3OH to H_2O, resulting in the formation of yolk-shelled ZIF-8@mSiO_2 structures. The ZIF-8 NCs exhibited a single rhombic dodecahedral morphology consisting of twelve major crystalline facets with diameters of about 130–140 nm. The yolk-shelled ZIF-8@mSiO_2 nanostructures maintained almost the original morphology similar to that of the ZIF-8 nanostructures (with diameters of ∼180–190 nm and inner core sizes of ∼90–95 nm), which suggests the synthesis method's feasibility.[63] The therapeutic platform was obtained by adding indole-nine-green (ICG) to a stirred mixture (CZ) at room temperature, which was finally coated with Pt NPs. The TEM images clearly demonstrated that Pt was homogeneously distributed on the surface of the direct-drawn single crystals and elemental maps and spectra of XPS measurements showed the presence of elements Co, Zn, N, Pt, and C in the CZIP. The XRD pattern showed characteristic peaks of Pt at 39.8° and 46.2°. The ζ-potential of CZIP was also reduced to −15.57 mV, and these results indicated that Pt was successfully modified on the CZP surface.[82]

Table 3 Some recently published works based on the applications of Zn-MOFs in cancer combination therapy

Zn-MOF composite	Particle size (nm)	Type of therapy	Anticancer efficacy	Ref.
FZIF-8/DOX-PD-FA	70	CT/PDT	Up to 57% DOX release at pH = 6.0, reducing tumor volume *in vivo* to 0.22 times the original size in tumor-bearing mice	22
PDA-MB-CAT-ZIF-8	—	PDT/PTT	60.32% of HeLa cells were apoptotic under 660 nm and 808 nm laser irradiation, tumors in PMCZ+PDT+PTT treated HeLa tumor-bearing mice were completely suppressed or even ablated	23
AIPH/PDA@CuS/ZIF-8	127	PDT/PTT/CDT	Almost no 4T1 cells in APCZ + laser group survived at the same concentration, the tumor was completely eradicated after two weeks of treatment	24
ACD	67.9 ± 5.5	CT/CDT	The smallest tumor size and growth rate in ACD-treated mice	25
ZCNs	—	PDT/PTT	The best photothermal effect at approx. 40 °C, phototherapeutic effect increases with increasing PA imaging power	78
IrO_2@ZIF-8/BSA-FA(Ce6)	74.6	PDT/PTT	The strongest fluorescence intensity for IZBFC + 808 + 660 nm laser-treated MNNG/HOS cells, with over 80% of cells killed	79
O_2–Cu/ZIF-8@Ce6/ZIF-8F127	95	PDT/CDT	The relative tumor volume of Balb/c mice carrying 4T1 tumors on day 15 is approximately one-third of the original tumor	80
A-NUiO@DCDA@ZIF-Cu	200	PDT/CDT	Shows a strong anti-tumor effect under white light, reducing tumor volume to 50% of the initial value	81
Co/ZIF-8/ICG/Pt	—	PDT/CDT	CZIP (50 ppm)+NIR (808 nm, 1.5 W cm^{-2}, and 10 min) reduced HeLa cell viability to 40%, CZIP+NIR group could effectively inhibit tumor growth in female Balb/c mice	82
LDNPs@Fe/Mn-ZIF-8	75.4	PDT/CDT	The survival rate of HeLa cells treated with 500 μg mL^{-1} LDNPs@Fe/Mn-ZIF-8+NIR decreased to 10.2%	83
PDA@Cu/ZIF-8	—	PTT/CDT	PDA@Cu/ZIF-8 inhibited 84.6% of tumor growth, tumor tissue suffered the most severe cell shrinkage and nuclear condensation	84
ICG@Cu_2–XSe-ZIF-8	250–300	PTT/CDT	ICG@Cu_2–XSe-ZIF-8+ a laser induces apoptosis in approximately 63.94% of breast cancer cells	85
FeNC@PAA	—	PDT/PTT/CDT	Cell viability of FeNC@PAA+NIR 4T1 cells was reduced by 95%, tumor weights of mice after 21 days of the treatment group were 53 times smaller than those of the PBS group	86
FA-BSA/ZIF-8CNPs-CPT	—	CT/PTT	Cell survival rate was 12.6% at 20 minutes of 808 nm laser irradiation, NIR group inhibited tumor growth optimally in tumor-bearing nude mice	88
PDA/DOX/ZIF-8	180	CT/PTT	NIR treatment group was more able to induce apoptosis in tumor cells than the other groups	89
ZSZIT	145–170	CT/PDT	Tumors in the ZSZIT+NIR irradiation group had the lowest tumor weight and the smallest size with the best inhibition rate	90
IR780/DOX@ZIF-D	126	CT/PDT	The laser treatment group showed 86.5% tumor inhibition in all treatment groups	91
DOX-Pt-tipped Au@ZIF-8	150	CT/PTT/PDT	Cell survival rate reduced to 21.5% under 1064 nm laser irradiation, complete inhibition of tumor growth *in vivo*	92
DIHPm	235	CT/PTT/PDT	DIHPm was the most effective tumor suppressor in mice bearing 4T1 mammary tumors, with only 8% of 4T1 cells surviving in a DIHPm (2 μg mL^{-1}) culture	93
CS/ZIF-8@A780/DOX NPs	128.2	CT/PTT/PDT	Reversal of P-gp-induced drug resistance with CS/NP treatment, 40-fold amplification of DOX therapeutic efficiency	94
HA-SS@CuS@ZIF-8@TPZ and TB macn	110 ± 5.6	CT/PTT/PDT	White light irradiation and 808 nm laser irradiation are the most toxic to MCF-7 cells, with strong concentration- and time-dependent killing effects on tumor cells under the light source	95
ZIF-8@GOx-AgNPs@MBN	—	CT/starvation therapy	0.08 mg mL^{-1} inhibited approximately 95% of tumor cells *in vitro* and 200 μg mL^{-1} inhibited 96.8% of tumors *in vivo* after 14 days of treatment.	96
AQ4N/GOx@ZIF-8@CM	250	CT/starvation therapy	The apoptosis rate of HepG2 cells: 88.43%	97
SG@GR-ZIF-8	234.6 ± 4.5	CT/starvation therapy	Inhibits 89% of tumor growth in mice bearing c5wn 1-tumors and inhibits pulmonary metastasis of HCC *in situ* C5WN1-bearing mice	98
CaO_2/DOX@Cu/ZIF-8@HA	150	CT/CDT	Cancer cell survival rate was 20%, *in vivo* tumor suppression rate was higher than that of control group	99
Cu/ZIF-8@DSF-GOD@MnO_2	145	CT/CDT	*In vitro* cellular analysis showed the highest tumor-killing rate and *in vivo*, U14 subcutaneous tumor-bearing mice showed a higher tumor suppression rate after two weeks of treatment than the other groups.	100

In the report by Zou *et al.*, Cu_2/XSe nanoparticles were synthesised and then added to methanol containing 2-methylimidazole, then zinc nitrate dissolved in methanol was added to the solution and reacted for 24 h at 25 °C to obtain an attachment material for malignant breast cancer and bone tumours. It is shown to be monodisperse, uniformly sized nanoparticles under TEM and SEM. DLS analysis reveals that the particle size remains unchanged after the incorporation of ICG into Cu_2–XSeZIF-8 nanoparticles. In the FTIR spectra, the overlapping of the characteristic peaks of the unsaturated C–H bond (3000 cm^{-1}), carbonyl group (1650 cm^{-1}) and carbon–carbon single bond (1090 cm^{-1}) indicated that the composite nanoplatform was successfully constructed. The results of N_2 adsorption–desorption isotherms showed that the inflection point induced by the complexes shifted to a relatively low pressure at the N_2 adsorption branch, which further confirmed the synthetic methodology. The feasibility of the synthesis method was further confirmed.[85] Sui *et al.* on the other hand,

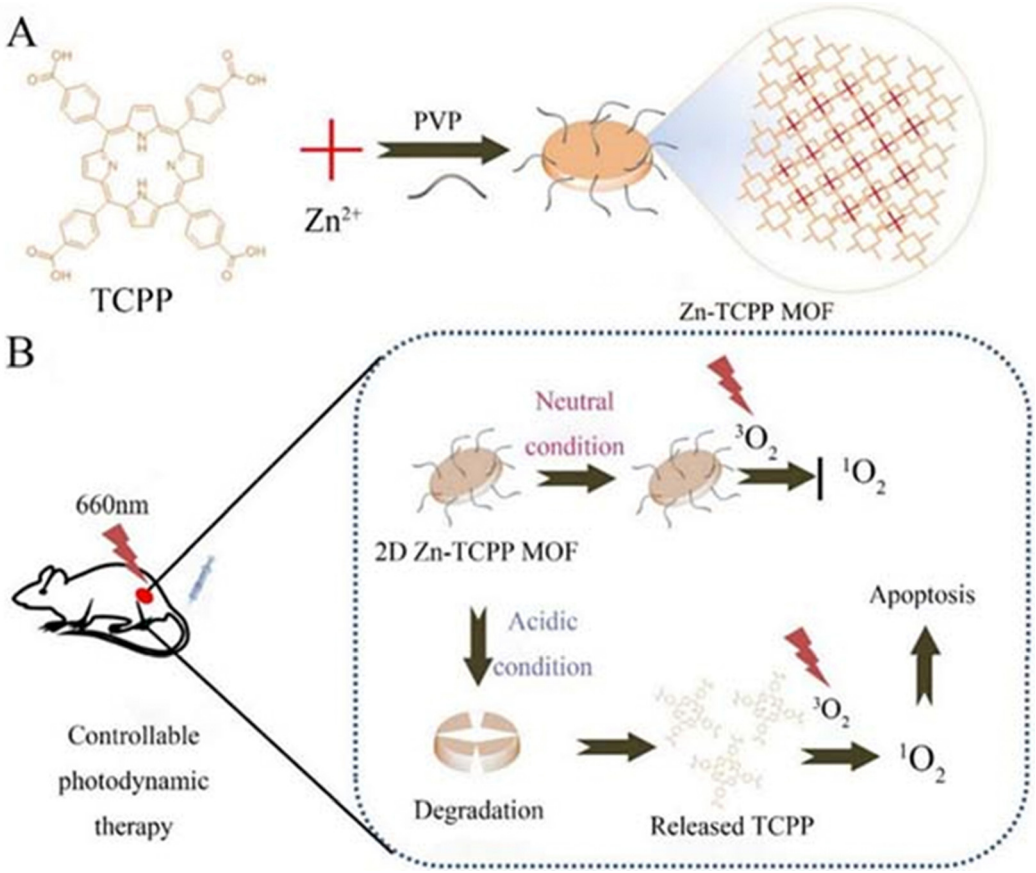

Fig. 2 Schematic showing the 2D Zn-TCPP MOF for controllable PDT. (A) A one-pot strategy to prepare 2D Zn-TCPP MOF. (B) The 2D Zn-TCPP MOF as a controllable photosensitizer for *in vivo* PDT. Reproduced from ref. 39 with permission from Springer nature, copyright 2023.

first synthesised ZIF-8(Fe/Zn) and ZIF-8(Zn) at room temperature as described previously,[130] and then obtained FeNC and ZnNC nanoparticles with polyhedral shapes and hierarchical porous structures, respectively, by simple pyrolysis. XRD and elemental mapping confirmed the homogeneous dispersion of elemental Fe in FeNC. Then, the successful synthesis of FeNC@PAA nanoparticles was further confirmed using the FT-IR spectra and ζ-potential changes of FeNC complexes modified with PAA (sodium polyacrylate), whose TEM images showed that PAA had no effect on the morphology of FeNC.[86]

In addition, good experimental results have been obtained for the core–shell preparations formed by ZIF-8 shells synthesised at room temperature with other nanostructures. Generally, the core particles were prepared before the coating of ZIF-8 and then the core particles were surface-modified with surfactants to attract Zn^{2+}, which facilitated the nucleation and growth of ZIF-8 shells on their surfaces. Polyvinylpyrrolidone (PVP) can be used as a stabiliser to prevent agglomeration and promote the formation of ZIF-8 shells. Huang *et al.* obtained circular ellipsoidal nanoparticles with good water solubility and biocompatibility by gradually growing the ZIF-8 material onto the surface of gold nanorods guided by a PVP polymer. Its TEM image clearly presents AuNR as the core and ZIF-8 as the shell. Energy dispersive X-ray (EDX) elemental mapping and XRD spectra also confirmed the constituents.[87] The method of Chao *et al.* is similar to the above. They first prepared uniform ZnS nano- and then surface-modified ZnS nanoparticles with PSS molecules to facilitate nucleation and growth of ZIF-8 shells on their surfaces. They found that in methanol solution ZIF-8 uniformly covered the ZnS surface, while in aqueous solution the individual nucleation and growth of ZIF-8 particles. In addition, they increased the final shell thickness to about 50 nm by gradually increasing the Zn^{2+} concentration during the synthesis process to facilitate loading of more drugs. The XPS analysis results were also in excellent agreement with the elemental maps showing the presence of ZnS and ZIF-8, which indicated the successful formation of a nucleoshell structure,[90] while in the report of Deng *et al.* they first synthesised iridium dioxide nanoparticles (IrO_2 NPs), then the ZIF-8 shell layer was encapsulated on their surface at room temperature, followed by conjugation of bovine serum albumin-folic acid (BSA-FA) on the surface of IrO_2@ZIF-8 as an active targeting agent, and finally adsorption of the photosensitiser Ce6 on the surface to form IrO2@ZIF-8/BSA-FA (Ce6).79 TEM, SEM elemental mapping and FTIR all confirmed that IrO_2 NPs were successfully encapsulated in ZIF-8. In contrast, the dimensions of IZBF NPs differed between TEM and DLS, which might be caused by the swelling of IZBF NPs in water. In addition, the absence of significant changes in the DLS and zeta potential of IZBF within 7 days of dialysis then indicates that IZBF has good physiological stability. It can be seen that this

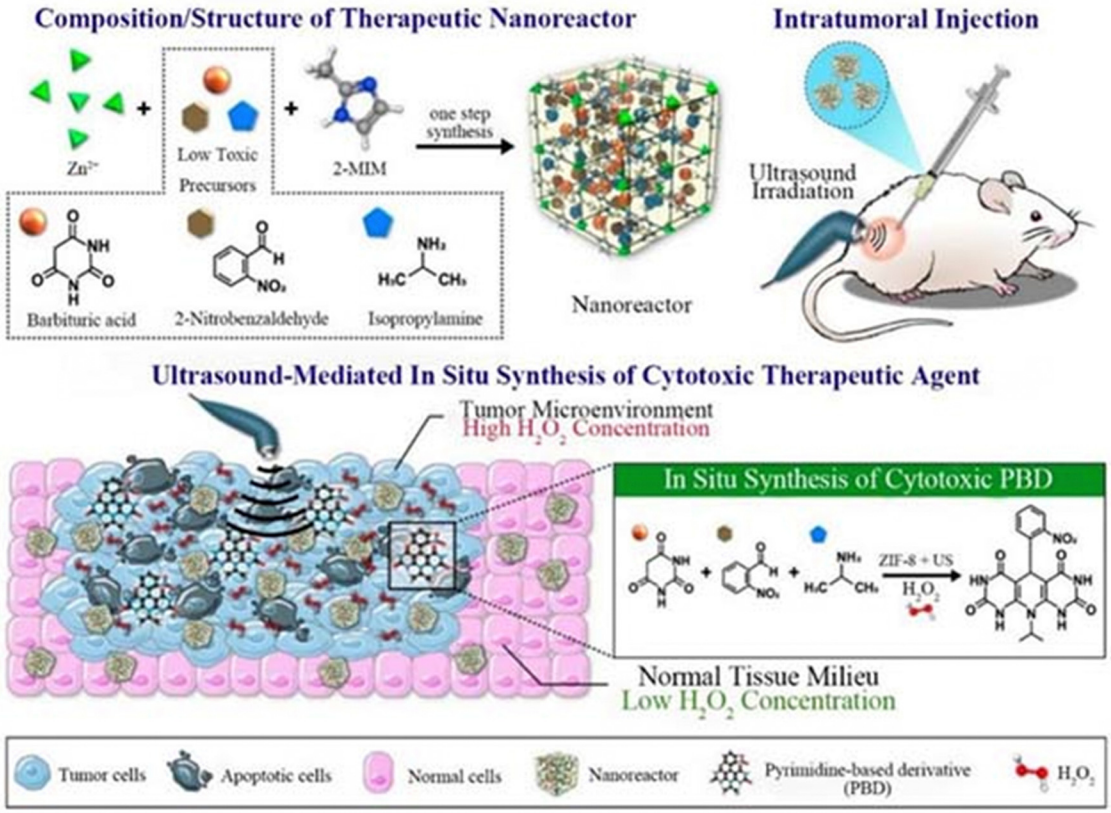

Fig. 3 Preparation of the as-proposed therapeutic NRs and their *in situ* synthesis of cytotoxic PBD upon irradiation with US following intratumoral injection. Reproduced from ref. 32 with permission from American Chemical Society, copyright 2023.

method can effectively synthesize the ZIF-8 core–shell structure we expected for cancer therapy.

In addition, the development of ZIF-90 has also attracted the attention of researchers. Jiang *et al.* added 2-ICA (imidazole acid-2-carboxaldehyde) in DMSO (dimethylsulfoxide), and $Zn(CH_3COOH)_2{\cdot}2H_2O$ in DMF, and the two solutions were mixed and stirred for ten minutes. Then DMF was added, stirred for five minutes and then washed with ethanol to get ZIF-9. Its SEM particle size was 75 ± 15 nm, which was larger than that of general ZIF-8. And the hydrated particle size was 85 ± 8.5 nm and zeta negative potential was −4.85, which was smaller than the value of general ZIF-8.[37] Pan *et al.* then added ICA to DMF and heated to 50 °C with stirring until ICA was completely dissolved and cooled and added DMF dissolved in $Zn(COOH)_2{\cdot}6H_2O$ drop by drop to the former, stirred for 10 min and then added trioctylamine (TOA) and stirred for 12 h at 25 °C, washed with DMF and EtOH, and dried at 40 °C. ZIF-90 prepared in this way still had a size of ∼80 nm even after encapsulation of the drug, and the average pore size was calculated to be 3 nm by the BET method and showed virtually no change in water over six days.[30] It can be seen that the particle size of ZIF-90 produced by different synthesis processes varies.

2.3 One-pot synthesis methods

A one-pot synthesis or simply a one-pot method is a chemical reaction strategy in which the reactants are subjected to successive multi-step reactions in a single reactor in order to save time and improve reaction efficiency. Yang *et al.* synthesized bio-bomb-loaded ZIF-8 by a one-pot method (Fig. 4B), and then adjusted the modified surface coating to make the biomimetic ZIF-8 nanovesicles (*i.e.*, BEFORE) into a core–shell structure with a size of 198.3 ± 2.1 nm, a PDI of 0.32 ± 0.08, and a ζ-potential of −23.0 ± 1.7 mV, which showed good stability.[69] The surface coating was then adjusted to make biomimetic ZIF-8 nanovesicles, *i.e.*, BEFORE. Li *et al.* dissolved dimethylimidazole (2-HMeIM), GOx and CQ in ddH_2O. Then, an appropriate amount of $Zn(NO_3)_2{\cdot}6H_2O$ solution was rapidly added to the mixture and stirred, centrifuged and rinsed at room temperature. It was then added to ice-cold phosphate buffered saline (PBS) with cell membrane fragments. After sonication for 5 min, mCG@ZIF was obtained by centrifugation for 20 min. Its TEM showed that a membrane-like layer was tightly covered on the surface of CG@ZIF, and the DLS data showed that the diameter of CG@ZIF changed from ∼147 nm to ∼171 nm, while the zeta potential went from ∼−12 mV to ∼−17 mV, which were all suggestive of the successful construction of mCG@ZIF. In addition, the size of mCG@ZIF remained almost unchanged in different media, suggesting that the mCG@ZIF fabricated by the one-pot method has good stability.[64] Jiang *et al.* employed one-pot stirring to prepare CEC@ZIF-8 by crystallising the ZIF-8 NP precursor (zinc nitrate and 2-methylimidazole) with CEC under stirring. The average size of the pure ZIF-8 NP was about 100 nm, and

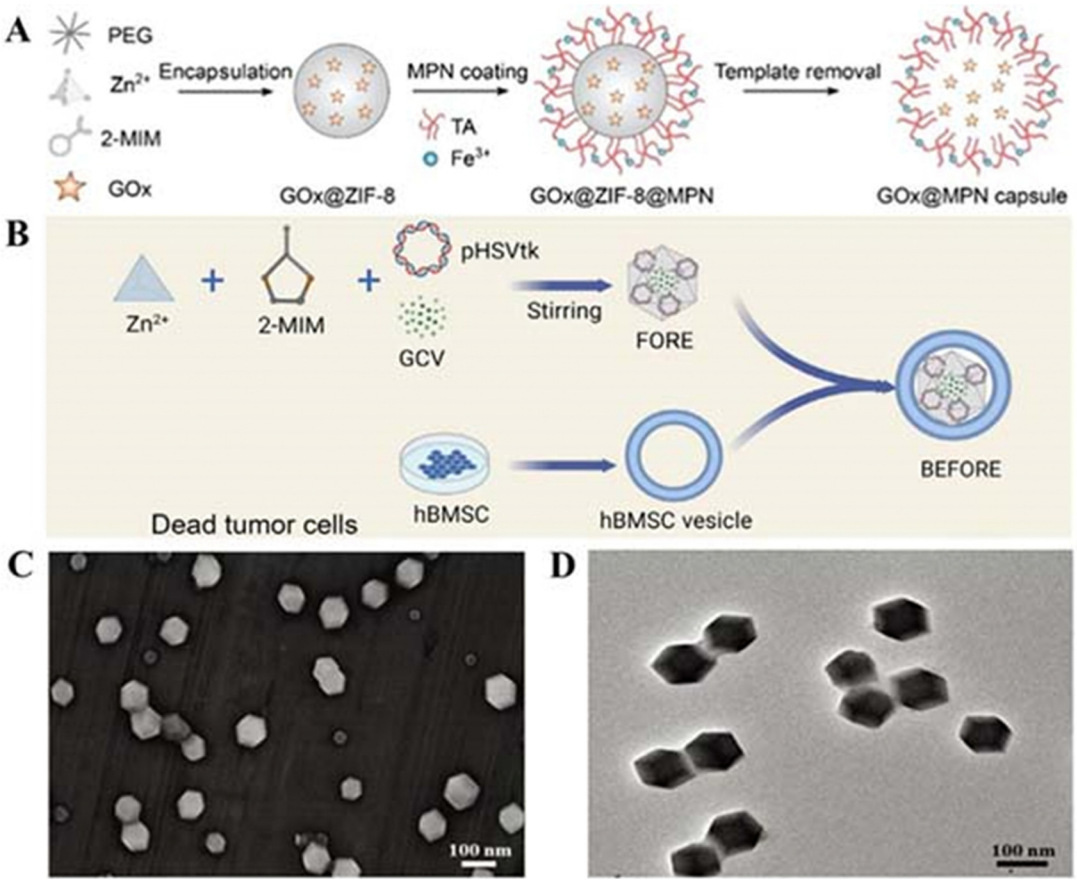

Fig. 4 (A) Preparation process of MPN capsules. Reproduced from ref. 60 with permission from American Chemical Society, copyright 2023. (B) Preparation process of BEFORE. Reproduced from ref. 69 with permission from Elsevier, copyright 2023. (C) Characterization of KN046@19F-ZIF-8. (D) SEM image of KN046@19F-ZIF-8. Reproduced from ref. 74 with permission from Wiley Online Library, copyright 2023.

encapsulation with CEC increased the average particle size to about 150 nm, suggesting the validity of the one-pot approach.[71] Lu *et al.* prepared chondroitin sulfate (CS)-functionalized ZIF-8 nanoplatforms using $Zn(NO_3)_2{\cdot}6H_2O$, 2,4-methylimidazole, hydrophobic ATO (A780), and chondroitin sulfate (CS) using a one-pot synthesis similar to the one-pot synthesis method described previously. TEM showed that the morphology of the CS-modified nanoparticles changed from *ortho*-hexagonal to spherical, and the enhanced permeability and retention (EPR) effect indicated that the complexes were suitable for passive targeting. In addition, the zeta potential of the complex was about −28 mV, and the complex dispersed in PBS showed remarkable dispersion and stability for 7 days. In addition, the size and morphology of the complex did not fluctuate over 180 days, indicating that the obtained particles have excellent storage stability.[94] Although the one-pot method is simple and efficient, it is only suitable for partial synthesis of Zn-MOFs. Some materials when added to Zn-MOF precursors at the same time are prone to cause agglomeration, which may lead to the failure of synthesizing the target product.

2.4 Ultrasound synthesis

Ultrasonic processing is widely used because it is cheap, environmentally friendly, convenient and gentle. Therefore, it is often implemented in combination with other synthesis methods.

Hang *et al.* encapsulated TPZ and GOx in nanoscale ZIF-8 (defined as GTZ) *via* a co-precipitation strategy, and subsequently, another ZIF-8 shell was fabricated on the surface of GTZ (defined as GTZ@Z) using epitaxial growth. Subsequently, the erythrocyte membrane was further wrapped around the nanoreactor by ultrasonic mixing to obtain GTZ@Z-RBM. Transmission electron microscopy images of the GTZ@Z-RBM NPS clearly showed a weak layer of dense corona RBM around the surface of the nanoparticles and the hydrodynamic diameter of the GTZ@Z nanoparticles on the RBM coatings (*ca.* 120.1 nm with a PDI of 0.122) was in agreement with the thickness of the RBM as previously reported. In addition, RBM-modified GTZ@Z in fetal bovine serum (10%) was more stable than GTZ@Z alone. The more negative ζ-potential of GTZ@Z-RBM indirectly also demonstrated the effectiveness of this ultrasound mixing approach,[109] whereas ZIF-8 particles were used as drug carriers in the study of Li *et al.* They prepared EHGZ nanosystems by encapsulating the ICD inducers EPI, GOx and haemoglobin chloride in ZIF-8 nanoparticles. The EHGZ nanoparticles were then dispersed in deionised water. A cell membrane solution with equal mass of nanoparticles was added to the above solution under stirring. The mixture was disrupted using an ultrasound probe at 45% power and centrifuged to obtain coated nanoparticles mEHGZ. After coating

the cell membranes onto EHGZ, DLS showed that the size of the nanoparticles increased from 123.66 ± 2.83 nm to 133.92 ± 2.93 nm. In addition, the surface charge changed from 17.77 ± 0.95 mV to −26.47 ± 1.98 mV after coating. The powder X-ray diffraction (XRD) pattern was identical to that of blank ZIF-8 nanoparticles, which indicated that the cargo in the ZIF-8 cavity and the sonication had no effect on the crystallinity of ZIF-8.[73] Zhou *et al.* on the other hand, co-encapsulated the chemotherapeutic drug mitoxantrone (MIT) and the DNA demethylating agent hydralazine (HYD) in ZIF-8 modified with hyaluronic acid (HA) and prepared (M+H)@ZIF/HA nanoparticles by dispersing the above synthesised product in an aqueous solution of HA under ultrasonication for 10 min. TEM images show that ZIF-8 and (M+H)@ZIF exhibit a rhombic dodecahedral morphology, whereas a thin smooth HA layer can be clearly observed in the rhombic shape of (M+H)@ZIF/HA. The increase in nanoparticle size and negative ζ-potential also further demonstrated that the negatively charged HA was successfully encapsulated on the (M+H)@ZIF surface. Since the HA carboxyl group is negatively charged, the negatively charged nanoparticles can thus effectively avoid severe protein adsorption and maintain the stability of the nanoparticles during blood circulation.[77] In the report of Liu *et al.* first, a methanolic solution of Fe_3O_4@PVP and a methanolic solution of gold nanoclusters were added to a methanolic solution of $Zn(NO_3)_2{\cdot}6H_2O$, which was sonicated for 5 min at room temperature. Subsequently, a methanolic solution of dimethylimidazole was added to the mixture, which was stirred for 5 min and then left to stand for 3 h. Finally, the reaction product was collected with a magnet and washed with methanol to obtain ZIF-8CNPs. Then, ZIF-8 CNPs-CPT was obtained by loading camptothecin (CPT) on its surface through simple physical adsorption (the loading capacity of the experimental sample was 35.7 mg g^{-1}) and finally FA-BSA/ZIF-8 cnps-CPT was obtained by modification with bovine serum albumin (FA-BSA). The ζ-potential of the FA-BSA-modified ZIF-8 CNPs-CPT changed from a strong positive charge to a weak positive charge as well as SEM images clearly showed that FA-BSA adsorbed on the surface of the sample, which confirmed the successful construction of the complexes.[88]

From the above, it can be seen that the low yield of the ultrasonic synthesis method can be avoided using a new strategy in combination with other synthesis methods. In addition, this strategy can avoid the agglomeration of the components when they are added simultaneously to the ZIF-8 precursor as well as reduce the reaction time, which is favourable economically and to the environment.

2.5 Other synthesis methods

In addition to the common room temperature synthesis methods, solvothermal methods and ultrasonic synthesis, there are other synthesis methods of Zn-MOFs that deserve our attention.

In a co-precipitation method, a solution containing two or more kinds of cations was used, which exist in the homogeneous phase in the solution; by adding a precipitant, after the precipitation reaction, various compositions of a homogeneous precipitation product can be obtained. It is not only possible to obtain products with uniform chemical composition directly through various chemical reactions in solution, but also easy to prepare nanopowder materials with small particle sizes and uniform distributions. ZIF-8 (ZnPc@ZIF) with water-insoluble PS zinc phthalocyanine (ZnPc) was synthesised by a one-step co-precipitation method by Xu *et al.* With the increase of ZnPc addition, ZnPc molecules gradually filled the micropores of ZIF-8. The luminescence intensity peaked when 0.25 mg of ZnPc was added.[40]

Hadi Ranji-Burachaloo *et al.* opted for a co-precipitation method to embed haemoglobin (Hb) and glucose oxidase (GOx) together in ZIF-8 nanoparticles with pH-responsive release and successfully prepared GOx&Hb@ZIF-8. TEM showed that ZIF-8 and GOx&Hb@ZIF-8 nanoparticles have a similar morphology with an average diameter of 400 ± 50 nm. In addition the DLS results (440 nm) are in agreement with the TEM results, suggesting that the nanoparticles are well dispersed.[66] The results of DLS (440 nm) are in agreement with the TEM analyses, suggesting that the nanoparticles are well dispersed.[66] Wang *et al.* first doped DOX into ZIF-8 nanoparticles by co-precipitation and then produced EGCG/iron nanocapsules encapsulating DOX (DOX@EGCG/Fe NCs) by suspending them in an aqueous solution of ferric chloride and EGCG and encapsulating a layer of EGCG-iron(III) complexes under mild conditions, after the template was removed. According to the DLS size distribution, DOX@EGCG/Fe NCs prepared with different Hmim/Zn molar ratios varied in size and their particle sizes were roughly in the range of 290–453 nm, which was a non-therapeutically critical factor for the nanoparticles, making nanoparticle sizes in this range suitable for cancer therapy. In addition, the typical folded morphology of DOX@EGCG/Fe NC capsules was observed in SEM images, and the high elastic deformation ability of such capsules could enable DOX@EGCG/Fe NCs to overcome the hydrodynamic flow obstacles of erythrocytes passing through the tumor tissues *in vivo*, which provides new possibilities for the application of Zn-MOFs in cancer.[68] The improved and innovative synthesis method also offers the possibility of preparing Zn-MOFs for cancer therapy. Jiang *et al.* synthesised amorphous ZIF-8 (aZIF-8) based on the original solvothermal method of preparing ZIF-8 by using a hydraulic pelletizer with a diameter of 20 nm at different pressures. The TEM images showed that its size was slightly larger than that of ZIF-8 (85–120 nm) and that it collapsed into aZIF-8 at a pressure of 0.34 GPa and increased with increasing pressure. ZIF-8 collapsed to aZIF-8 at a pressure of 0.34 GPa and the grain size increased with increasing pressure.[34] Hong *et al.* on the other hand avoided the conditions of organic solvents, high temperature and high pressure required for conventional MOF synthesis and used green and natural biomineralisation to synthesise aluminium-containing nanoparticles of ZIF-8 for antigen delivery. $AlCl_3{\cdot}6H_2O$ and OVA (ovalbumin) were added to the conventionally synthesised ZIF-8 at room temperature and the products all had a particle size of about 80 nm and a ζ-positive potential of 14.4 ± 0.1 mV. Gentle and simple synthesis without organic solvents or stabilizers achieved a high antigen-loading capacity of 30.6% and pH-dependent antigen release.[35] Li *et al.* on the other hand prepared ZIF-8 particles coated with Bi nanodots by a reduction method by dissolving $Zn(NO_3)_2{\cdot}6H_2O$, $Bi(NO_3)_3{\cdot}5H_2O$

and 2-methylimidazole in deionised water and stirring for 5 min. Afterwards, $NaBH_4$ in deionised water was quickly added to the above mixture and stirred for 1 min, washed and dried to obtain the product. Electron microscopy showed a size of about 100 nm and the hydrated particle size was also about 100 nm and its small size was attributed to the short reaction time and fast stirring rate.[53] Kaang *et al.* innovatively used a flow-assisted method to prepare a Pdop@enzyme@ZIF-8 (urease-powered nanomotor) system. They used beakers to improve the experimental procedure and to achieve bulk synthesis. Slowly diffusing Zn^{2+} ions preferentially interacted with catechol groups on the surface of the Pdop NP, leading to exclusive nucleation of ZIF-8. The Pdop core flow acted as a synthetic barrier, with the mass of reagents from the sheath flow being able to control the amount of transfer and the mass transfer of reagents in the sheath flow, effectively coiling the enzyme into a self-assembled, amorphous ZIF-8 shell, with quenching of core–shell products, and membrane filters were necessary to remove unreacted reagents in a timely manner.[57] Zhao *et al.* first synthesised DNAzyme-loaded nanoparticles to mimic viral nucleocoats containing genomes. Zn^{2+}-dependent DNAzyme (named TD) was encapsulated into ZIF-90 nanoparticles (named Z@TD) using a one-step synthesis procedure. The particle size of Z@TD was significantly reduced to 103 nm after DNAzyme encapsulation. Z@TD was modified by the Mn^{2+}-ZIF-90 exchange by Mn^{2+} modification. Finally, DSPE-PEG-cRGD and DSPE-PEG-HA2 peptides, which resembled spiny glycoproteins, were modified on the erythrocyte membrane by lipid insertion to complete the structural mimicking of herpesvirus.[72]

Their results undoubtedly provide new ideas for the preparation of Zn-MOFs and their nanocomposites; however, there are still many novel synthesis methods of Zn-MOFs that deserve our attention and exploration.

Applications in monotherapy. The number of clinical therapies is gradually expanding with advances in medical technology. Advanced nanotechnology has opened promising avenues for improving the performance of various clinical therapies. In this part of the review, we explore and discuss the role of Zn-MOFs and their complex applications in cancer monotherapy, hoping to provide an idea for future therapeutic research in cancer.

3. Chemotherapy

Chemotherapy(CT) is a common cancer treatment method that involves chemical reactions at the site of the tumor, which has a positive impact on cancer treatment. However, it also has drawbacks such as multidrug resistance, systemic toxicity, and low aggregation at the site of the tumor. Choosing appropriate nano drug delivery systems (DDs) can reduce damage to normal cells, while apoptotic cancer cells are present. The performance of Zn-MOFs studied in this article is worthy of attention. Although they have low stability and high cytotoxicity without modification, their performance has been well improved after loading, modification, and application. Especially, ZIF-8, which can achieve precise targeting of cancer cells, efficiently kills cancer cells and reduces damage to normal cells, has low aggregation in areas such as the kidneys, and plays an indispensable role in CT. The simplest method is to load relevant drugs onto Zn MOFs and target them to cancer cells, which then internalize them and exert their effects. Paclitaxel, gemcitabine hydrochloride (Gem), camptothecin (CPT), fluorouracil (5-FU), doxorubicin (DOX), *etc.* have all been proved to be able to effectively load ZIF-8 in high doses and target cancer cells.[27–29,101,102] By using simple methods to load cancer drugs onto Zn-MOFs, almost no specific conditions are required. Cancer drugs can be loaded onto Zn-MOFs through simple mechanical stirring or immersion methods. Here, 5-FU is used as an example: (1) Javanbakht *et al.* immersed MOF-5 in 5-FU reserve solution and measured the drug dosage using UV visible spectroscopy at 266 nm absorbance to remove the unloaded drug and obtain the predetermined product;[29] (2) Kulkarni *et al.* added ZIF-8 to a solution containing 5-FU and then centrifuged to obtain the predicted product;[103] (3) Jiang *et al.* mixed ZIF-8 and aZIF-8 induced by different pressures in PBS with 5-Fu by stirring in darkness for 72 hours, and freeze-dried to obtain the predetermined product.[34] The modification of hydrophilic/hydrophobic biodegradable polymers (such as polylactide glycolic acid (PLGA)/chitosan) can control the release rate of drugs, improve the biocompatibility, and increase the drug loading, thus improving the cell killing rate.[101] Modification of target molecules such as gallic acid (GA) enables more precise apoptosis of cancer cells and improves drug utilization.[27] The coating of related substances on the surface of Zn-MOFs can make the drug system more targeted. Javanbakht *et al.* designed an efficient oral drug delivery system by using the pH sensitivity of carboxymethylcellulose (CMC) with different degrees of dissolution in the gastrointestinal tract (GIT), coating CMC on the surface of MOF-5, and accumulating 5-FU in the pores of MOF-5. The formed nano material is spherical. Although the porosity and surface area of MOF-5-encapsulated 5-FU are reduced, the crystal structure of MOF-5 will not be damaged by drugs and the drug encapsulation rate is also high (84.1%). The electron microscope structure shows that the surface of its hydrogel is wrinkled significantly, which is conducive to the drug system as an oral drug delivery system to release 5-FU under the action of water after entering the microenvironment, The release of the drug in the microenvironment for 8 hours reaches 70%, and various properties have a satisfactory inhibitory effect on cancer cells.[29] Zhang *et al.* have modified Zn-MOFs using the property that the electrostatic interaction of ascorbyl palmitate (AP) hydrogel with the site of inflammation can preferentially target and adhere to the gastric mucosa of inflamed mice, but its long-term biosafety and target reliability need to be further investigated.[20] There is also 2-ME coated with homologous cell membranes that accurately targets cancer cells/TK-CPT@ZIF-90@C(MTZ@C). Under the action of homologous cell membranes, not only does its surface become smooth and easier to be internalized, but its stability is also improved, better targeting mitochondria and inducing higher levels of ROS. The experimental results show that its activity on 4T1 cells has decreased to about 30.4%, which is similar to that of 4T1 cells ZIF-90@C. The viability of co-

cultured cells is about 93.1% and in addition, NaN_3 and MTZ@C cells treated in combination are more effective than those treated alone with MTZ@C. The treated cells have higher vitality.[30] Even magnetic nanoparticles can be introduced for targeted drug delivery through the action of *in vitro* magnetic fields dropping the drug system to selectively localize to specific tissues.[102]

However, it is inevitable that there will be some problems, such as the early release of some drugs not only causing unexpected damage, but also reducing treatment efficiency, or the insufficient motivation to continue the action after acting deep in cancer cells. In response to these shortcomings, researchers have conducted in-depth research, and CPT has become a major hotspot. Due to the loading of hydrophobic drug CPT, regardless of the traditional ROS production program, the drug system is engulfed by cancer cells and produces ROS within the cancer cells. Even without external energy input and oxygen participation, it can induce exogenous ROS, completely avoiding the inactivation of traditional ROS grade nanomaterials in extremely hypoxic cancer centers, achieving significantly deep catalytic therapy, and prioritizing the promotion of cancer cell apoptosis.[14,18] The deep catalytic treatment of cancer has brought hope for better suppression of cancer. Due to the strong toxicity of certain drugs, direct delivery can cause damage to other cells and reduce their toxicity to cancer cells. *In situ* generation of drugs within cells may be an ideal method. Delivery of low toxicity prodrugs, *in situ* synthesis of compounds with high cytotoxicity in a specific microenvironment (TME) within cancer cells, thus achieves efficient and precise treatment. The pyrimidine-based derivative (PBD) that can only be activated in a TME, the low toxic compound disulfiram (DSF) and the highly cytotoxic copper chelate transformed by Cu^{2+} in a TME all provide evidence for this conclusion. Unlike traditional nanomedicine development, anticancer drugs are not pre-synthesized, but generated specifically *in situ*, avoiding the inevitable toxicity of non-targeted transportation.[23,24] The prodrug is generated *in situ* at the tumor site based on TME, which not only inhibits the tumor with higher toxicity, but also avoids unexpected toxicity caused during transportation. Combined with responsive "switches", it will definitely bring hope for cancer treatment. Regardless of the method used, when designing a drug delivery system, multiple factors should be considered together to achieve a more comprehensive drug delivery system.

If other means are added and combined with drugs, the therapeutic effect of CT will be greatly improved. The ZIF-based compound for *in situ* synthesis of PBD using the specific environment of TME above was deeply aggregated in tissues at specific tumor sites under ultrasound (US) conditions, and the precursor was induced to be synthesized *in situ* at the tumor sites mediated by US and TME and selectively activated by US irradiation. After ultrasound irradiation, the mechanical energy associated with US physically increased the penetration of f-NR into the tumor tissues and even completely covered the lesion tissues and the biodistribution within the tumor remained unchanged for 6 hours and was metabolically eliminated after 24 hours, maximizing the therapeutic effect and minimizing the associated toxic side effects.[32] As shown in Fig. 5, coating the drug system of the ZIF-8 carrier to form a Raman scattering (SERS) imaging probe enhances Raman signals and improves the stability and biocompatibility of SERS tags, while treating cancer Au@Ag $NRs^{4\text{-}ATP}$@ZIF-8/FA can load 60.31 g of DOX per 100 mg. Under the action of targeted drug folic acid (FA), HeLa cells exhibit sufficiently strong SERS signals, and are almost non-toxic to LNCaP cells, MDA-MB-231 cells, QGY-7703 cells, MCF-7 cells, and HCT-116 cells. Cell viability exceeds 89%, combining diagnosis and treatment.[36] There is also titanium dioxide (TC) loaded with lactoferrin (Lf) to form a core–shell structure compound with an MOF, along with 5-FU, which is used synergistically with phototherapy against neuroblastoma to reduce the side effects associated with conventional CT.[103] Abandoning the role played by CT alone and combining multiple treatment modalities together will certainly provide new ideas for the treatment of tumor cancer.

Among the ZIF family, in addition to ZIF-8, ZIF-90 has also attracted the attention of researchers. ZIF-90 has certain advantages that ZIF-8 does not possess, in addition to its relative excellence in biocompatibility, *in vivo* survival rate, and cytotoxicity of the drug release rate compared to ZIF-8; most importantly, ZIF-90 provides better mitochondrial targeting, achieving dual control through dual targeting of the cell membrane and mitochondria, resulting in better efficacy.[37] This aspect has been studied by a number of researchers with important results. Drugs such as DOX, thioketone-linked hippur (hippurine prodrug, TK-CPT), 2-methoxyestradiol (2-ME), and atovaquone (AVO) have been used in studies, and structures have shown that these drugs can achieve bidirectional mitochondrial targeting under high adenosine triphosphate (ATP) conditions and increase the oxidative stress effect of tumor cancer to induce apoptosis. The 2-ME/TKCPT@ZIF-90 (MTZ) studied by Pan *et al.* had a good therapeutic effect on solid tumors, with significantly smaller tumor size than the control group (shown in Fig. 6) and a significant apoptotic effect on tumor cells.[30] The IRGD/AVO-hemin@ZIF-90 studied by Lu *et al.* also had excellent effects in inducing apoptosis of tumor cells (as shown in Fig. 7), and the longest median survival time of mice treated with it could reach 70 days, and it effectively accumulated in the tumor area through the EPR effect and tumor cell targeting ability, releasing mitochondria-loaded AVO and heme chloride to kill tumor cells. It also has low cytotoxicity, with no significant cytotoxicity *in vivo* in the dose range of 0–75 mg kg^{-1}, although it caused weight loss and liver necrosis in mice in the range of 100 mg kg^{-1}, but this did not affect the excellent performance of IRGD/AVO-hemin@ZIF-90 in CT treatment of tumorigenic carcinoma.[38] The ZIF-90-based strategy to induce a mitochondrial cascade response has a significant synergistic therapeutic effect and is important in CT to overcome the low specificity and bioavailability and low serious side effects in CT for the treatment of tumor carcinoma.

In CT, Zn-MOFs deliver cancer treatment drugs to the cancer site and collapse in the acidic environment of the cancer site to release the drugs, resulting in the killing of cancer cells by cancer treatment drugs, and the simultaneous release of Zn^{2+}

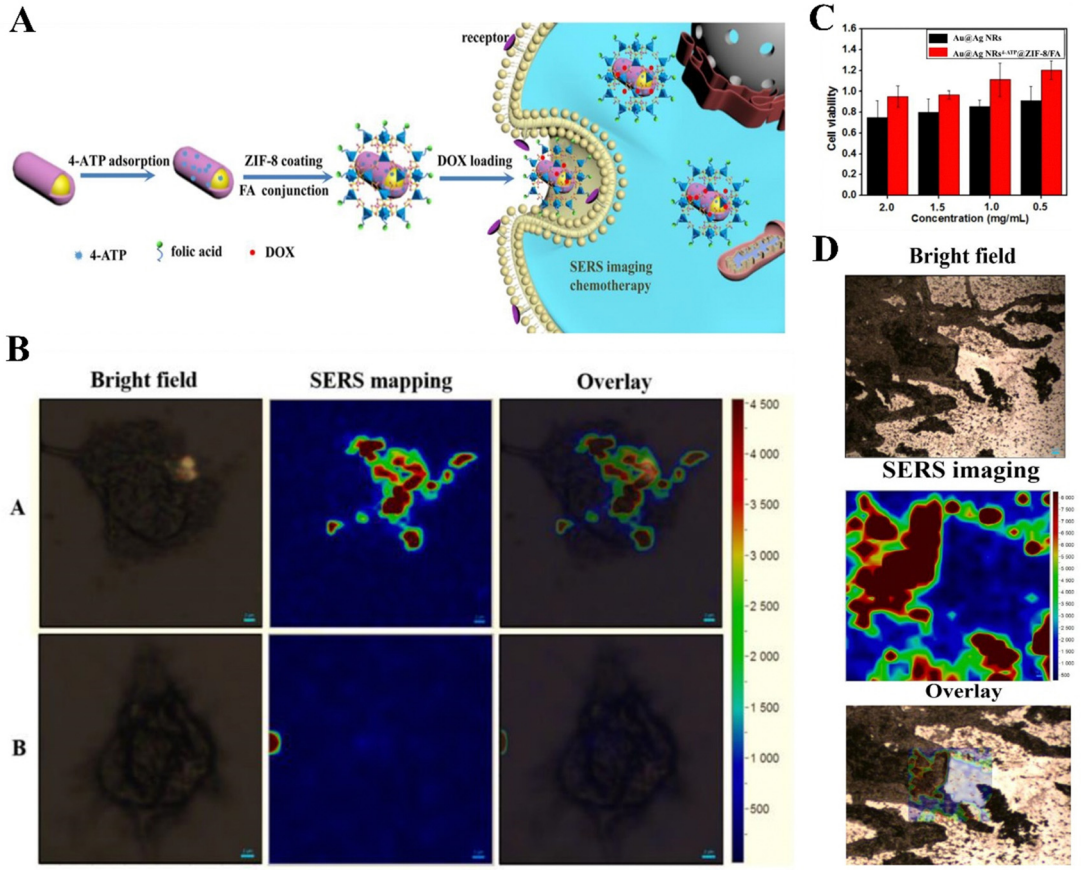

Fig. 5 (A) Synthetic route and application explanation of multifunctional composite nanomaterials. (B) SERS images of HeLa cells with Au@Ag NRs4-ATP@ZIF-8/FA [(A)]; Au@Ag NRs4-ATP@ZIF-8 [(B)]. (C) Cell viability of HeLa cells incubated with various concentrations of Au@Ag NRs4-ATP and Au@Ag NRs4-ATP@ZIF-8/FA; (D) SERS image of tumor sections of the human colon cancer. Reproduced from ref. 36 with permission from Elsevier, copyright 2023.

also provides support to kill cancer cells. The MOFs are widely used in the preparation of drug delivery systems and are pivotal in CT due to their excellent properties, which can be used for loading drugs for swelling cancer therapy or modified to confer different properties with more superior effects in targeting, drug delivery and release, apoptosis, and multiple actions. Although their specific degree of cytotoxicity remains to be explored, their excellent performance cannot be ignored. In the future, it is expected that CT and phototherapy, ultrasound and bioimaging can be used to achieve two or more synergistic treatments to compensate each other's defects and maximize the therapeutic effect.

4. Photodynamic therapy

Photodynamic therapy (PDT) is non-invasive and has minimal toxicity, but its efficiency depends on the tumor aggregation of photosensitizers (PSs) and the production efficiency of singlet oxygen in tumors. The hypoxia in tumors inevitably hinders the progress of PDT. The Zn-MOFs reviewed in this article can bring unexpected effects when used in PDT due to their large specific surface area, adjustable pores, and modifiable sites. The most significant one is ZIF-8, which can be modified to have different effects to cope with different TMEs. For example, by embedding tetra (4-carboxyphenyl) porphyrin (TCPP), zinc phthalocyanine (ZnPc), and others into ZIF-8, ZIF-8 can be released after collapsing in an acidic environment. This drug delivery system not only has efficient $^1O_2$ production efficiency but also excellent luminescence intensity. Due to ZIF-8's targeted drug delivery, it highly aggregates at the tumor site, reducing its damage to normal tissue.[39,40] However, direct delivery of drugs inevitably leaves residues in other tissues, which inevitably cause damage to the residual sites during laser irradiation. Therefore, a more effective method of *in situ* generation of oxygen should be considered. CaO_2@ZIF-8@THPP (THPP, porphyrin (tetrakis(3-hydroxyphenyl)-porphyrin)) studied by Yang *et al.* utilized the *in situ* oxygen-generating property of CaO_2 and the photosensitizing property of porphyrin to propose a self-oxygenation strategy, which decomposed and released the encapsulated CaO_2 of CaO_2@ZIF-8@THPP in an acidic tumor microenvironment and the drug loading of THPP was 28% higher than that in CaO_2 alone by 10-fold with a drug loading of 28%, which was 10-fold higher than that in CaO_2 alone, and the oxygen concentration reached 11.7 mg mL^{-1} after 6 h. CaO_2@ZIF-8@THPP showed significant cytotoxicity under

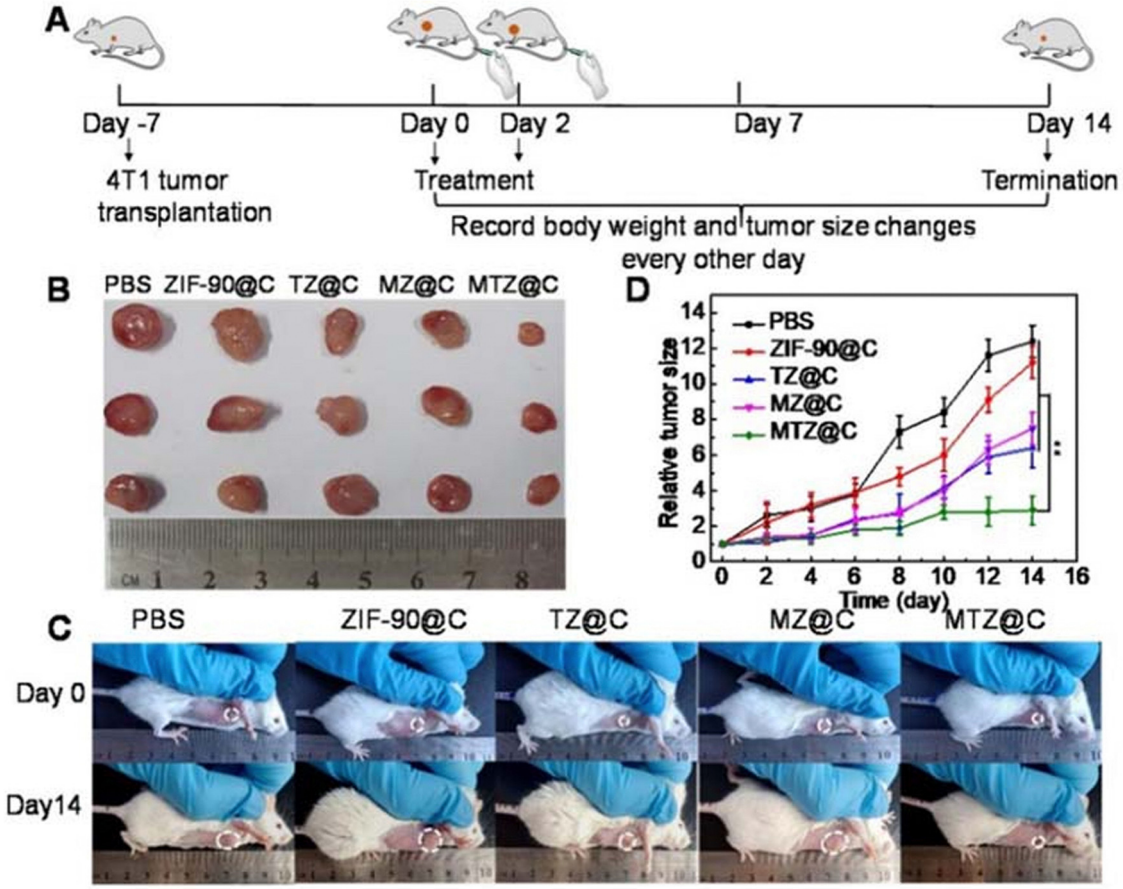

Fig. 6 (A) Diagrammatic representation of the therapeutic experiment. (B) Photographs of dissected tumors after the mice were treated with different materials for 14 days. (C) Photographs of the mice taken before treatment (0 days) and at the 14th day with different treatments. (D) Tumor growth curves within 14 days after the mice received different treatments. Data are presented as the mean ± SD (n = 5), $^{**}P < 0.01$. Reproduced from ref. 30 with permission from Ivyspring International Publisher, copyright 2023.

650 nm laser irradiation, with an IC_{50} value of 14.5 lg mL^{-1}, and the apoptosis and necrosis rates increased to about 86.5%, and overcame the hypoxic PDT limitations.[41] It can also load bovine serum albumin manganese dioxide nanoparticles (BSA, bovine serum albumin) with catalase-like activity on the surface of ZIF-8, realize oxygen self-supply in the hydrogen peroxide environment of acidic solution, and greatly alleviate the hypoxic state of cancer cells under the irradiation of 650 nm light with a low power density (230 mW cm^{-2}).[17] In addition to the possibility of drug residues in other tissues during transportation, after the drug reaches the cancer site and is swallowed by cancer cells, it may also seep back into the blood vessels due to size issues, causing damage as blood flows to other tissues. Therefore, the size controllability of nanomedicines should be considered. Wang *et al.*'s research based on accumulation-induced emission of TBD@ZIF-8-PMMA-S-S-mPEG (TBD, 2-((4-(7-(2,2-bis(4-methoxyphenyl)-1-phenylvinyl) phenyl) benzo[*c*][1,2,5] thiadiazol-4-yl) phenyl) (phenyl) methyl) malononitrile, PMMA, polymethyl methacrylate, S-mPEG, disulfide bonded methoxy polyethylene glycol group) has obtained satisfactory results, approximately 50 nm in original size of PS@ZIF-8-PMMA-S-S-mPEG. After ordered self-assembly within cancer cells, the size exceeded 200 nm. After 120 minutes of treatment with glutathione (GSH), the compound was assembled into ordered triangular particles with a size greater than 200 nm, with 94.5% of the assembly exceeding 170 nm. After expansion, it showed significant tumor aggregation, with very effective $^1O_2$ production and reduced blood reflux. At the same time, research has shown that the compound synthesized with ZIF-8 can load different drugs, to achieve targeted and precise treatment.[42] In addition to loading conventional drugs, programmable chiral organisms can be loaded into ZIF-8, integrating cofactor enzymes such as L-His DNAase into ZIF-8 to promote tumor-specific accumulation using biocatalysis and generate cytotoxic singlet-linear oxygen $^1O_2$ from molecular oxygen, and this ATP-responsive and self-sufficient l-CHA@l-His-ZIF-8 NPs can also accurately and specifically detect intracellular miRNA-21 expression, providing a precise and efficient therapeutic and diagnostic platform.[43] The drug itself can generate ROS in PDT, achieving PDT treatment. However, it is worth noting that in drug-loaded Zn-MOFs, Zn-MOFs release Zn^{2+} in acidic environments. Due to the release of coordination bonds and specific catalytic effects, drug-loaded Zn-MOFs show enhanced PDT effect and increase ROS production. Here are a few examples of this. (1) Hang *et al.* demonstrated that the enhanced PDT was due to the release

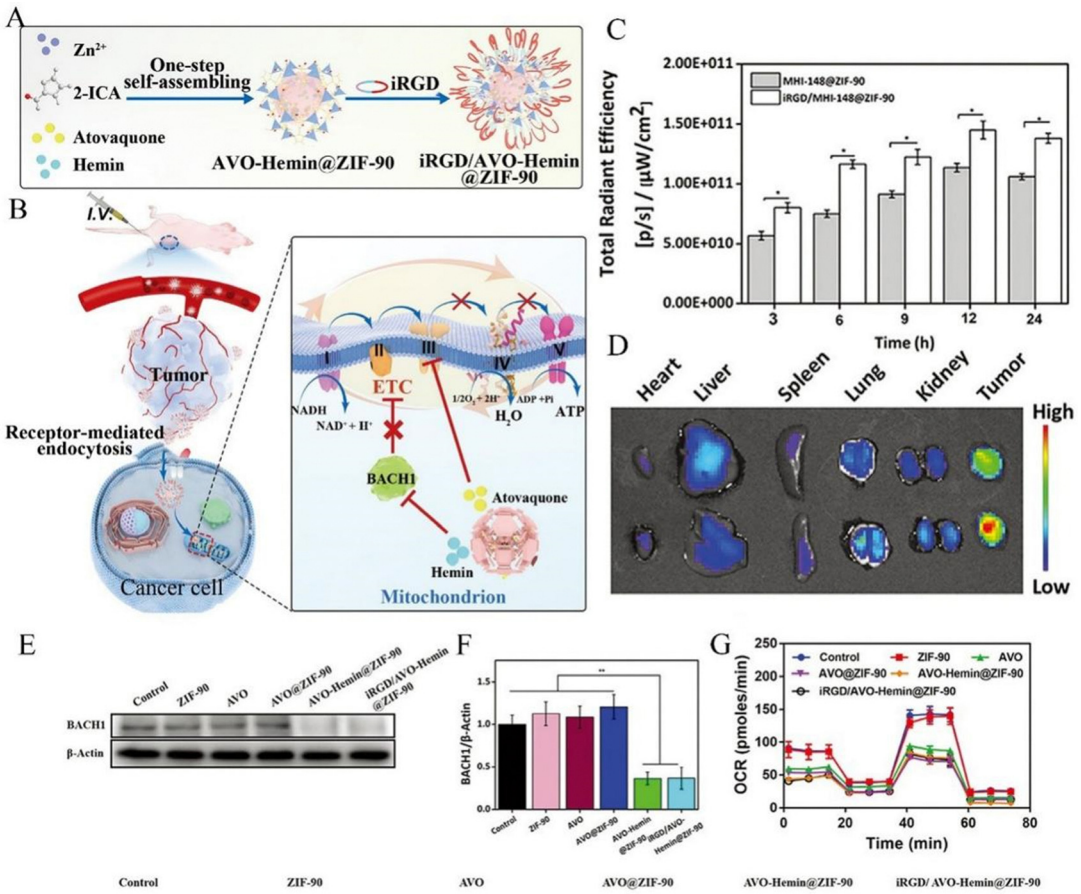

Fig. 7 (A) Schematic representation of preparing the iRGD/AVO-hemin@ZIF-90 through host–guest chemistry. (B) The potential mechanism for the breast cancer treatment by iRGD/AVO-hemin@ZIF-90. The mitochondria-targeted nano-system exhibited antitumor abilities by acting on the mitochondrial metabolism. BACH1 degraded by hemin can effectively improve the inhibition abilities of AVO towards breast cancer through increasing dependency on mitochondrial respiration. (C) The quantitative analysis of the fluorescence intensities of MHI-148@ZIF-90 and iRGD/MHI-148@ZIF-90 at tumor sites at different time intervals (n = 3, $^*P < 0.05$). (D) *Ex vivo* IVIS imaging of major organs and tumor after intravenous injection at 24 h. (E) Western blot analysis of BACH1 levels in MDA-MB-436 cells treated with various formulations for 48 h. (a) Control, (b) ZIF-90, (c) AVO, (d) AVO@ZIF-90, (e) AVO-hemin@ZIF-90, and (f) iRGD/AVO-hemin@ZIF-90. (F) Western blot densitometric analysis on the expression of BACH1 in MDA-MB-436 cells incubated with various formulations for 48 h (n = 3, $^{**}P < 0.01$). (G) Seahorse XFp analysis of MDA-MB-436 cells pre-treated with different formulations (n = 3). Reproduced from ref. 38 with permission from John Wiley and Sons, copyright 2023.

of TCPP from the decomposition of the weak 2D Zn-TCPP MOF ligand bond that the 2D Zn-TCPP MOF has between the hard Lewis base and the soft Lewis acid.[39] (2) Zhang *et al.* prepared a stimulus-responsive gating system using zinc(II) protoporphyrin IX (Zn(II)-PPIX), compared the ROS generation efficiency of the Zn(II)-PPIX/K^+-ion-stabilized G quadruplex tetrahedra to the ROS generated by Zn(II)-PPIX in the presence of the (II)-modified tetrahedra, and Zn(II)-PPIX/G-quadruplex tetrahedra were found to enhance the formation of ROS products by 2.5-fold and significantly enhanced ROS indicator fluorescence was detected in miRNA-21-responsive NMOF.[46,104] (3) Wang *et al.* compared TBD-PMMA S-S-mPEG and TBD@ZIF-8-PMMA-S-S-mPEG and found that ZIF-8 in the self-assembly promoted O_2 translocation of loaded organic PSs to achieve tumor-activated ROS enhancement of organic PSs and that hydrophobic fused PMMA and ZIF-8 in the assembly also protected PSs from environmental disturbances by isolating the PSs from contact with water to protect PSs from environmental interferences, demonstrating that the ZIF-8-PMMA-S S-mPEG nanoplatform could achieve optimal cancer cell clearance of loaded organic PSs in a bioremediation-specific manner.[42] (4) Zheng *et al.* showed that DF-BODIPY@ZIF-8 (BODIPY, boron dipyrrolylidene methylidene) had the highest intracellular ROS production rate due to its own catalytic effect on O_2 production from endogenous H_2O_2 catabolism, overcame the limitations of hypoxic environments in *in vitro* experiments, and significantly improved the efficiency of PDT under the same conditions.[44] (5) UCNPs-g-C_3N_4-CD@ZIF-8 obtained by Yang *et al.* were believed to be capable of efficiently transmitting deep-penetrating photon energies to sequentially activate the photosensitizers of g-C_3N_4 and CD, which can rapidly generate ROS and efficiently kill cancer cells, even in the absence of oxygen. In addition, the presence of the ZIF-8 shell layer not only stores a large amount of O_2 or H_2O required for the photodynamic effect, but also prevents the fluorescence intensity from being affected by an environment superior to mesoporous silica.[48]

Most PDT drugs have hydrophobicity and undergo aggregation and self-quenching during delivery to the tumor site.

However, Zn-MOFs, due to their unique site relationship, allow PSs to be well isolated in the framework, limiting their aggregation behavior. Studies have shown that drugs fixed by Zn-MOFs have more significant cytotoxic effects than free drugs after release at the tumor site. It was also proved that the ZIF-8 coating enhances their ability to escape within the body. At the same time, utilizing the gaps in the framework to transport oxygen can improve the efficiency of drug system ROS production in the tumor site. DF-BODIPY@ZIF-8 by Zheng *et al.* and HPMOF@ZIF-8 (HPMOF, photosensitive MOF) by Yang *et al.* demonstrated this idea well, utilizing the restrictive effect of the ZIF-8 framework to reduce PS aggregation and self-quenching, which provided a good basis for PDT therapy.[44,45]

To further improve the treatment efficiency of PDT, consideration should be given to its controllability. After reaching the tumor site, the drug is released in a specific environment and PDT is carried out in a specific environment. Controlling the entire treatment process will inevitably drive PDT to a new level. The classic material ZIF-8 has an undeniable effect in this regard and plays an important role in pH control. Zhang *et al.* addressed this issue by constructing a stimulus-responsive gating system and conducted an in-depth study of nanocarriers composed of vascular endothelial growth factor (VEGF)-responsive tetrahedral gated NMOFs loaded with the photosensitizer Zn(II)-PPIX, which acted as a door to cancer cells after the hairpin was opened and released in the ''chamber'' under catalytic DNA hairpin assembly or miRNA detection. In ATP-directed vector overexpression in cancer cells, tetrahedral-gated NMOF cytotoxicity and selectivity are enhanced because ROS product formation is enhanced approximately 2.5-fold and epithelial MCF-10A cells are less affected after Zn(II)-PPIX loading, and NMOFs also protect Zn(II)-PPIX from nuclease degradation and enhance loaded cell uptake and promote internalization of the endocytic pathway;[46,104] gating and hairpins allow the entire PDT process to be controlled, giving it visualization and maximizing results.

The Zn-MOF loads a PS in PDT and delivers it to the cancer site. After irradiation at a specific wavelength, the PS delivered by the Zn MOF to the lesion tissue is activated, leading to a luminescence chemical reaction that destroys the lesion. Modifying and loading different PSs on ZIF-8 not only improves the efficiency of $^1O_2$ generation and the tumor inhibition rate, but also achieves precise cancer treatment. Different Zn MOF compounds are synthesized through different methods, bringing different possibilities to PDT. In the future, the focus can be on the further controllability of complexes based on zinc-based metal organic frameworks in PDT, such as achieving different therapeutic effects under different fluorescence intensities or even combining them with other different treatment methods to achieve diverse treatments of a single system under different fluorescence intensities, maximizing the effectiveness of drugs.

5. Photothermal therapy

Photothermal therapy (PTT) also is non-invasive and causes minimal harm, while the currently used photothermal agents (PTAs) may have potential long-term toxicity and low accumulation in cancer, and the carriers loaded with PTAs also have instability issues, which hinder their further application in PTT. Zn MOFs in the MOF family are widely used as carriers for PTAs in PTT due to their excellent performance, with ZIF-8 being the most typical. However, unmodified Zn MOFs have high toxicity and their original biodegradability ensures that they will not accumulate permanently in the body. However, on the other hand, there are obvious side effects such as cell apoptosis, major organ abnormalities, and experimental animal death, and there are few reports of ZIF applications *in vivo*.[49] After modification, the performance of both PTAs and Zn MOFs has been significantly improved.[50] After loading organic dyes into a Zn-MOF, the compound exhibits good water solubility and photostability, strong near-infrared absorption rate, and strong photothermal conversion efficiency. The low solubility, low selectivity, and rapid elimination of organic dyes have also been improved, this was well demonstrated by Cy@ZIF-8 NPs (Cy, near infrared dye cyanine) studied by Li *et al.* and ICG@ZIF-8 NPs (ICG, indocyanine green) studied by Wang *et al.* The compounds studied by them had effective cellular uptake and were mainly concentrated in the swollen cancers and the liver, which reduced the damage to the normal cells, and importantly, no recurrence of swollen cancers was detected, which demonstrated an effective inhibition of the growth of swollen cancers.[51,52] It is noteworthy that their preparation is simple, although only simple mixing without considering the size matching problem can also yield compounds with uniform size.

In addition to organic dyes, metal nanoparticles are also widely used in PTAs, but they are not cheap or rare, which limits their large-scale clinical application. A non-toxic and low-cost ''green metal'' – bismuth (Bi) has attracted the interest of researchers. The first application of Bi nanoparticles and gambogic acid (GA) in liver cells has shown good photothermal properties and biomedical applications. Cell damage (such as apoptosis) caused by heating at lower temperatures (such as 45 °C) can be repaired with the help of heat shock protein (Hsp90), which brings defects to photothermal therapy. However, GA loaded Bi@ZIF-8 (BZ) (abbreviated as GBZ) can overcome this problem, inhibit Hsp90, effectively induce cancer cell apoptosis under low-temperature heating (such as 43 °C), improve the efficiency of cancer treatment, and at the same time, GBZ can reduce non-specific heating of high-temperature cancer under a strong laser, reducing damage to normal organs.[53] In short, GBZ has high potential for development in PTTs due to its high penetration depth and Hsp90 inhibition. The excellent performance of metal nanoparticles in PTAs has made researchers keen to study them even though they are expensive, such as gold nanoparticles, which have been shown to be combined with single-atom catalysts (SACs) for the modification of ZIF-8, the synergistic effect of the metal particles, gold and SAC made the PTAs show good redox capacity (the H_2O_2 content was greatly increased), and the temperature could even be as high as 65 °C after loading with gold, which did not produce significant skin damage despite the usual

treatment temperature range of 50–60 °C. What is more, these compounds have excellent enzyme-like catalytic ability, which can effectively catalyze the decomposition of hydrogen peroxide, and their heat conversion efficiency was calculated to be up to 63%.[54] Meanwhile, if we want to avoid the problem of expensive and costly metal nanoparticles, we can consider a liquid metal (LM), which is modified on a drug-loaded ZIF-8 framework with autophagy activation ability for resisting mild PTT-induced thermal resistance, allowing cancer cells to be killed even at a mild PTT temperature (45 °C) and without recurrence. The material (CLALN) prepared by this method has higher photothermal conversion efficiency to overcome the bottleneck of conventional PTT and also has the ability to induce autophagy activation, providing better PTT efficiency.[55] In conclusion, the application of metallic materials to Zn-MOFs can provide satisfactory results.

However, GBZ is only used for PTT treatment in a single aspect. To achieve a more precise effect in PTT treatment, it is necessary to consider the diversity of the tumor environment and the multiple control of PTT, so that the compounds used for PTT can act under different conditions in the tumor to achieve a precise treatment effect. Also using metallic nanomaterials, compounds based on dual release control have been applied to PTT. An *et al.* developed Au@ZIF-8 for the design of therapeutic agents with sequential response steps characterized by two tumor cancers. Although Au is more expensive compared to Bi, Au@ZIF-8 is capable of dual release in synergy with GSH and lower pH (both conditions are present for this to occur) to avoid interfering diagnostic signals from normal tissues and to reduce damage to normal tissues during treatment. As shown in Fig. 8, the excellent performance was demonstrated both in the confocal fluorescence image of 4T1 cells after staining and in the photothermal performance after laser irradiation.[56] ZIF-8 is unstable in a H^+ or GSH overexpressing microenvironment, but Au is only activated without release under H^+ and released in the presence of GSH, thus the excellent photothermal properties of Au@ZIF-8 have the potential to enhance the treatment of tumor cancer. In this study GSH is like a door for PTT, which can be used only when the door is open. In an earlier study, polydopamine (PDA) and tetradecanol (PCM) were used as a thermal response switch to achieve NIR-controlled synergistic thermotherapeutic precision drug release, and PDA-PCM@ZIF-8/DOX was developed. On the one hand, the thermal properties of PDA melted PCM and had some thermal therapeutic effect, and on the other hand, the acidic environment in the

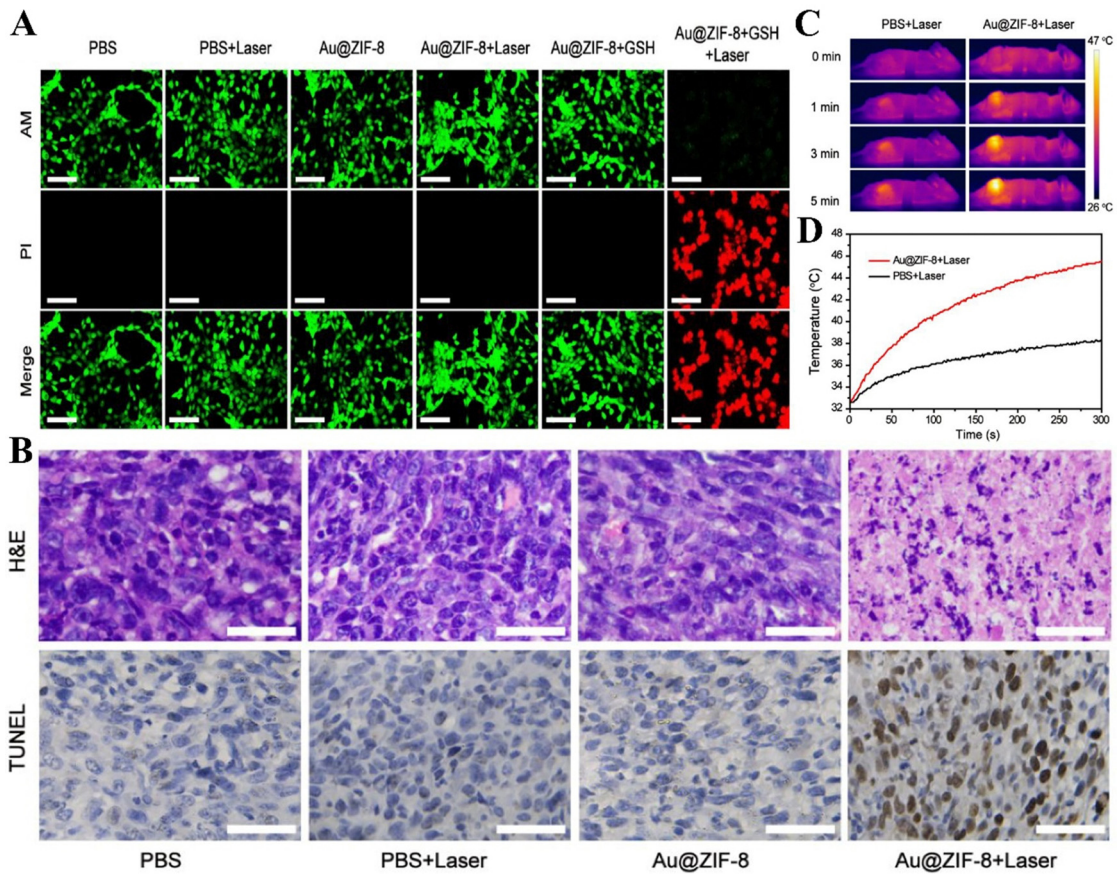

Fig. 8 (A) Confocal fluorescence images of 4T1 cells after treatment with different conditions and stained with Calcin-AM/PI (scale bar = 100 μm). (B) H&E- and TUNEL-stained histopathology slices of tumor tissues treated with PBS, PBS+laser, Au@ZIF-8, and Au@ZIF-8+laser (scale bar = 50 μm). (C) Photothermal images of PBS (200 μL) and Au@ZIF-8 (10 mg kg^{-1} body weight) 12 h after intravenous injection and irradiation by a 808 nm laser (0.9 W cm^{-2}) for 5 min. (D) Corresponding heating curves at the tumor site shown in (A). Reproduced from ref. 56 with permission from American Chemical Society, copyright 2023.

swollen cancer region degraded ZIF-8, thus achieving a dual drug release control. And it was shown that PDA-PCM@ZIF-8/DOX degraded slowly under neutral conditions and quickly under acidic conditions, achieving a moderate rate of degradation, and could be used as a good pH-responsive drug carrier.[49] Different tumors have different complex environments; therefore, the targeted design of drug systems is crucial. It is a major challenge in the treatment of tumors to deeply understand the microenvironment in which different tumors are located and to design and prepare efficient targeted drug delivery systems according to the different characteristics of drugs.

Zn MOFs load PTAs with high photothermal conversion efficiency required for PTT and deliver them to the cancer sites, causing them to aggregate in the tumor tissue. Under the irradiation of external light sources, the light energy is converted into heat energy to kill cancer cells. Both organic stains and metal nanoparticles have improved their performance after modifying with Zn-MOF carriers and have shown excellent therapeutic effects in PTT. From a single aspect of therapy to a dual release control in different environments, the application of Zn-MOF-based carriers in PTT has achieved a great leap and it is believed that further applications can be realized to combine their application in PTT with other biomedical applications such as bioimaging.

6. Chemodynamic therapy

The mechanism of action of chemodynamic therapy (CDT) is to promote the conversion of tumor-specific H_2O_2 to reactive oxygen species (ROS, *e.g.*, OH and O_2) by using oxidoreductase-like catalysis, transition-metal catalysis, or transition-metal-catalyzed Fenton reactions to induce apoptosis of tumor cells. CDT does not depend on the light and oxygen levels, and therefore is more conducive to the treatment of hypoxic tumors at the deeper tissues, but at the same time has been subject to the limitations of inefficient ROS generation and insufficient H_2O_2 in cancer tissues, in addition to difficulties such as damage to the immune system, high cost, and side effects on normal human tissues. The emergence of multifunctional nanomaterials provides a new pathway to address the shortcomings of CDT.

In previous studies, Pd cube nanoenzymes have been proved to catalyze H_2O_2 to produce ROS by simulating the activity of horseradish peroxidase (HRP). However, there will be some problems when directly combining GOx with Pd nano-enzymes, such as limited double-enzyme cascade efficiency, relatively low enzyme loading, inevitable enzyme degradation in blood circulation and so on. Biomimetic mineralization can effectively deal with the above problems. In Jin *et al.*'s research, in order to solve the problem of the low level of reactive oxygen species in tumor tissues, Gox and Pd cubic nanoenzymes were combined into ZIF-8 through biomimetic mineralization to obtain GOx@Pd@ZIF-8, which was used as an effective ROS generator to fight cancer. The cytotoxicity of ZIF-8, GOx@ZIF-8, Pd@ZIF-8 and GOx@Pd@ZIF-8 was evaluated by CCK-8 analysis of A549 cells. At 110 g mL^{-1}, the relative survival rate of cells was 96.8%. However, lower cell viability was observed after treatment with GOx@ZIF-8, Pd@ZIF-8 or GOx@Pd@ZIF-8. This fact shows that the GOx@Pd@ZIF-8 complex has effective anticancer activity. In addition, the inhibitory effects of different nanomaterials on the migration of cancer cells were also evaluated. Among them, the GOx@Pd@ZIF-8 complex showed good inhibitory ability. Subsequently, the effects on apoptosis and proliferation of tumor cells were evaluated by comparative experiments in mice. Ki67 staining and TUNEL determination were carried out. At the same time, the important organs of mice were sliced and compared and it was concluded that the GOx@Pd@ZIF-8 complex had anticancer activity and had almost no side effects on the main organs. It can be seen that this not only provides a new choice for effective treatment of cancer, but also helps us to understand the relevant molecular mechanism and improve the chemicals of the GOx@Pd@ZIF-8 complex.[59] In Qian *et al.*'s research, MOFs had a new way of application, the imidazolium zeolite framework (ZIF-8) was used as a sacrificial template and applied to the design of MPN capsules to achieve the purpose of adjusting their size and thickness.

As shown in Fig. 9, ZIF-8 NPs were encapsulated by doping GOx, and after encapsulation in MPN capsules, the template was removed under mild conditions (such as EDTA solution) and GOx@MPN was obtained. This substance can not only transport GOx, but also trigger intracellular cascade reaction through Fenton reactions and increase the level of ROS, thus increasing the death rate of cancer cells. Then, the ROS level induced by GOx@MPN capsule was detected by flow cytometry and fluorescence microscopy. Compared with the control group, the fluorescence degree of the GOx@MPN capsule group was stronger, which became strong evidence that GOx@MPN could produce higher intracellular reactive oxygen species. At the same time, through MTT assay and live/dead cell imaging, it was confirmed that the synergistic effect of Gox and Fe^{2+} gave GOx@MPN higher cytotoxicity.[60] This model provides a new idea for the potential biological application of MPN capsules combined with enzymes, but whether this substance will cause damage to other tissues of the human body still needs further experiments to explore. In addition to monotherapy, PDT can also be combined with CT for anti-cancer treatment. Wang *et al.* encapsulated chlorin e6 (Ce6)-, doxorubicin (DOX)- and HIF-1α siRNA into ZIF-8, so as to obtain a nano-particle (CDHNs) therapeutic platform that can be used to enhance chemotherapy (CT) and photodynamic therapy (PDT) strategies and obtain various therapeutic gains. In the fluorescence experiment, the average life span of DOX decreased from 3.97 ns to 3.27 ns, which was because the ROS produced by PDT was released from the nanocarriers with therapeutic agents. These results show that CDHNs irradiated with light can effectively produce ROS for PDT and at the same time promote the release of various therapeutic agents through lysosome escape in living cells. In addition, the zinc content of the tumor obtained by the researchers through inductively coupled plasma atomic emission spectrometry (ICP-AES) increased significantly 4 h after injection of CDHNs, which just proved that the effective tumor-specific accumulation of CDHNs and the environmentally

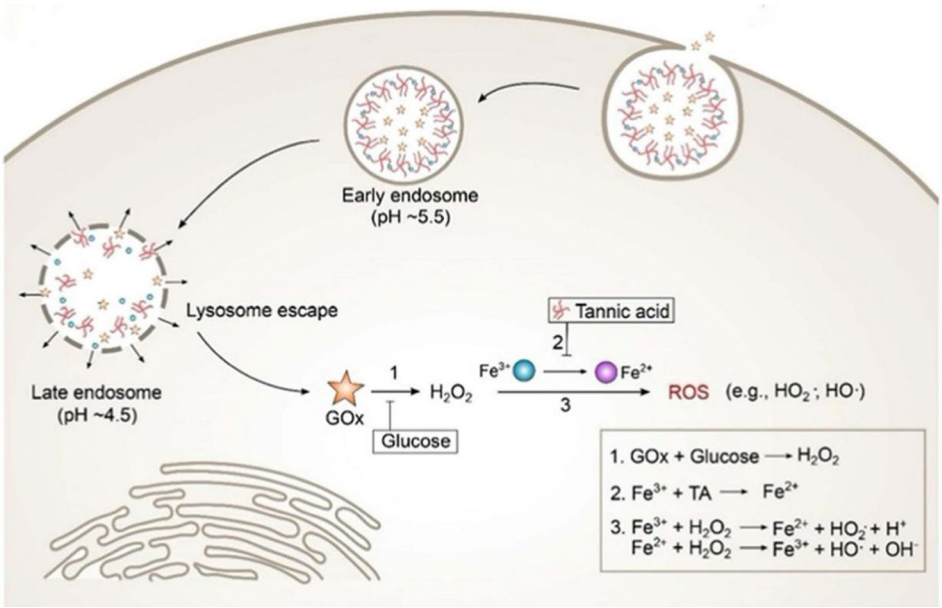

Fig. 9 Synthetic process for GOx@MPN capsules and (A) intracellular cascade reactions triggered by GOx@MPN capsules. (1) GOx catalyzes the intracellular glucose to generate H_2O_2. (2) Fe^{3+} was reduced to Fe^{2+} by tannic acid (TA) in an acidic environment. (3) ROS generation by iron ions and H_2O_2 *via* Fenton reactions. Reproduced from ref. 60 with permission from American Chemical Society, copyright 2023.

responsive dissociation of acidic tumors after intravenous injection had no long-term physiological toxicity. Undoubtedly, CDHNs provide a more comprehensive and powerful tool for cancer treatment through a collaborative strategy, and at the same time, it also sets a good example for PDT to be combined with other therapies.[105]

CDT induces tumor cells to undergo apoptosis by using redox enzyme-like catalysis, transition metal catalysis or Fenton reactions catalyzed by transition metals, thus promoting the production of reactive oxygen species (ROS, for example, OH and O_2) in tumor areas, and thus achieving the effect of killing tumor cells. From the above, it can be concluded that the compounds with Zn MOFs as the main carrier and other substances (such as Gox) have improved the cytotoxicity and the ability to kill cancer cells and because Zn MOFs themselves have good biocompatibility, they are more helpful to be put into cancer treatment after loading other substances. In addition, Zn- based MOFs provide a potential and good carrier, which helps the therapeutic effect of CDT therapy to some extent.

7. Sonodynamic therapy

Ultrasound uses a periodically vibrating mechanical sound wave that can activate acoustic sensitizers to produce reactive oxygen species (ROS), which can induce cancer cell death. This therapeutic strategy is commonly referred to as sonodynamic therapy (SDT), where ultrasound has the ability to penetrate deeper into the tissue and induce multiple biological effects that may reverse the immunosuppressive tumor microenvironment (TME) and further enhance the tumor immune response. Therefore, these unique advantages of ultrasound make SDT more effective and safer in the treatment of deep and large tumors. Zn MOFs have good biodegradability and good drug-carrying properties, which make them ideal carriers to promote the efficacy of SDT with high quality.

In Wang *et al.*'s research, it is reported that ZIF-8 NCs with specific M–N active sites will be expected to be potential bioactive acoustic sensitizers to improve the efficacy of SDT. At the same time, it reveals their possible SDT mechanism in cells and expands the scope of action of MOFs. They tested ROS by ESR and UV-Vis absorption spectra. Compared with the control group, the signal intensity of oxidized derivatives of ZIF-8+US, TEMP and DMPO increased by 2.81 and 31.04 times, respectively, which indicated that ZIF-8 NCs could significantly enhance the production of ROS under US irradiation. Combined with the experiments of mice and cells with cancer, it further indicated that ZIF-8 NCs had the potential to kill cancer cells in cancer treatment. In addition, the results also show the sonodynamic performance and biological activity of ZIF-8 NCs, which prove their potential as a bioactive anticancer agent and nano-sensitizer with high tumor inhibition efficiency (84.6%). However, more experiments are needed to explore whether they can have a long-term therapeutic effect *in vivo* and whether their structure is stable.[61] In Zhu *et al.'s* research, a two-dimensional (2D) coordination nanoplate composed of Zn^{2+} and tetra (4-carboxyphenyl) porphyrin (TCPP) was designed and prepared. This substance not only can be used as a sound sensitive agent for non-invasive SDT to stimulate cytotoxic reactive oxygen species (ROs), but also shows extraordinary loading capacity.

Therefore, as shown in Fig. 10, Zhu *et al.* further combined Zn TCPP with immune adjuvant CpG to prepare Zn-TCPP/CpG nanosheets, revealing the mechanism of Zn-TCPP/CpG nanosheets inducing specific immune response in tumor tissues *in vivo*.

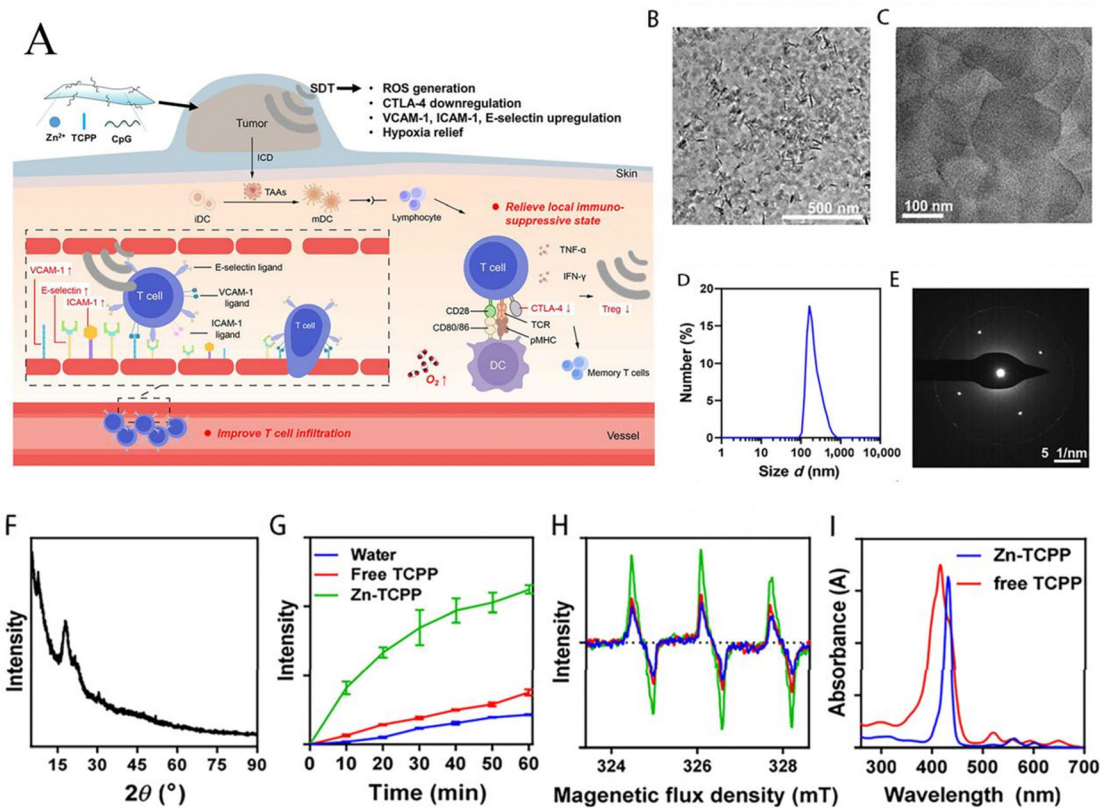

Fig. 10 Characterization of 2D Zn-TCPP nanosheets. (A) Schematic image of the synthesis of Zn-TCPP/CpG nanosheets and the mechanism of immune responses induced by Zn-TCPP/CpG-based SDT. Briefly, SDT with Zn-TCPP/CpG could induce ICD of cancer cells and release TAAs, which could be engulfed and presented by DCs with the assistance of CpG. The immune system could be activated to suppress tumor metastasis owing to the antigen presentation by matured DCs. Moreover, ultrasound itself could strengthen anti-tumor immune responses by improving the tumor-infiltration of T cells and limiting regulatory T cells in the tumor microenvironment. (B) and (C) TEM images of 2D Zn-TCPP nanosheets. (D) Dynamic light scattering (DLS) data of 2D Zn-TCPP in aqueous solution. (E) The SAED pattern of Zn-TCPP nanosheets. (F) The powder XRD spectrum of 2D Zn-TCPP nanosheets. (G) The UV-Vis-NIR spectra of free TCPP and 2D Zn-TCPP nanosheets in aqueous solutions. (H) and (I) ESR spectra (H) and SOSG fluorescence (I) of ultrasonically irradiated free TCPP and Zn-TCPP. Experiments were repeated three times. Data are presented as mean ± SD (n = 3). Reproduced from ref. 62 with permission from Springer Nature, copyright 2023.

The researchers used the methods of incubating cancer cells and measuring the ROS level *in vivo*. The results showed that Zn-TCPP/CpG nanosheets played an important role in enhancing tumor-associated antigens produced in cancer cell fragments after SDT treatment and promoting DC activation.[62] This result is obviously worthy of recognition, which provides us with a new way to treat tumors, and at the same time gives us the possibility of synergistic treatment with other local treatment methods. Metal–organic framework (MOF)-based egg yolk–shell nanocomposites are composed of an organic/inorganic shell and a MOF core, and are some of the most classic egg yolk–shell nanostructures. However, although a lot of research work has been done, how to accurately adjust the size of the yolk shell nanostructure, especially its core size, is still a huge challenge. In Wang *et al.*'s research, they applied Zn MOFs to a new structure-yolk–shell nanostructure. For the first time, they demonstrated a solvent-dependent adsorption-driven mechanism, which was used to synthesize an egg yolk shell MOF-based nanostructure with adjustable size and morphology, and its substance (ZIF-8@mSiO_2) was coated with a mesoporous silica shell. The selective and competitive adsorption of methanol (CH_3OH) and water (H_2O) on ZIF-8 nucleus was found to be decisive for inducing the morphological evolution of yolk–shell nanostructures. When they pretreated ZIF-8 nanocrystals with different concentrations of CH_3OH–H_2O (10%, 20%, 40% and 80%), they obtained a series of egg yolk-shaped ZIF-8@mSiO_2 nanostructures. The results show that with the increase of methanol concentration from 10% to 80%, the core size of ZIF-8@mSiO_2 nanostructure in yolk shell gradually increases, which shows that the absorption of methanol and H_2O by ZIF-8 is different. Therefore, they put forward a guess that the absorption of H_2O by ZIF-8 is low in low concentration of CH_3OH, but it is just the opposite in high concentration of CH_3OH. This mechanism affects the etching rate of the ZIF-8 NC core and leads to a disordered structure of the ZIF-8 core. Subsequently, they tested the cytotoxicity of ZIF-8@mSiO_2 and its performance as a sound sensitive agent using a fluorescence probe and the MTT test. It is worthy of recognition that this study not only provides the formation mechanism of an egg yolk–shell nanostructure based on MOFs, but also provides a novel direction of sound sensitive agents. However, whether this substance can play a long-term role still needs more experimental exploration.[63]

Liang *et al.* have confirmed that the cationic nature of glycidyl methacrylate functionalized quaternary chitosan (QCSG) can effectively promote blood coagulation and has good antibacterial activity, but its mechanical strength is still insufficient. Hyaluronic acid (HA) has great potential to enhance the strength of the QCSG gel network through electrostatic interactions. In addition, the transplantation of dopamine (DA) onto hyaluronic acid (HA–DA) will make it have good wet tissue adhesion, thus improving its ability to seal the wound quickly. So they synthesized a series of antibacterial shape memory multifunctional frozen gels by combining dopamine-modified ZIF-8(ZDH) loaded with dopamine monomethyl ether (HMME), dopamine modified hyaluronic acid (HA–DA) and glycidyl methacrylate-functionalized quaternized chitosan (QCSG). They used a contact method to simulate the antibacterial effect of frozen gel after contact with bacteria. The results showed that frozen gel showed good antibacterial ability to both Gram-positive *Staphylococcus aureus* and Gram-negative *Escherichia coli*. Moreover, when ZDH nanoparticles containing Zn^{2+} were added to the frozen gel system, the antibacterial rate of cold glue was greatly improved to over 98% due to the dual antibacterial effects of Zn^{2+} and quaternary ammonium cation groups. What is more surprising is that the cold glue has a good antibacterial effect in dealing with MRSA (methicillin-resistant *Staphylococcus aureus*), which just eliminates the concern about bacterial antibiotic resistance. In addition, the hemostatic effect and hemolysis ability of frozen gels were tested by using a rat animal model. The results showed that the blood loss in frozen gels was significantly different from that in control group ($P < 0.001$), gauze group ($P < 0.001$) and gelatin sponge group ($P < 0.01$). The blood loss in the frozen gel group was less and the hemostasis time was shorter with the increase of the HA–DA content in the frozen gel. Furthermore, there was no obvious inflammation in the contact area between the tissue and the gel in the subcutaneous wound of rats, and the tissue grew well. The above research results confirmed that a bio-friendly wound hemostatic gel, in addition to its structure can also be used as a sound sensitive agent to stimulate the production of ROS and inhibit tumor regeneration.[106] Hemoglobin (Hb) is an efficient and safe oxygen carrier, which can release oxygen in the hypoxic tumor site, thus improving the oxygenation of the tumor. At the same time, hemoglobin has a satisfactory ultrasonic sensitization effect. This effectively avoids the problem of low quantum yield of ROS caused by the accumulation of hydrophobic porphyrin. In order to improve the efficacy of SDT, Yuan *et al.* explored the biological characteristics of Hb, which carried O_2 and combined it with ZIF-8 to prepare O_2@Hb@ZIF-8 (OHZ) nanoparticles. They found that the $^1O_2$ production efficiency of OHZ nanoparticles at pH 5.5 was significantly higher than that of HZ nanoparticles, which showed that the O_2 in the substance could promote the production of 1 O_2. They speculated that OHZ nanoparticles could improve the hypoxic state in tumor microenvironment. Subsequently, tumor model and mouse experiments were used to test the biocompatibility and cytotoxicity of OHZ by live/dead cells. These experimental results show that the side effects of OHZ nanoparticles and US radiation on mice can be ignored and US with high tissue penetration depth can trigger OHZ nanoparticles to produce highly cytotoxic ROS, thus inducing tumor cell apoptosis. On this basis, researchers also measured the levels of Apaf-1 and ATP in the tumors of each group, as well as the expression level of apoptosis-related proteins. The results showed that the synergistic effect of US radiation and OHZ nanoparticles activated the mitochondrial apoptosis pathway.[19]

In addition to being used in SDT therapy, some acoustic sensitizers also show the ability of combined therapy with other therapies. In Gao *et al.*'s research, they designed and synthesized a cascade nano-platform based on ZIF-8. Through one-pot synthesis under mild conditions, subminiature MnO_2 nanoparticles (NPs), CaO_2 nanoparticles and acoustic sensitizer Ce6 were loaded into ZIF-8 nanoparticles together, in order to obtain a cascade nano-platform MnO_2/CaO_2/Ce6@ZIF-8 (MnCaCZ), which can improve the tumor microenvironment and enhance CDT/SDT combined therapy by circulating O_2. It was found that MNCAZNP had better ROS production ability in the process of ultrasonic treatment under the action of circulating oxygen supply and reducing GSH concentration. In the cytotoxicity evaluation of MNCAZNP, the cell survival rate was higher than 90% after 24 hours by gradient setting, which just proved the low toxicity and good biocompatibility of the nano-platform. This study shows us the feasibility of combining SDT with other therapies. From the above research results, we can see that MOFs play an indispensable role in sonodynamic therapy. In terms of its ROS production efficiency, the spatial structure of MOFs is conducive to acoustic cavitation to increase its efficiency.[107]

SDT is a therapeutic mechanism that activates the acoustic sensitizer in the tumor area without direct contact with the lesion in the form of ultrasound and then produces reactive oxygen species, which attacks the tumor cells and causes them to die. The safety and high efficiency of its materials, Zn-MOFs, show great potential value in these studies, but at the same time, the research products still have different shortcomings, such as whether the stay time of ZIF-8@mSiO_2 in the human environment is long enough still needs a lot of research to improve our understanding of these substances. Undeniably, MOFs have shown the prospects that people expect.

8. Starvation therapy

As we all know, hunger therapy can inhibit tumors through the consumption of components (that is, glucose depletion, oxygen scavenging and nutrient intake blocking) that are essential for tumor growth or vascular obstruction. There are two typical treatment schemes to achieve growth by cutting off the nutrition and energy supply of tumor tissue. One is to block the blood supply to tumor tissue by vascular embolization; the other is to directly consume nutrients in cancer cells. Especially, tumor cells are extremely sensitive to the fluctuation of the intracellular glucose level because of their active aerobic glycolysis, which makes it possible to develop tumor hunger therapy by accelerating glucose consumption.

Nowadays, glucose oxidase (GOx) has attracted extensive attention. It can reduce the glucose content in cancer cells by converting glucose into gluconic acid and hydrogen peroxide (H_2O_2). Excessive H_2O_2 can not only cause energy shortage, but also cause systemic toxicity, thus improving tumor killing efficiency. However, this process will consume oxygen and increase local hypoxia in the body. At the same time, considering the inherent hypoxic conditions in solid tumors, the lack of oxygen supply inhibits the effect of GOx-mediated cancer hunger treatment. Therefore, people have made a lot of efforts to improve the hunger effect mediated by GOx. Li *et al.* encapsulated chloroquine (CQ) and glucose oxidase (GOx) in zeolite imidazolium framework 8(ZIF-8) NPs, and at the same time wrapped their surface with cell membranes, aiming at enhancing the anti-cancer effect through the combination of starvation therapy and an autophagy regulation strategy. Cell membrane coating endows mCG@ZIF with excellent isotype targeting ability *in vivo*, and the cumulative release curve of mCG@ZIF *in vivo* experiment can be seen. Under the condition of pH 7.4, only about 20% of CQ was released from mCG@ZIF nanoparticles after 24 hours. In contrast, it was observed that CQ was rapidly released from mCG@ZIF NPs at pH 5.5 and released more than 60% after 24 hours. This result clearly shows the pH-responsive CQ release characteristics of mCG@ZIF, which are beneficial to the accurate release of CQ in the microenvironment with moderate acidity (pH5–6) and effectively reduce the occurrence of side effects. At the same time, the ATP level was significantly decreased in 4T-1 cells treated with mCG@ZIF. The expression level of LC3-II protein in 4T-1 cells treated with mCQ@ZIF and mCG@ZIF is high, which means that CQ released from ZIF-8 NPs successfully inhibits induced autophagy, because the inhibition of autophagy regulated by CQ leads to the accumulation of autophagosomes and the increase of LC3-II protein. Obviously, the participation of CQ can further aggravate the hunger of cancer cells induced by mG@ZIF. We can know that mCG@ZIF provides a new treatment mode for anti-cancer.[64] Finding drugs that can target key enzymes involved in different steps of glycolysis is a promising method to prevent glucose metabolism. One of the outstanding methods is to inhibit hexokinase 2(HK2). Metformin can damage glycolysis by selectively inhibiting the activity of HK2, but the effect of its single treatment is not satisfactory. Therefore, Meng *et al.* chose GOx in combination with it to enhance the therapeutic effect. ZIF-8 is a promising drug delivery nano-system for co-delivery of GOx and Met. However, the designed ZIF-8 is still inefficient in targeting cancer sites through passive targeting. L-Histidine (His) is a common amino acid with an imidazole ring and amino acid groups. This unique structure makes His have high affinity for Zn^{2+}, forming a ZIF-8 nanostructure. The amino groups exposed on the surface of ZIF-8 can be used as pliers for amino acid groups to grasp carboxylated recognition molecules through amide bonds. So Meng *et al.* encapsulated glucose oxidase (GOx) and methionine into histidine/zeolite imidazolium skeleton 8 (His/ZIF-8) and then coated it with the arginine-glycine-aspartic acid (RGD) peptide to obtain the required nano-drug (Met/Gox@His/ZIF-8∼RGD). In this study, they creatively constructed a new structure based on glycolysis. The researchers used a comparative experiment, which showed that the cell survival rate was only 30.4% in the Met/Gox@His/ZIF-8∼RGD group under normal glucose conditions, and only 22.3% of the cells survived under low glucose conditions. This result showed that Met/Gox@His/ZIF-8∼RGD had the best anti-tumor effect under normal or low glucose conditions. In addition, with the increase of the Met content and GOx concentration, Met/Gox@His/ZIF-8∼RGD showed higher cancer cell killing efficiency, which reflected that Met/Gox@His/ZIF-8∼RGD had a strong synergistic effect by blocking glycolysis and activating hunger therapy. At the same time, the subsequent fluorescence experiments and mouse experiments showed that Met/Gox@His/ZIF-8∼RGD was more concentrated in tumor sites, so as to effectively release GOx and Met to treat cancer, with outstanding biocompatibility and negligible side effects.[65] Here, Meng *et al*. provided another new way to cooperate with hunger therapy to fight cancer, which has a promising prospect, but the stability of Met/Gox@His/ZIF-8∼RGD remains to be explored. Hadi Ranji-Burachaloo *et al.* reported that GOx&Hb@ZIF-8 was used for hemoglobin co-production of free radicals and nutritional hunger. They used flow cytometry to monitor the fluorescence of DCFH-DA to analyze the ability of GOx&Hb@ZIF-8 to stimulate ROS. After the cells were incubated with GOx&Hb@ZIF-8 nanoparticles for 2 hours, the ROS levels produced in HeLa and MCF-7 cells were 8.1 times and 3.7 times higher than those of untreated cells, respectively. Obviously, GOx&Hb@ZIF-8 promoted the ROS production in cancer cells, and the survival rates of HeLa and MCF-7 cells decreased to 64% and 39%, respectively. From the above results, it can be seen that the prepared GOx&Hb@ZIF-8 effectively promoted the apoptosis of cancer cells, but the influence on normal cell apoptosis was relatively low, indicating that it has relatively low. Therefore, we can know that GOx&Hb@ZIF-8 nanoparticles provide an example for the combination of Fenton's therapy and hunger therapy.[66]

In Yu *et al.*'s research, compared with the hunger treatment strategy targeting at a single carbon source, they chose zeolite imidazole acid skeleton (ZIF-8) as the drug carrier platform to deliver glucose oxidase (GOx) and α-cyano-4-hydroxycinnamate (CHC) together and made a new nano drug CHC/GOx@ZIF-8, which could deprive glucose and lactic acid together. Both deprivation methods are through the ZIF-8 platform. The researchers compared the therapeutic effects of GOx@ZIF-8 as the control group with CHC/GOx@ZIF-8. For example, in the cell experiment, 44.3% of the cells in the group treated with GOx@-ZIF-8 were apoptotic, while 71.7% of the cells in the group treated with CHC/GOx@ZIF-8 were apoptotic, which indicated the synergy of the dual deprivation strategies. The introduction of CHC improved the anoxic environment in TME and enhanced the catalytic ability of GOx. In addition, in the subsequent mouse experiments, the weight of mice in CHC/GOx@ZIF-8 group did not change significantly, and on this basis, the tumor tissue decreased, which showed that CHC/GOx@ZIF-8 had good biocompatibility. Under this advanced hunger treatment strategy, CHC/GOx@ZIF-8 is a promising anti-tumor nano-drug.[67]

In Wu *et al.*'s research, an efficient Zn^{2+}-activated mRNA cleaving DNA enzyme with a common motif with ''8–17''

deoxyribozyme was selected. After transforming it into a therapeutic DNA enzyme, the enzyme can specifically recognize and digest GLUT1 mRNA in cells, thus down-regulating the expression of glucose transporter 1(GLUT1). Then the GLUT1 and deoxyribozyme (GD) were encapsulated into ZIF-8, Finally, HZ@GD was successfully synthesized through a HA connection, and a double-grid-controlled ''nano-energy interrupter'' was constructed to enhance the anti-cancer efficiency of hunger therapy. Researchers measured the inhibitory ability of ''nano-enabled energy blockers'' in metabolic pathways by the levels of LA and ATP secreted by B16-F10 cells. HZ@GD, HZ@RD and HZ groups decreased by 55.0%, 20.0% and 19.9%, respectively. Approximately, the ATP level of the HZ@GD group (39.3%) was significantly lower than those of the HZ@RD group and the HZ group. Then, C57BL/6 mice bearing the B16-F10 tumor were used to evaluate the anti-tumor effect of the ''nano-enabled energy interrupter'' *in vivo*. The experimental results showed that HZ@GD significantly reduced the tumor volume, and the tumor growth inhibition rate was as high as 80.8%, which was much higher than that of the control group. These results just reveal that HZ@GD has more outstanding energy depletion ability than other preparations due to the synergistic effect of GLUT1 depletion activated by Zn^{2+} and glycolysis inhibition mediated by Zn^{2+} interference.[21] Undeniably, Wu *et al.*'s research provide promising support for energy exhaustion in hunger treatment. Natural enzymes have the characteristics of high catalysis and specificity, but at the same time, they have the disadvantages of poor tolerance, short half-lives *in vivo* and low operational stability, which precisely organize their wide-ranging applications. Immobilization of enzymes on metal–organic framework (MOF) carriers is an effective method to maintain their biological activities by improving the stability of enzymes. Bai *et al.* designed an innovative cascade bioreactor with glucose oxidase (GOx) and horseradish peroxidase (HRP) nanostructures (ZIF-8@GOX/HRP) supported by ZIF-8 for synergistic cancer hunger/oxidation treatment. In the study, about 90% of HeLa cells treated with ZIF-8@GOx/HRP were wiped out, which indicated that the hunger/oxidation synergistic treatment based on ZIF-8@GOx/HRP had great potential for effectively eliminating cancer cells, and at the same time, it showed gratifying biocompatibility in hemolysis tests, which not only reflected the effectiveness of synergistic treatment of hunger and oxidation, but also gave a promising path for effective cancer treatment.[108] Another combination therapy was provided in the research of Hang *et al.* They designed a nano reactor with core–shell structure as an ''ON/OFF'' intelligent treatment system to encapsulate TPZ and GOx for multi-mode cancer treatment. The synthesized GTZ@Z-RBM nanoparticles can be used as an ''ON/OFF'' nanoreactor, which can reduce the toxicity of the system under acidic conditions and release GOx as needed. The GTZ@Z-RBM nanoreactor can inhibit tumor metastasis and prolong the survival time of mice with metastatic breast cancer. Therefore, the GTZ@Z-RBM nano-reactor can minimize systemic toxicity, achieve effective multi-mode tumor treatment, and inhibit tumor metastasis at the same time and combine starvation therapy with deoxyintensive chemotherapy, showing the expected therapeutic effect.[109]

Hunger therapy can inhibit the proliferation of tumors by consuming components that are essential for tumor growth or vascular obstruction (namely, glucose consumption, oxygen scavenging and nutrient intake blocking). From the above, it can be seen that Zn-MOFs play an indispensable role in hunger therapy and their unique pH response performance can promote autophagy of cancer cells and inhibit glycolysis so that they can accurately release drugs at the focus and their side effects cannot be reduced without this characteristic. In addition, Zn^{2+} in Zn-MOFs also plays a very important role in energy barrier regulation (such as HZ@GD), which shows that Zn-MOFs have broad application prospects in this therapy.

9. Gene therapy

Clinical anticancer drugs have many disadvantages, such as low bioavailability, low specificity, short cycle life and they cause great damage to normal tissues. Therefore, there is an urgent need to develop a new generation of anti-tumor weapons for cancer treatment. Gene therapy has become a powerful tool to treat challenging diseases such as cancer. Most anticancer drugs have limited selectivity to cancer cells relative to surrounding normal cells, especially normal cells with high mitosis rate. Therefore, it is urgent to develop methods for targeted delivery of anticancer drugs to tumor sites.

Nanotechnology provides a new strategy for eradicating tumors, including nanocarriers that can accurately target drugs to tumor tissues. Recently, nano-sized metal–organic framework nanoparticles (MOF NPs) have been used to load therapeutic agents or imaging agents because of their good biocompatibility, simple preparation, porous structure and multifunctional characteristics. Among these MOF NPs, zeolite imidazolium framework-8 nanoparticles (ZIF-8 NPs) composed of Zn^{2+} and 2-methylimidazole (2-MIM) have unique pH-sensitive biodegradability, which makes them an ideal nano-carrier for transporting various goods to living cells. Wang *et al.* designed a green tea polyphenol-metal network nanocapsule to stimulate the response of active oxygen. The results show that the cytotoxicity of DOX@EGCG/Fe NCs will increase with the increase of the incubation time of cancer cells, while the trend of cytotoxicity of free DOX is just the opposite, which makes DOX@EGCG/Fe NCs show good tumor growth inhibition (84.2%) and slight systemic toxicity. In addition, the drug release rate of DOX@EGCG/Fe NCs is greatly increased when the ROS level is high and the high dose of DOX@EGCG/Fe NCs has the highest tumor growth inhibition rate (84.2%). It can be seen that DOX@EGCG/Fe NCs have the characteristics of ROS response, which is helpful for the rapid release of drugs in the focus to eliminate side effects and has become one of the promising ways to treat cancer.[68] Suicide therapy uses tumor-specific drug-activated enzymes (suicide genes, such as herpes simplex virus type I thymidine kinase, abbreviated as HSVtk) to complete systemic delivery. HSVtk can also catalyze the phosphorylation of ganciclovir (GCV), which can be incorporated into the DNA of actively proliferating cells, thus stopping its DNA replication and cell division. In Yang *et al.*'s research, they reported a biomimetic

ZIF-8 nanovesicle BEFORE. The researchers explored the cycle life and biological distribution of BEFORE in the body. As shown in Fig. 11C, pHSVtk or FORE shows much less fluorescence at the tumor site, which is consistent with the *in vitro* imaging of extracted organs. The quantitative analysis of fluorescence intensity shows that BEFORE has accurate selectivity for tumor cells, which is beneficial to the development of accurate cancer treatment.

At the same time, the circulating life of BEFORE has been prolonged and tumor accumulation has been enhanced, which will contribute to the effectiveness of tumor treatment and reduce the side effects caused by repeated administration (Fig. 11D). Later, the anti-cancer ability of BEFORE was evaluated by mouse experiments. During the treatment, the weight of mice did not show significant changes and the researchers further removed the tumor for weight analysis. There was obvious infiltration of tumor cells in saline, BEFO, BEFOR and BEFOE groups and the tumor volume in the BEFORE group was significantly reduced, which means that BEFORE has good cancer cell killing ability and biocompatibility. Yang *et al.* constructed a new biomimetic metal–organic framework, which can accurately direct biological bombs to tumors and enhance the therapeutic effect on lung cancer. This strategy opens up a new way for cancer treatment and needs further clinical application research.[69] Yang *et al.* chose a ZIF-8 framework with pH response as biological macromolecule nanocarrier to complete the intracellular delivery of protein to cancer cells overexpressing epidermal growth factor receptor (EGFR). They provided clickable ligands (MIM-Nor modified by norbornene) by partially introducing norbornene into imidazole ligands, embedded them into ZIF-8 during the formation of particles, and then combined with cetuximab (Cet). The researchers evaluated the cytotoxicity of nanoparticles on HeLa and A431 cell lines. From the results of CCK-8, there was no significant cytotoxicity at a concentration as high as 100 $\mu g\ mL^{-1}$, which indicated that the antibody-coated nanoparticles had good biocompatibility. At the same time, the subsequent experimental results also show that nanoparticles coated with antibodies with specific target recognition can not only improve selective cell uptake but also successfully release functional proteins. Thus, Cet@protein@ZIF-8N shows efficient intracellular delivery and pH-responsive release of functional proteins with cell type selectivity. Yang *et al.* successfully developed a simple and effective ''clickable'' ZIF-8N nanoplatform, and its ''clickable'' mechanism is expected to provide a customizable and universal method, so that other targeting ligands can modify the surface of ZIF-8N more conveniently, thus achieving other types of selectivity. This strategy will provide a useful platform for future protein-based therapies.[70]

In human cancers, point mutations in the DNA binding domain of TP53 gene account for a large proportion, which leads to the cell accumulation of highly stable mutant P53 protein (mutp53) with cancer-promoting properties. Therefore, eliminating mutp53 by inducing proteasome degradation or

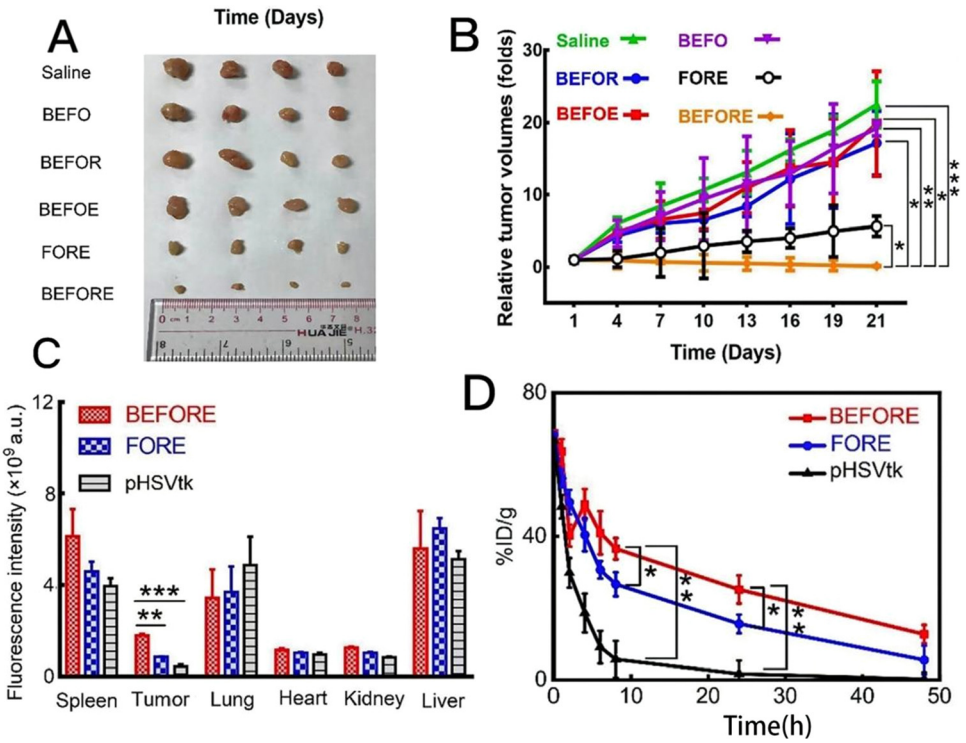

Fig. 11 (A) Macroscopic images of the tumor volumes after various treatments (n = 4). (B) Tumor growth curves after different treatments at different time points (n = 4, $^*P < 0.05$, $^{**}P < 0.01$, $^{***}P < 0.001$ compared with the BEFORE group). (C) The statistics of fluorescence intensity in different organs (n = 4, $^{**}P < 0.01$; $^{***}P < 0.001$ compared with the BEFORE group). (D) Circulation lifetime of different formations (n = 3, $^*P < 0.05$; $^{**}P < 0.01$ compared with the BEFORE group). Reproduced from ref. 69 with permission from Elsevier, copyright 2023.

autophagy is an effective strategy to treat p53 mutant cancer, but so far, the reported explanation inducer is more or less defective, which is not enough. Zhang *et al.* reported the unexpected activity of ZIF-8 in inducing proteasome degradation mediated by strong ubiquitination of broad-spectrum mutant p53 and revealed a series of mechanisms, including the continuous increase of intracellular Zn^{++} through the decomposition of ZIF-8 in acidic endosome, the decrease of intracellular GSH: GSSG ratio, the enhancement of glutathionization of mutant p53, and finally the ubiquitination and degradation of mutant p53. The researchers further designed an improved ZIF-8, which showed higher stability than unmodified ZIF-8 in an acidic tumor microenvironment and increased cell internalization, resulting in lower toxicity, enhanced degradation ability of mutp53 and a better therapeutic effect. However, the potential targeting effect of ZIF-8 on mutp53 still needs more experiments to improve.[110] AIE-Mit-TPP, a mitochondrial targeting material with aggregation-induced emission (AIE) characteristics, can induce extensive ubiquitination-dependent proteasome degradation of mutp53 protein and can also induce a lot of mitochondrial damage and autophagy. In Wang *et al.*'s research, AIE molecules with different organelle targets were designed, in which AIE materials targeting mitochondria (AIE-Mit-TPP) can successfully induce the degradation of mutp53 protein, leading to the proliferation of cancer cells and the decrease of cell migration. Therefore, they proposed a strategy of combining AIE-Mit-TPP and autophagy inhibitors for targeted treatment of mutp53-related tumors. In order to study the combined antitumor effect of AIE-Mit-TPP and autophagy inhibitor CQ *in vivo*, Wang *et al.* used a tumor mouse model to apply different treatments, but during the treatment period, no significant weight difference was observed between different treatment groups. The combined treatment of AIE-Mit-TPP and CQ induced a more significant reduction in tumor quality in a TOV112D tumor model. The results showed that the combination therapy of AIE-Mit-TPP and autophagy inhibitor CQ effectively inhibited the proliferation of cancer cells in the TOV112D tumor model. At the same time, TUNEL staining and immunofluorescence assay proved that the apoptosis in the tumor treated in the groups of AIE-Mit-TPP and CQ in the TOV112D tumor model increased, and the level of mutp53 decreased more obviously. Overall, these experimental results confirmed the combined anti-cancer effect of autophagy inhibitor and AIE-Mit-TPP *in vivo* and *in vitro*, and AIE-Mit-TPP showed excellent targeted damage effect. However, the relationship between mitochondrial damage and mutp53 protein degradation is still unknown, and the potential mechanisms of mitochondrial damage and mutp53 protein degradation need to be studied in detail in the future.[111] Cecropin (CEC) is an amphipathic polypeptide derived from insect venom, which has many pharmacological effects, including anti-inflammatory, antibacterial, antiviral and antitumor activities. In Jiang *et al.*'s research, CEC-encapsulated zeolite imidazolium-8 (ZIF-8) nanoparticles (CEC@ZIF-8 nanoparticles) were prepared by a one-pot stirring method. ZIF-8 can protect CECs from proteasome degradation, enhance the bioavailability of peptides, promote the uptake of HeLa tumor cells and increase the anti-tumor effect. The researchers measured the potential anti-tumor efficacy of CEC@ZIF-8 nanoparticles by MTT assay. HeLa cells were incubated with specified concentration of ZIF-8 NPs, free CEC, CEC@ZIF-8 NPs, carrier (negative control) or cisplatin (positive control) for 24 hours. Compared with the negative control group, the survival rate of all doses of ZIF 8 nanoparticles exceeded 80%, which indicated that ZIF 8 nanoparticles were in this concentration range. Compared with the free CEC with the same concentration of 80 g mL^{-1}, the combination of CEC with ZIF-8 nanoparticles increased the cytotoxicity, which indicated that nanocarriers greatly enhanced the effective endocytosis of CEC and at the same time greatly enhanced the accumulation in intercellular space of cells, and exhibited toxicity towards cervical cancer cell lines. This work has formed a strong support for highlighting the potential of Zn MOFs as a simple, stable and efficient drug delivery carrier for cancer treatment.[71] Zhang *et al.* established a PER-based DNA machine initiated by survivin mRNA in cells, that is, components including hairpins, primers and KFC were encapsulated by ZIF-8 nanoparticles and delivered to living cells together. This instrument can sensitively image the expression level of survivin mRNA and selectively kill cancer cells without affecting normal cells. The ability of ZIF-8 NPs to co-deliver protein and nucleic acid provides an excellent platform for designing various protease-based nucleic acid amplification reactions in living cells for disease diagnosis and treatment. The researchers found that only when the primers that triggered the reaction existed can the PER-based machine react in HeLa cells and produce substances. This further proves the reliability of the PER-based machine. Similarly, we can know that the PER-based machine has the potential to selectively kill cancer cells and has no effect on normal cells. After incubating with different nanoparticles, the researchers evaluated the cell viability of HeLa cells, LO2 cells and MCF-7 cells. Compared with untreated cells or cells treated with other nanoparticles, the cell viability of HeLa cells and MCF-7 cells incubated with BSA+KFP@ZIF-8/HP+/HP+primer NPs decreased significantly. On the contrary, even when cells were treated with BSA+KFP@-ZIF-8/HP+primer NPs, the cell viability of LO2 cells hardly changed. In addition, these results strongly prove that the PER based machine started by survivin mRNA can effectively produce gene drugs to induce apoptosis and provide a promising strategy for selectively killing cancer cells.[18] Wang *et al.* firstly prepared copper/zinc bimetallic MOF nanoparticles in coordination and then encapsulated deoxyribozyme targeting human early growth response-1 (EGR-1) into copper/zinc bimetallic MOF nanoparticles to establish a nano-platform for combined chemotherapy-gene therapy. In this design, after being swallowed by cancer cells, the nanoparticles will decompose in the acidic environment of lysosomes and at the same time release Zn^{2+}, Cu^{2+} and deoxyribozyme drugs to trigger the CuAAC reaction. The resveratrol derivatives produced subsequently can kill cancer cells with minimal side effects. At the same time, Zn^{2+} can activate DNAzyme, which strongly inhibits the proliferation and metastasis of cancer cells. Wang *et al.* compared the cytotoxicity of deoxyribozyme@Cu/ZIF-8 to different cell lines. The results showed that deoxyribozyme@Cu/ZIF-8 nanoparticles

showed stronger cytotoxicity towards MCF-7 cells than normal cells (293T cells and LO2 cells). Subsequently, they evaluated the synergistic therapeutic effect of the platform by cDNACu/ZIF-8 and deoxyribozyme @ZIF-8, respectively. CDNA@Cu/ZIF-8 and deoxyribozyme@ZIF-8 inhibited MCF-7 cell proliferation by 63% and 40%, respectively, while deoxyribozyme @Cu/ZIF-8 inhibited cell proliferation by as much as 75%. This is much higher than gene therapy alone (24.7%) or *in situ* drug synthesis alone (35.0%). These results prove that DNAzyme@Cu/ZIF-8 system has better therapeutic performance and this combination therapy not only effectively avoids the side effects of traditional chemotherapy, but also effectively blocks tumor metastasis, which provides an example for gene therapy to cooperate with other therapies.[112]

Gene therapy mainly induces the death of tumor cells from the gene level, and its way is that some genes are introduced into cancer cells through drug-carrying platforms, and cancer cells are killed by translating proteins that induce cell death, so as to achieve the therapeutic purpose. From the above research, we can see that Zn MOFs provide a better choice for overcoming the shortcomings in gene therapy, such as low selectivity, insensitive responsiveness and difficult drug structure to reach the focus stably. In gene therapy, the induced characteristics of Zn MOFs have played a gratifying role, and Zn^{2+} can also be used as an auxiliary factor to promote the process of cancer cell death. It can be said that in the aspect of gene therapy, Zn MOFs have shown a refreshing effect.

10. Immunotherapy

The use of T cell-mediated immune responses is an important strategy in tumor immunotherapy. However, tumors actively adopt various immune escape mechanisms to attenuate or even silence anti-tumor immunity; therefore, tumor cells cannot be effectively removed. With the development of tumorigenesis and anti-tumor immune mechanisms, immunotherapy with polymeric nanoparticles and gels to modulate the immune response has been explored; however, both techniques are challenged by stability issues and weak loading capacity.

Lactate is a characteristic metabolite of the tumor microenvironment (TME), and drives immunosuppression and promotes tumor development. The material engineering strategy of lactate regulation in tumors shows its potential in tumor immunotherapy. However, there is still a lack of understanding of the internal relationship between lactic acid regulation, metabolism and immunity promoted by materials in TME. Zhao *et al.* successfully developed a catalytic metabolic reprogramming strategy, which eliminated lactate through intra-tumor catalysis, realized local and systemic immune remodeling at the same time, and catalyzed the generation of OH for tumor treatment. The research focused on how the catalytic metabolic regulation of lactic acid helped to enhance immune function and its influence on related energy metabolism. The results showed that USL inhibited the progress of HCC by catalyzing the production of lactic acid and triggering the cytotoxicity of reactive oxygen species. At the same time, because the activation of systemic immunity is inseparable from the stimulation of peripheral factors, the researchers then detected the secreted proteins in the serum of tumor-bearing mice treated with PBS, U or USL. The secretory protein group in USL group was different from the secretory protein group in PBS and U group. The expression level of representative cytokines was also verified by ELISA. The results showed that USL triggered accelerated M1-polarized macrophage and cytotoxic T cell stimulation, and inhibited Treg differentiation. The remodeling of systemic immunity is the immunological basis for improving TME, which provides a prerequisite for enhancing local anti-tumor immunity. From the above results, we can know that the catalytic oxidation of lactic acid initiated by USL recombines the paracrine pathway in peripheral serum, which is very important for systemic immune remodeling. This catalytic metabolic reprogramming strategy targeting lactate may open up a promising and safe way for tumor treatment, which can be extended to other characteristic metabolites in TME.[113] Virus-based immunotherapy is becoming a very promising tumor treatment method. The high metabolic activity and immunosuppression of tumors increase their susceptibility to viruses, and viruses can specifically target tumor cells by recognizing the over-expression of tumor-associated antigens on their surfaces. However, despite the potential therapeutic advantages of natural viruses, their clinical application is greatly limited due to the risk of serious side effects caused by uncontrollable replication and the insertion of genetic materials into the host genome and the short board that it is difficult to achieve therapeutic effects too quickly. In Zhao *et al.*'s research, a kind of nano-particle (named Vir-ZM@TD) was designed to mimic herpes virus. In this bionic system, manganese-doped zeolite imidazole framework -90(ZIF-90) nano-particle (ZM@TD) loaded with DNA enzyme mimics the virus core–shell containing genome. Erythrocyte membrane mimics the virus envelope. Two functional peptides, RGD and HA2 peptide, were prepared by imitating the structure and infection process of herpes virus and their specific action mechanism is shown in Fig. 12. The effective accumulation of Vir-ZM@TD in tumor tissue can be known by *in vitro* fluorescence imaging. Next, ICP-MS was carried out to further quantitatively analyze the drug content in major organs and tumor tissues by measuring the Zn level. Compared with the control group, Vir-ZM@TD showed the highest tumor accumulation, which reflected its targeting. In the subsequent experiments, it was also revealed that the mice treated with Vir-ZM@TD showed stronger tumor growth inhibition due to the effective activation of innate immunity, and about 68% of the tumors completely subsided. However, Zhao *et al.* did not stop there. They also built a remote tumor model to evaluate the anti-recurrence ability of Vir-ZM@TD. After the treatment of Vir-ZM@TD, the growth of distant tumors was significantly delayed, with an inhibition rate of 63%, and the weight of mice did not change significantly. Subsequently, the activation of systemic immune response was found. This was confirmed by H&E staining. From this, we can see that Vir-ZM@TD can not only inhibit the growth of tumors, but also play its long-term protective role by promoting the systemic immune response. This effect shows that

Vir-ZM@TD has sufficient prospects for cancer treatment.[72] In the study reported by Li *et al.* a biomimetic nanosystem was constructed to trigger a tandem reaction to generate reactive oxygen species to amplify the ICD effect and increase the sensitivity of tumor cells to anti-PD-L1 antibody therapy. CLSM images show that mEHGZ can strongly induce CRT transport from ER to cell membranes. These DAMP results show that the self-amplification delivery system induces a powerful ICD effect. At the same time, the researchers found that the powerful ICD induces DCs to mature and CD8+T cells to infiltrate into tumor tissues for adaptive immune response, thus creating an immune-activated microenvironment. After treatment with the anti-PD-L1 antibody and mEHGZ, the tumor growth was effectively inhibited and the lung metastasis of the tumor was limited. This shows that the nano-system can be used as a nano-vaccine to enhance the antigenicity and auxiliary possibility and improve the anti-PD. In addition, after treatment with EPI and mEHGZ, the tumor growth weight decreased from 3449.54 mg in the blank group to 1020.34 mg and 416.24 mg, respectively. MEHGZ has an effective anti-tumor effect in the mouse model carrying CT26. Therefore, mEHGZ is expected to be a nano-system that can effectively induce ICD to activate a tumor immune microenvironment and enhance the therapeutic effect of the anti-PD-L1 antibody.[73]

In the research of Jiang *et al*, a new recombinant humanized PD-L1/CTLA-4 bispecific single domain antibody Fc fusion protein (KN046) was designed, which can bind to PD-L1 and CTLA-4 and effectively enhance the killing effect on tumor cells. Intelligent nano-delivery agents with high biocompatibility and biodegradability can not only protect the active components of immunotherapy from damage, but also accurately deliver antibodies to tumor areas. Therefore, coating KN046 with ZIF-8 can reduce the adverse reactions in normal tissues, improve its enrichment in tumors and prevent it from being cleared by the immune system. Jiang *et al.* designed a new intelligent drug KN046@^{19}F-ZIF-8 to overcome many limitations in immunotherapy. KN046 is a novel recombinant humanized PD-L1/CTLA-4 bispecific single domain antibody-Fc fusion protein. After combining it with PD-L1 and CTLA-4, the drug can be safely and effectively delivered to the tumor through ZIF-8. In the experiment, the results show that KN046@^{19}F-ZIF-8 is more

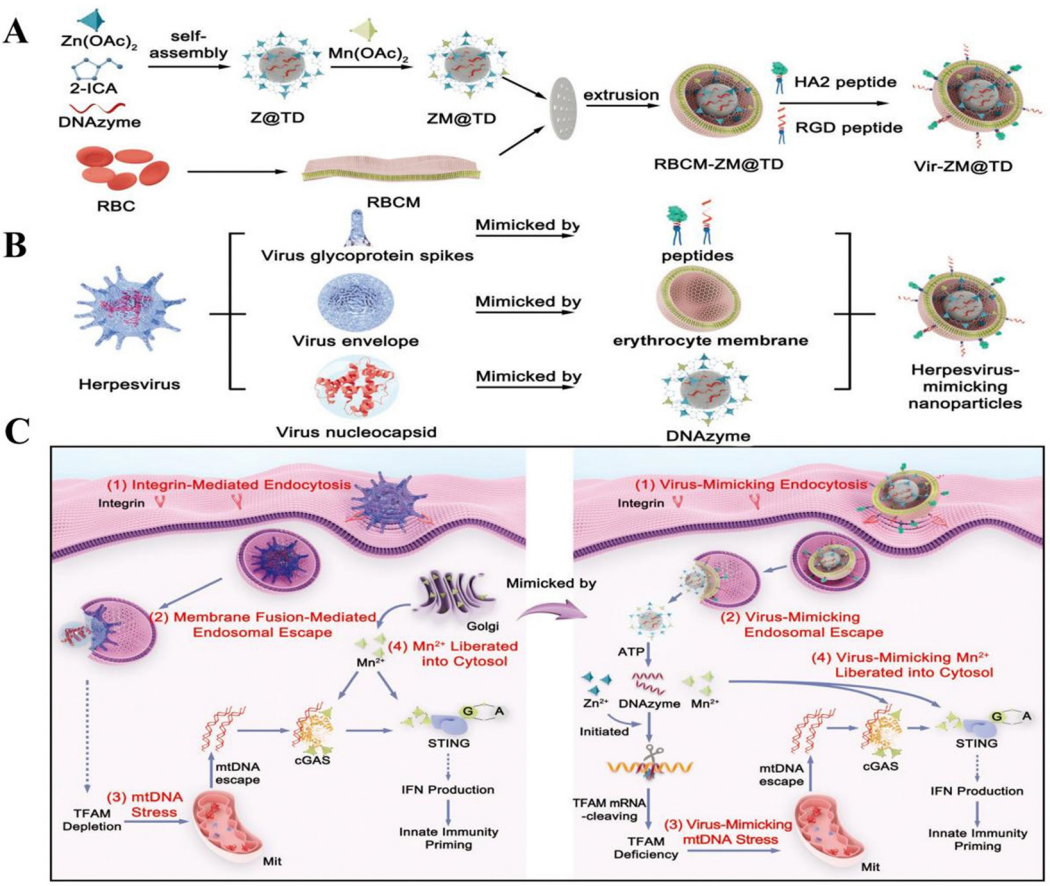

Fig. 12 Schematic illustration of herpesvirus-mimicking nanoparticles (Vir-ZM@TD) that activate antitumor innate immunity. (A) Preparation procedure for Vir-ZM@TD. (B) Schematic illustration of Vir-ZM@TD, which closely mimics the structure of herpesvirus. (C) Schematic illustration of Vir-ZM@TD mimicking the infection processes of herpesvirus for robust innate immune responses: (1) Vir-ZM@TD specifically targets tumor cells through the integrin receptor. (2) HA2 peptide-mediated membrane fusion triggers endosomal escape of ZM@TD. (3) The ATP-responsive released DNAzymes catalyze the cleavage of TFAM mRNA to induce TFAM deficiency and mtDNA stress, releasing mtDNA into the cytosol. (4) Cytosolic Mn^{2+}, mimicking the organellar Mn^{2+} liberated into cytosol during herpes virus infection, synergistically potentiates antitumor innate immunity. Reproduced from ref. 72 with permission from John Wiley and Sons, copyright 2023.

effective than KN046 alone, and in the mouse model, the weight of mice only changes slightly and the hemolysis degree is less than 2%, which is enough to prove that KN046@^{19}F-ZIF-8 has good biocompatibility. More importantly, KN046@^{19}F-ZIF-8 provides persistent PD-L1/CTLA-4 double blocking immunotherapy, which can effectively induce significantly enhanced anti-tumor immune response and reduce the immunosuppression of tumor cells, thus achieving higher anti-tumor efficacy. At the same time, this study provides an engineering strategy for the clinical application of more effective immunotherapy.[74] Ge *et al.* designed a pH-sensitive autophagy control nanocarrier CUR-BMS1166@ZIF-8@PEG-FA(CBZP), loaded with curcumin (CUR), and activated immunogenic cell death (ICD) through autophagy cell death, thus enhancing the immunotherapy response blocked by PD-1/PD-L1. At the same time, BMS1166 inhibits the interaction of PD-1/PD-L1, enhances the immunogenicity of tumor and improves the immunity of anti-tumor T cells. By detecting the expression of calreticulin and HMGB1, ICD is studied *in vivo*. The experimental results showed that no significant HMGB1 release and calreticulin exposure were observed in saline and blank ZP groups. However, CZP and BZP significantly increased the exposure of calreticulin and the release of HMGB1, which indicated that CZP and BZP promoted the maturation of DC compared with the untreated group and blank ZIF group. In addition, CBZP induced DC maturation more obviously, which confirmed the robust ICD production mediated by CBZP treatment. Similarly, Ge *et al.* also observed that the percentage of the CD3+CD8+CD44+CD62L effect or memory T cells (TEM) in spleen in the CBZP group was much higher than that in CZP and BZP groups. These results show that CBZP treatment successfully provides a strong immune memory effect with long-term efficacy. In short, CBZP can synergistically treat the OS (osteosarcoma) effect by combining ICD induction with checkpoint blocking, which just reveals autophagy control as a potential clinical therapy for OS.[75]

Dai *et al.* reported the synthesis of a bimetallic organic framework (MOF) nanoparticle (Gd-MOF-5) containing Gd^{3+} and Zn^{2+}, which was used as an immunomodulator to reduce the immunosuppressive PS signal and as an ICD inducer to improve the immunostimulatory signal. The results showed that Gd-MOF-5 nanoparticles with acidity reactivity successfully released Gd^{3+} and Zn^{2+} in cancer cells, in which Gd^{3+} and Ca^{2+} competed for the binding of TMEM 16F, thus inactivating TMEM 16F, inhibiting PS externalization and making its immunosuppression largely ineffective. At the same time, intracellular Zn^{2+} overload leads to mitochondrial dysfunction, activates endoplasmic reticulum (ER) pressure, destroys cellular calcium balance, leads to ICD induction, up-regulates immune stimulation signals, greatly improves the effect of cancer immunotherapy, and provides an example for the synergistic treatment of cancer with bimetallic nanoparticles.[76] Zhou *et al.* put forward another immunotherapy mechanism, designed a nano-platform based on a metal–organic framework (MOF), and encapsulated mitoxantrone (MIT) and a DNA demethylation agent hydrazine (HYD) in ZI by destroying MDSC-mediated immunosuppression. On the one hand, HYD can up-regulate the expression of GSDME, and the released MIT can induce the activation of caspase-3, leading to focal droop of tumor cells. On the other hand, HYD can prevent the formation of MGO in MDSCs, so as to eliminate T cell paralysis. The results show that (M+H)@ZIF/HA can greatly promote the maturation of DC, from 18.8% to 36.6%, which is to transform non-inflammatory apoptosis into inflammatory ptosis, which leads to a stronger immune effect. In addition to enhancing immunity, the researchers evaluated the long-term immune memory and the anti-metastasis ability of (M+H)@ZIF/HA by re-attacking mice with 4T1 cells and found that compared with any other treatment group, the number of metastatic nodules in (M+H)@ZIF/HA group was significantly reduced and then the central memory T cells (TCMs) in the spleen of each mouse were evaluated to reveal the anti-metastasis mechanism. This expression of (M+H)@ZIF/HA stimulated the T cell immune memory response to inhibit tumor metastasis. This nanoplatform shows a powerful transition from apoptosis, which reduces immune escape through HYD and improves the killing rate of cancer cells.[77] As an endogenous gas molecule, carbon monoxide (CO) can significantly accelerate mitochondrial respiration. These metabolic processes will lead to mitochondrial depletion and produce a large number of reactive oxygen species (ROS). More importantly, CO can affect the recruitment of innate immune cells and the differentiation of bone marrow cells and can also kill cancer cells without affecting drug resistance. In view of the above advantages, Xiao *et al.* first integrated the g-C_3N_4–Au (CA) nanocomposite into a photocatalyst, and then co-encapsulated CA into ZIF-8 to enhance CO_2 collection. Finally, an intelligent multifunctional CO nano generator CO_2–g-C_3N_4–Au@ZIF-8@F127(CCAZF) was made, which can trigger the conversion of carbon dioxide into CO to amplify ICD and activate immune cells. In this study, the combination of gas therapy and anti-PD-L1 not only effectively inhibited the growth of primary tumors, but also greatly prevented the proliferation and lung metastasis of distant tumors. Compared with traditional co-nano-drugs and immunotherapy, CCAZF has obvious advantages. This paper innovatively combines gas therapy with immunotherapy, which breaks the limitations of single therapy and provides a new way for CO gas therapy.[114]

Immunotherapy mainly uses the immune response mediated by T cells to stimulate the immune response of the body itself and ''actively'' remove tumor cells, thus achieving the purpose of anti-tumor treatment. In immunotherapy, Zn MOFs have multi-level applications, for example, as a drug carrier, delivering substances into cancer tissues, reducing the degradation rate of drugs releasing of Zn^{2+}, overloading the concentration of Zn^{2+} in cells, inducing the death of organelles, strengthening the expression of ICD, and so on. Obviously, Zn MOFs are indispensable substances to maximize the immune effect.

10.1 Application in combination therapy

Currently, although combination therapy has been applied in clinical cancer treatment, it still fails to solve the problem of coordinating the pharmacokinetics and site of action differences of each drug. Zinc-based MOFs may be a potential tool to address the aforementioned shortcomings of combination therapy as they can be loaded with multiple cargoes to synergise multiple therapies and provide targeted and sustained

delivery to target tumour cells. In this section, we will describe the role of Zn-MOFs in PDT/PTT/CDT, CT/PTT/PDT, CT/starvation therapy and CT/CDT in the hope of providing an idea for future therapeutic studies for cancer.

11. PDT/PTT/CDT

11.1 PDT/PTT

It is difficult to achieve a comprehensive anti-cancer effect with monotherapy. Oxygen-deficient conditions in the tumour microenvironment diminish the therapeutic effect of oxygen-dependent photodynamic therapy (PDT). It has been found that the integration of photothermal therapy (PTT) and PDT into the same nanoplatform can enhance the antitumour effect and solve the problem of hypoxic conditions in the tumour microenvironment, but there are problems of complex synthesis protocols and low efficacy. Therefore, optimising the experimental method and improving the efficiency of photothermal therapy are the focus of our research. In 2018, Yang *et al.* found that an increase in nanoparticle size enhanced the overall PDT/PTT anticancer effect by simply pyrolysing ZIF-8 to develop ZIF-8-derived carbon nanoparticles (ZCNs) that can act as both photothermophiles and photosensitisers. The researchers found that the phototherapeutic effect and photoacoustic (PA) imaging ability of ZCNs enhanced with increasing nanosize through *in vitro* anticancer experiments. The phototherapeutic effect of ZCNs improved accordingly as the carbonisation temperature increased. They demonstrated that ZCN-110 (900 °C) showed the best photothermal effect at a temperature of about 40 °C. Also the excellent photothermal effect promoted the increase in absorbance of ZCNs at 808 nm. *In vivo* experiments also confirmed that PA imaging-guided ZCNs can completely inhibit tumours.[78] Yet, ZCNs damaged nearly 10% of A549 cells (normal cells) within 24 hours. Thus, it is not enough to focus on the cancer cell killing effect, but we should also focus on the non-specific damage caused by the nanocarriers to the neighbouring hypoxic healthy tissues. In order to overcome the non-specific damage caused to neighbouring healthy tissues, while incorporating the pH responsiveness of ZIF-8. In 2020, Feng *et al.* designed multifunctional PDA-MB-CAT-ZIF-8 (PMCZ) nanoparticles.[23] PMCZ exhibited an effective controlled release of the photosensitiser methylene blue (MB) and catalase (CAT) triggered by the acidic pH of the tumour upon entry into cancer cells. MB was not prematurely released under normal physiological conditions and 60% of MB could be released after incubation at pH 5.0 for 25 h. Meanwhile, PMCZ produced more O_2 in acidic than in alkaline environments further confirming that CAT loaded onto ZIF-8 could catalyse the generation of O_2 from H_2O_2 to alleviate the hypoxic microenvironment of the tumour, which reduced the damage to the adjacent healthy tissues. Under 660 nm and 808 nm lasers, 50 mg mL^{-1} PMCZ could cause 60.32% of HeLa cells to apoptosis, and PMCZ+PDT+PTT could completely inhibit or even ablate the tumours in HeLa-loaded mice. They also verified that the ''off-target'' nanoparticles could be effectively removed from the mice, showing the good biocompatibility of PMCZ. In addition, nano-enzymes are artificial simulated enzymes that have both catalysing ability similar to catalase and good biocompatibility. Among other things, sodium iridium oxide (IrO_2) can also alleviate hypoxia in the tumour microenvironment, thereby expanding PDT efficacy.[115,116] In view of the above, in 2022, Deng *et al.* developed an IrO_2@ZIF-8/BSA-FA(Ce6) nanoplatform (*i.e.*, IZBFC) for achieving synergistic PTT–PDT targeting for cancer treatment.[79] As shown in Fig. 13B, IZBFC + 808 nm + 660 nm laser-treated MNNG/HOS cells exhibited the strongest fluorescence intensity, and more than 80% of MNNG/HOS cells were killed, which can be attributed to the combined effect of PTT and PDT. They also found that IZBFC NP-treated MNNG/HOS cell-carrying Balb/c mice could reach a temperature of ~58.1 °C after laser irradiation, significantly enhancing the photothermal effect. The process of *in vivo* tumour efficacy assessment in animal models is depicted in Fig. 13A. As shown in Fig. 13C, the PTT-PDT combination treatment group demonstrated good combined anti-tumour effects compared to both the control and laser-only groups, but also demonstrated that the damage to tumour cells by single doses of PTT and PDT was limited. Most importantly, all groups did not show any toxic reactions throughout the process. Unlike PMCZ, IZBFC-incorporated and FA-mediated targeting effects promoted the enrichment of NPs at the tumour site, resulting in a much higher anticancer effect.

11.2 PDT/CDT

The overexpression of glutathione and hydrogen peroxide in the tumour microenvironment severely hampers the development of chemodynamic therapy for cancer treatment. Happily, it has been found that combining CDT with PDT therapy *via* Zn-MOFs can solve the above problems, while enhancing the therapeutic effect of PDT. To simultaneously overcome hypoxia and overexpression of glutathione in the tumour microenvironment, Xie *et al.* designed a novel biodegradable O_2–Cu/ZIF-8@Ce6/ZIF-8F127 (OCZCF) therapeutic system.[80] The instability of copper-based materials *in vivo* limits the biological applications of these copper-based MOFs in CDT.[117] At the same time, the oxygen storage capacity of ZIF-8 is inferior to that of Cu-MOFs. Thus, Xie *et al.* cleverly doped Cu^{2+} into ZIF-8, which increased the O_2 storage by a factor of one. On this basis, Ce6 was further integrated into it, increasing the amount of ROS generated by Ce6 under 650 nm laser irradiation. The complex could degrade and release 90% Ce6 and 85% Cu^{2+} in the tumour microenvironment (pH = 6.5), and Cu^{2+} could oxidize GSH in tumours to reduce ROS consumption. More importantly, the by-product Cu^{+} reacted with H_2O_2 to produce cytotoxic –OH and Cu^{2+}, which enhanced PDT and CDT by depletion of GSH and supplementation of O_2. The researchers covered with a further layer of highly biocompatible polymer F127 to improve the biocompatibility of the complex. The results of the final *in vivo* and *ex vivo* experiments validated their ideas. However, Dong *et al.* concluded that it is not enough to improve the ability to consume GSH, but also to improve the wavelength emission, fluorescence brightness, ROS generation ability and photostability of photosensitisers. They focused on UiO-66 as a carrier for aggregation-induced emission-active luminophores (AIEgens) to

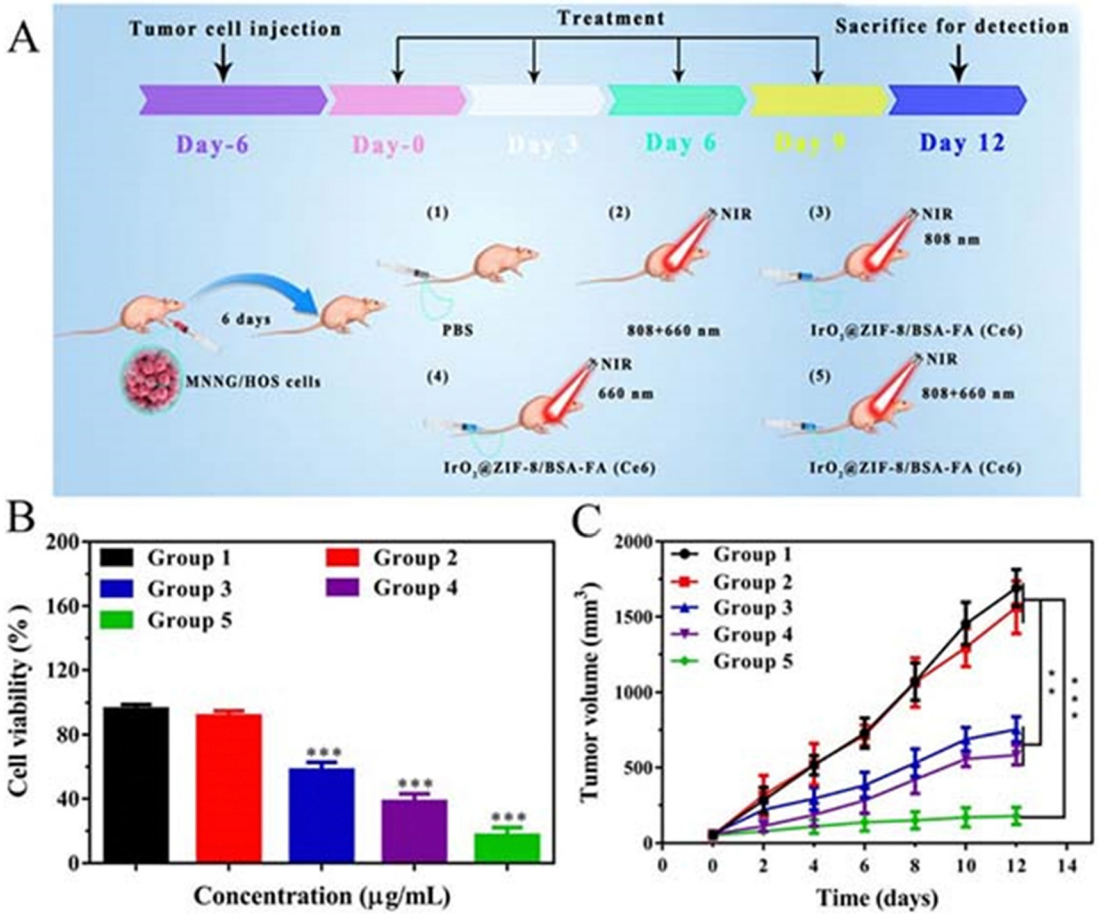

Fig. 13 (A) The combined effect of induced PTT/PDT on tumor ablation. (B) MNNg/HOS cells' viability after different treatments. (C) Curves of tumor volume growth for each tumor-bearing mice group. (1) control group, (2) 808 + 606 nm laser-irradiated group, (3) iZBFC + 808 nm laser irradiation, (4) iZBFC + 660 nm laser irradiated and (5) iZBF + 808 nm + 660 laser-irradiated group, respectively). Reproduced from ref. 79 with permission from Taylor and Francis Group, copyright 2023.

solve the problems of fluorescence quenching and ROS generation inhibition of conventional photosensitisers. Thus they designed the A-NUiO@DCDA@ZIF-Cu therapeutic system.[81] The researchers demonstrated that TME with low pH and overexpression of GSH and H_2O_2 could trigger the fluorescence "switch-on", particle self-assembly, GSH depletion and ROS generation of A-NUiO@DCDA@ZIF-Cu. When the concentration of A-NUiO@DCDA@ZIF-Cu was increased to 300 μg mL^{-1}, 86% of MCF-7 cells, 80% of HeLa cells, 78% of 4T1 cells, and 54% of normal cells (LO2) died in the *in vitro* CDT experiment. In contrast, in the *in vitro* PDT experiments (under white light irradiation) the cell survival rate of MCF-7 cells was 12% and about 35% of LO2 cells survived. In the *in vivo* experiments, "A-NUiO@DCDA@ZIF-Cu + white light" showed a strong anti-tumour effect compared to other groups, with tumour volume reduced to 50% of the initial value. In conclusion, A-NUiO@DCDA@ZIF-Cu achieved significant TME stimulation in response to tumour accumulation, fluorescence imaging capability and PDT/CDT combination therapeutic effect. However, its damage to normal cells should not be ignored and its clinical application needs further in-depth exploration. Similarly, Li *et al.* believe that it is also possible to start with ZIF-8 itself, which could enhance the overall effectiveness of cancer therapy by addressing the problem of ZIF-8's wide forbidden band and response to UV light. They focused on the fact that doping Mn and other transition metal ions into ZIF-8 could give ZIF-8 a very narrow band gap. They also discovered that rare-earth doped upconversion (UC) nanoparticles enable conversion of near-infrared to ultraviolet-visible light and that lanthanide-doped down-conversion (DC) nanomaterials are suitable for high-sensitivity *in vivo* optical imaging. Thus, they developed Fe/Mn bimetallic-doped ZIF-8-coated lanthanide-doped nanoparticles,[83] (LDNPs@Fe/Mn-ZIF-8, as in Fig. 14A). The double doping of Fe^{2+}/Mn^{2+} replaces the Zn position in the ZIF-8 framework, which enables the sp–d exchange interaction between the conduction band electrons consisting of the 4s4p orbitals of Zn and the d electrons of Fe/Mn ions to significantly reduce the forbidden bandwidth of the ZIF-8 photosensitizer from 5.1 eV to 1.7 eV, which ultimately generates more O_2 for PDT and extends the excitation threshold of ZIF-8 extended to the visible region (650 nm), allowing Fe/Mn-ZIF-8 to be efficiently excited by UC photons for photocatalytic-driven PDT. In addition, the combined effect of higher levels of H_2O_2, GSH, and H+ in the TME on the degradation of Fe/Mn- ZIF-8 led to a highest release of Fe/Mn/Zn ions from PBS (pH 5.6, GSH 10 mM) than that in in PBS (pH 5.6, GSH 10 mM)

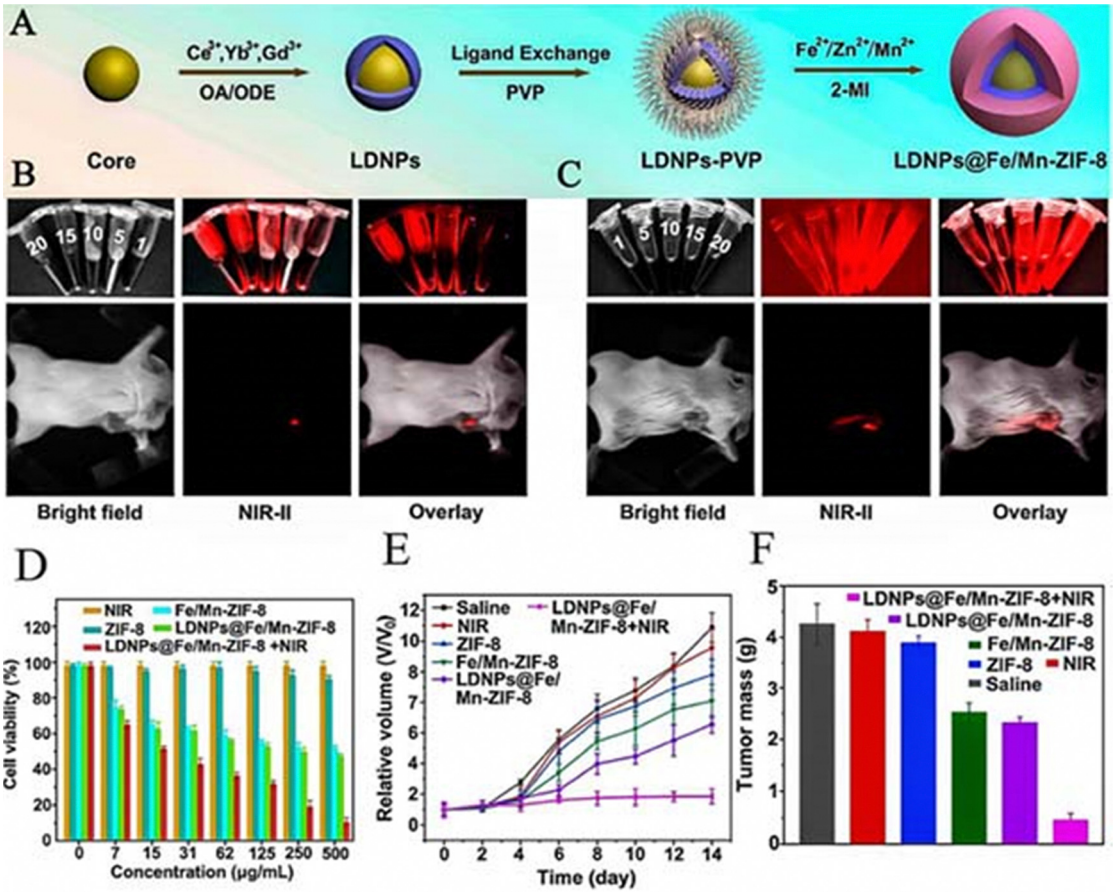

Fig. 14 (A) Synthesis procedure of LDNPs@Fe/Mn-ZIF-8 nanoplatform. (B) *In vitro* NIR II fluorescence imaging of LDNPs@Fe/different concentrations of Mn-ZIF-8 solution and *in vivo* NIR II fluorescence imaging of LDNPs@Fe/Mn-ZIF-8 solution (500 μg mL^{-1}). (C) *In vivo* NIR II fluorescence imaging of LDNPs@Fe/Mn ZIF-8 degraded in PBS (pH 5.6) for 12 h. (D) Viabilities of HeLa cells in groups of NIR, ZIF-8, Fe/Mn-ZIF-8, LDNPs@Fe/Mn-ZIF-8, and LDNPs@Fe/Mn-ZIF-8plusNIR(0.72 W cm^{-2}). (E) Changes in the relative tumor volume growth curves of different groups of tumor-bearing mice. (F) weights of tumors obtained from different groups of tumor-bearing mice. Reproduced from ref. 83 with permission from American Chemical Society, copyright 2023.

and in PBS (pH 5.6, GSH 0 mM), which in turn enhanced CDT rate than in PBS (pH 5.6, GSH 0 mM), which in turn enhanced CDT. What is more, the high-valent metal ions generated by the reaction could deplete the excess GSH in cancer cells through redox reaction to keep reactive oxygen species (ROS) from being scavenged by GSH and improve the anticancer effect of the final CDT/PDT. Meanwhile, the degradation of Fe/Mn-ZIF-8 endowed the nanosystems with tumour self-enhanced near-infrared (NIR) imaging, which provided accurate guidance and monitoring of the CDT/PDT process. As shown in Fig. 14B, the NIR-II fluorescence signals became more and more obvious when the concentration of LDNP@Fe/Mn-ZIF-8 increased. Compared with LDNPs@Fe/Mn-ZIF-8 in pH = 7.0 (Fig. 14B), the NIR-II signal degradation of LDNPS@Fe/Mn-ZIF-8 was stronger in pH = 5.6 at 12 h (Fig. 14C). To verify the anticancer effect of CDT/PDT; as in Fig. 14D, cell survival in the NIR group was measured at 93.4%, whereas the survival of HeLa cells treated with 500 μg mL^{-1} LDNPs@Fe/Mn-ZIF-8 + NIR decreased to 10.2%. As shown in Fig. 14E and F, tumour growth was significantly inhibited in the LDNPs@Fe/Mn-ZIF-8 plus NIR group. These showed that LDNPs@Fe/Mn-ZIF-8 could provide a new idea for the application of Zn-MOFs in tumour diagnosis and treatment.

Unlike the above, Jiang *et al.* focused on PDT/CDT synergistic therapy by addressing the problems of hypoxia and hydrogen peroxide (H_2O_2) overexpression in the tumour microenvironment. They constructed a Co/ZIF-8/ICG/Pt (CZIP) nanoplatform to synergise CDT with PDT for cancer treatment by taking advantage of the properties using which Co^+ can catalyse the H_2O_2 reaction to produce cytotoxic hydroxyl radicals (−OH).[82] At pH = 7.4, 23.7% Co^{2+} was released cumulatively from CZIP within 1 h, while at pH = 5.0, more than 80% of Co^{2+} was released. The researchers further confirmed the good potential of CZIP as a CDT agent by the methyl blue experiment. Dissolved oxygen instrumentation and single-line-state oxygen sensor green (SOSG) were also used to confirm the good potential of CZIP as a PDT agent, which is closely related to the catalytic generation of O_2 and ICG from H_2O_2 by the modified Pt NPs. Both *in vivo* and *ex vivo* results demonstrated the good anti-tumour properties and high biosafety of CZIP.

11.3 PTT/CDT

In addition, Zn-MOFs can combine CDT with PTT to address GSH and hydrogen peroxide overexpression in the tumour microenvironment, thereby effectively killing tumour cells. In

2020, Ana Peking *et al.* designed Cu^{2+}-doped zeolite imidazolium salt backbone-coated polydopamine nanoparticles (PDA@Cu/ZIF-8 nanoparticles) for glutathione-triggered and photothermally enhanced sequential catalytic treatment of breast cancer using a simple chemical coordination approach.[84] These PDA@Cu/ZIF-8 nanoparticles not only reduced the intracellular levels of reduced glutathione, but also increased the production of cytotoxic reactive oxygen species *via* a copper ion-mediated Fenton-like reaction. Based on the significant NIR absorption of PDA, the temperature of PDA@Cu/ZIF-8 aqueous solution exhibited a significant concentration-dependent effect, reaching up to 70 °C within 10 min. And it also showed a significant photothermal conversion effect and photostability. GSH expression was significantly reduced in MCF-7 cells treated with PDA@Cu/ZIF-8 together with NIR irradiation compared with PDA@Cu/ZIF-8 alone. When irradiated with an 808 nm laser, PDA@Cu/ZIF-8 inhibited tumour growth by 84.6%, while tumour tissues suffered the most severe cell shrinkage and nuclear condensation. *In vivo* experiments showed that PDA@Cu/ZIF-8 nanoparticles had no significant side effects on normal tissues and exhibited good biocompatibility. In addition, Zou *et al.* focused on the fact that the combination of reactive oxygen species-associated CDT and PTT based on transition-metal materials could improve the treatment of tumour-related diseases.[118] Thus, they developed a zeolite imidazolium salt backbone-8-capped Cu_2–XSe composite nanotherapeutic platform (ICG@Cu_2–XSe-ZIF-8) (Fig. 15A).[85] The rational design of ZIF-8-wrapped Cu_2–XSe reduced the damage to normal cells. After treating normal mammary cells (Hs578) and pro-osteoblasts (BMMs) with 1 μg mL^{-1} ICG@Cu_2–XSe-ZIF-8, the viability of these two cells was nearly 100%, which demonstrated that the nanosystem was safe for the two types of normal cells. ICG@Cu_2–XSe-ZIF-8 could release a large amount of Cu^+ and Cu^{2+} to trigger the ROS overproduction, exhibiting high anti-tumour activity of CDT. Meanwhile, in combination with ICG, Cu_2–XSe could also be used as a photothermal agent and ICG@Cu_2–XSe-ZIF-8 + laser could induce apoptosis in about 63.94% of breast cancer cells and they found that PTT-induced hyperthermia could further enhance the CDT effect in tumours. As expected, ICG@Cu_2–XSe-ZIF-8 exhibited a synergistic PTT/CDT effect in *ex vivo* breast cancer experiments (Fig. 15B and C). Most surprisingly, selenium in Cu_2–XSe could also be involved in the formation of selenoproteins, which inhibited osteoclastogenesis and suppressed cancerous bone metastasis by initiating an antioxidant mechanism affecting the expression of selenoenzymes in osteoblasts in contact with tumour cells. In addition, ICG@Cu_2–XSe-ZIF-8 NPs inhibited tumour growth and reduced MDA-m b-231 cell-induced osteolytic bone loss by inhibiting IL-8 cytokine secretion in a mouse breast cancer bone metastasis model (Fig. 15D). ICG@Cu_2–XSe-ZIF-8 facilitates the use of Zn-MOFs for the treatment of bone metastasis and osteolysis in breast cancer, a promising therapeutic strategy.

11.4 PDT/PTT/CDT

Despite the popularity of the combination of photodynamic therapy (PDT) and chemodynamic therapy (CDT) in tumour therapy, hypoxia and glutathione (GSH) overproduction in the tumour microenvironment (TME) limit their further application. Thus, the introduction of another therapeutic synergy strategy to treat tumours is necessary. The radical initiator 2,2′-azobis[2-(2-imidazolin-2-yl)propane]-dihydrochloride (AIPH) has become a research hotspot for the rapid generation of toxic alkyl radicals (R) upon thermal stimulation and without the need for oxygen molecules.[119,120] In 2021, Li *et al.* invented a novel nanogenerator AIPH/PDA@CuS/ZIF-8 (*i.e.*, APCZ).[24] The excellent pH responsiveness allows the outer ZIF-8 layer to rapidly degrade the self-reinforcing Fenton-like nano-agent CuS, which releases CDT, at the TME. APCZ also shows good glutathione and H_2O_2 consumption capabilities. In addition, APCZ exhibited excellent photothermal properties, generating high temperatures under 1064 nm laser excitation that not only allowed NIR-II-excited PTT but also synergised with CDT. APCZ also triggered the decomposition of AIPH into toxic alkyl (R) for oxygen-independent PDT. The APCZ+laser group demonstrated a more significant PDT/PTT/CDT therapeutic outcome, with almost no 4T1 cells surviving at the same concentration as well as complete eradication of the tumour after two weeks of treatment. More importantly, GSH depletion by PDA/CuS reduced the antioxidant activity of the tumours and further enhanced R-/OH-based treatment. In addition, they found that APCZ as a contrast agent improved PA imaging. The discovery of APCZ provides a new idea for the application of Zn-MOFs for effective diagnosis and treatment of deep and hypoxic tumours.

The synergy of PDT/PTT/CDT can also be achieved by irradiating a single MOF derivative with a single wavelength laser. Sui *et al.* were inspired by the fact that Zn–N–C nanomaterials synthesized by pyrolysis of ZIF-8 (Zn) can be used as photosensitisers for tumour photodynamic therapy.[121] Thus, they envisioned the synthesis of FeNC@PAA nanoparticles for CDT/PDT/PTT synergistic treatment of tumours by simple pyrolysis of the precursor ZIF-8 (Fe/Zn), followed by PAA modification.[86] FeNC@PAA is capable of triggering an iron-based Fenton-like reaction with H_2O_2 to produce OH and O_2 for chemodynamic therapy (CDT) and O_2 precipitation. In the CDT effect assay, FeNC above 150 mg L^{-1} concentration was observed to cause more than 50% reduction in cell viability. Meanwhile, the porphyrin-like metal centres in FeNC@PAA nanoparticles can be used as photosensitizers for photodynamic therapy (PDT) of tumours and the photosensitizers can be enhanced by the O_2 generated in the above CDT. Thus, in *in vitro* experiments, 200 mg L^{-1} FeNC@PAA caused damage to more than 60% of 4T1 cells under 808 nm laser irradiation at 4 °C. In addition, FeNC@PAA nanoparticles were found to have high absorption in the near infrared region (NIR). In photothermal therapy (PTT), the photothermal conversion efficiency of FeNC@PAA nanoparticles at 808 nm was 29.15%. A significant reduction in 4T1 cell viability by 95% was observed with FeNC@PAA (FeNC concentration, 50 mg L^{-1}). In an *in vivo* synergy assay in CDT/PDT/PTT, under 808 nm laser irradiation, the temperature at the tumour site of FeNC@PAA-injected 4T1-homozygous Balb/c mice increased to 48 °C within 4 min of irradiation and further to 53 °C at 10 min of irradiation. In contrast, no significant change in tumour site temperature was

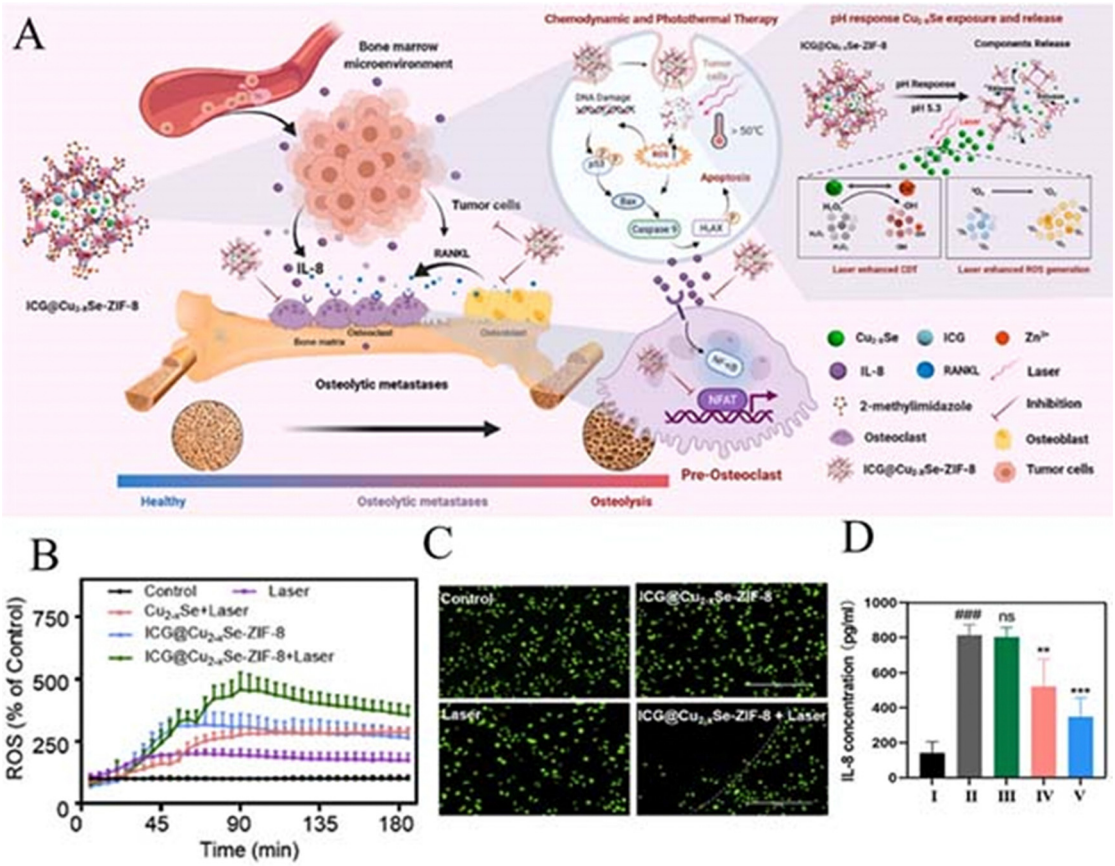

Fig. 15 (A) Schematic diagram of *in vivo* chemotherapy (CDT) photothermal therapy (PTT) for treating bone metastases and osteolysis in malignant breast cancer. (B) Excessive induced ROS levels by various nanosystems (12.5 μg mL^{-1}) in MDA-MB-231 cells under laser irradiation (808 nm) at 1 W cm^{-2} for 5 min. (C) Fluorescence images of MDA-MB-231 cells stained with Calcein AM (green) after the thermal therapy with ICG@Cu_2–XSe-ZIF-8 (12.5 μg mL^{-1}) and a laser (808 nm) at 1 W cm^{-2} for 1 min. (D) IL-8 levels in mouse serum were measured by ELISA. Black for healthy, grey for saline, green for saline+laser, pink for ICG@Cu_2–XSe-ZIF-8, and blue for ICG@Cu_2–XSe-ZIF-8 + laser. Reproduced from ref. 85 with permission from Elsevier, copyright 2023.

observed in PBS-injected mice. Moreover, after 21 days of treatment, the tumour weight of FeNC@PAA mice was about 53 times smaller than that of the PBS group. What is more, all the results of *ex vivo* and *in vivo* toxicity tests clearly revealed the low biotoxicity of FeNC@PAA nanoparticles *in vivo*.

Overall, Zn-MOFs play an essential role both in the two combination therapies and in the three combination therapies of CDT/PDT/PTT. Zn-MOFs can effectively encapsulate photothermal agents, photosensitisers, metal-based nano-enzymes, *etc.*, due to their porous structure and some Zn-MOFs become photothermal agents and photosensitisers by altering their synthesis. Once these Zn-MOF complexes enter cancer cells, tumour acidic low pH stimulation and photothermal properties promote degradation of the Zn-MOF shells, releasing the photothermite, photosensitizer, nano-enzyme, *etc.* in a controlled manner. In the combination of PDT and PTT, the NIR-induced local thermal effect not only helps in promoting the release of the loaded drug, but also amplifies the ROS-induced cell killing ability. In addition, the loaded nanoenzymes catalyse endogenous H_2O_2 for *in situ* tumour oxygenation and enhancement of PDT. In the synergy of PDT and CDT, the main targets of the Zn-MOF complexes are to overcome tumour hypoxia, reduce GSH levels and induce more hydroxyl radicals (−OH) from Fenton/Fenton-like reactions within the tumour. The nanoenzymes released by Zn-MOFs (such as platinum nanoparticles) can catalyse the production of oxygen from H_2O_2 at the tumour site and be used to overcome tumour hypoxia. Strategies to reduce GSH levels are critical for effective PDT/CDT, and Zn-MOFs release metal ions such as Cu^{2+}. Cu^{2+} can deplete intracellular GSH to form Cu^{+}. The reduced GSH can enhance PDT, and the generated Cu^{+} can react with H_2O_2 in TME to induce efficient Fenton-like reactions to generate −OH and O_2 required for CDT, achieving synergistic treatment of PDT and CDT. In the synergy of PTT and CDT, the metal ions released from Zn-MOFs catalyse the local H_2O_2 through a series of chemical reactions to generate highly toxic −OH by highly efficient Fenton-like reactions, realizing CDT. Meanwhile, the released photothermolysis can generate a large amount of heat under laser irradiation, which not only amplifies the generation of ROS, but also amplifies the consumption of GSH, further expanding the intracellular oxidative stress, realizing synergistic photothermal-chemical kinetic therapy. We believe that the combination of three therapeutic modalities can provide

more possibilities for patients, such as reducing the treatment time, compared to the combination of two therapeutic modalities. At the same time, we think we can pay more attention to other useful aspects of Zn-MOFs itself, such as focusing on the role of other Zn-MOFs (*e.g.* ZIF-90) in cancer therapy. Also, we need to pay attention to whether the amount of metal ions doped in will affect the human body, as well as exploring more and simpler modifications of Zn-MOFs for enhanced cancer therapy.

12. CT/PTT/PDT

12.1 CT/PTT

Among the various types of combination therapy, chemo-photothermal (CT/PTT) therapy has attracted attention due to the following advantages: (1) thermotherapy can make the tumours more sensitive to chemotherapeutic drugs; (2) high heat can make the cells absorb more drug carriers; and (3) the photothermal effect can trigger local drug release;[122] (4) chemotherapeutic agents can reduce heat shock reactions caused by high temperatures;[123] (5) reduce the dose of chemotherapeutic drugs. However the therapeutic efficacy and application potential of CT/PTT largely depend on the controllability and biocompatibility of the functional nanoplatforms. Thus therapeutic Zn-MOFs exhibit biocompatibility, targetability and responsiveness to the tumour microenvironment showing advantages in achieving precise CT/PTT treatment of cancer. In 2019, Feng *et al.* prepared a stimulus-responsive Zn-MOF for targeted drug delivery, pH-stimulated release and synergistic enhancement of chemo/photothermal therapy for tumour therapy using PDA as a functional interface.[124] The strategy developed in this approach certainly leads to ideas for the combined chemo-photothermal therapy performed next by ZIF-8. Currently, gold nanorods (AuNRs) with tunable optical properties have been shown to be ideal components for the construction of core–shell nanoplatforms for tumour therapy.[125] However, the low drug-carrying capacity of nanoshell materials, toxic synthesis methods, and high tendency to cause aggregation have limited their application to chemical photothermal therapy. Inspired by the unique properties of ZIF-8 mentioned above, Huang *et al.* envisioned a way to overcome the shortcomings of shell materials by combining AuNR and ZIF-8 shell materials. They synthesised Au@ZIF-8/DOX by a simple method. The remarkable surface area and guest-matched pore size of ZIF-8 enabled Au@ZIF-8/DOX to achieve a DOX loading efficiency of $\sim$37%. Au@ZIF-8 exhibited a high photothermal effect under near-infrared radiation. At a high concentration of 200 ppm and irradiated by an 808 nm laser, the temperature of Au@ZIF-8 suspension rapidly increased from 23 °C to 54 °C within 5 min. The heat generated not only killed the cancer cells directly, but also synergistically promoted the release of DOX from the pores of the shell. Under NIR radiation, the release rate of DOX under acidic conditions (68%) was 33% faster than that at pH 7.4 and exhibited better cell viability inhibition properties than free DOX. Finally, the results of *in vivo* loaded nude mouse experiments also demonstrated the superior tumour elimination obtained by Au@ZIF-8/DOX+NIR compared to the other groups (DOX, DOX+NIR, and Au@ZIF-8/DOX), even without any significant adverse effects.[87]

Nowadays more and more photothermal agents are being used for PTT of tumours, such as the gold nanorods (AuNRs) mentioned above.[87] However, their cost may be relatively high and too much retention in the human body may cause other side effects. Fe_3O_4 nanoparticles have the advantages of low cost, a simple preparation process, and good biocompatibility compared with precious metal nanoparticles and carbon nanomaterials. Therefore, in 2022, Liu *et al.* synthesised FA-BSA/ZIF-8CNPs-CPT using Fe_3O_4 nanoparticles as a photothermite by a simple method. FA-BSA/ZIF-8CNPs-CPT entering the tumour cells generated local high temperatures and exhibited high photothermal stability under NIR laser irradiation (808 nm). In addition, ZIF-8 degraded and released camptothecin (CPT) in pH 5.3, and the release rate of CPT could reach 76.3% after 15 h. The results showed that ZIF-8 CNPs were highly stable to NIR laser irradiation (808 nm) and showed high photothermal stability. *In vivo* experiments confirmed that when FA-BSA/ZIF-8cnps-CPT was co-cultured with tumour cells and irradiated with an 808 nm laser for 20 min, the cell survival rate was only 12.6%, showing good photothermal/chemotherapeutic synergy. In addition, AuNCs conferred fluorescence properties to the composites. As shown in Fig. 16A, the cytoplasmic fraction emits strong fluorescence that does not overlap with the blue fluorescence of the nuclear fraction. This indicates that the nanoparticles are mainly distributed in the cytoplasm after entering the tumour cells. As shown in Fig. 16B, the cells exhibited strong fluorescence, but the fluorescence intensity decreased significantly with the increase of incubation time. This may be due to the degradation of ZIF-8 in the acidic microenvironment of the entering tumour cells leading to the escape of AuNCs from ZIF-8, resulting in a sharp decrease in fluorescence intensity. This shows that it not only fulfilled the purpose of drug tracking and tumour imaging, but also guided photothermal therapy.[88] It is conceivable that such composites with drug-releasing, photothermal conversion and fluorescence properties would be promising candidates for anti-tumour therapy.

The synergy of chemo-photothermal therapy can also be achieved by designing novel biosensors for MOFs. In 2021, Wang *et al.* reported a multifunctional polydopamine (PDA)-coated metal–organic framework (MOF) biosensor (PDA/DOX/ZIF-8).[89] They found that the decomposition of the PDA/DOX/ZIF-8 structure in an acidic environment could release a large amount of free Zn^{2+} as a trigger for AIE signal amplification, which enabled the ultrasensitive detection of miRNA-122 and the accurate differentiation of cells with different expression levels of miRNA-122 (*i.e.*, it could find fluorescence signals from AuNCs only in MCF-7 cells, but not in HepG2 cells where no fluorescence signal was found) with an ultra-low detection limit of 12.5 pM (at 498 nm). The composite also released 83.0% DOX, and the DOX release was significantly higher than that of the control group, achieving a good chemotherapeutic effect (with an 808 nm laser). In addition, the modification by the PDA coating resulted in better biocompatibility and photothermal effect of the biosensor. Only PDA-coated MOFs showed

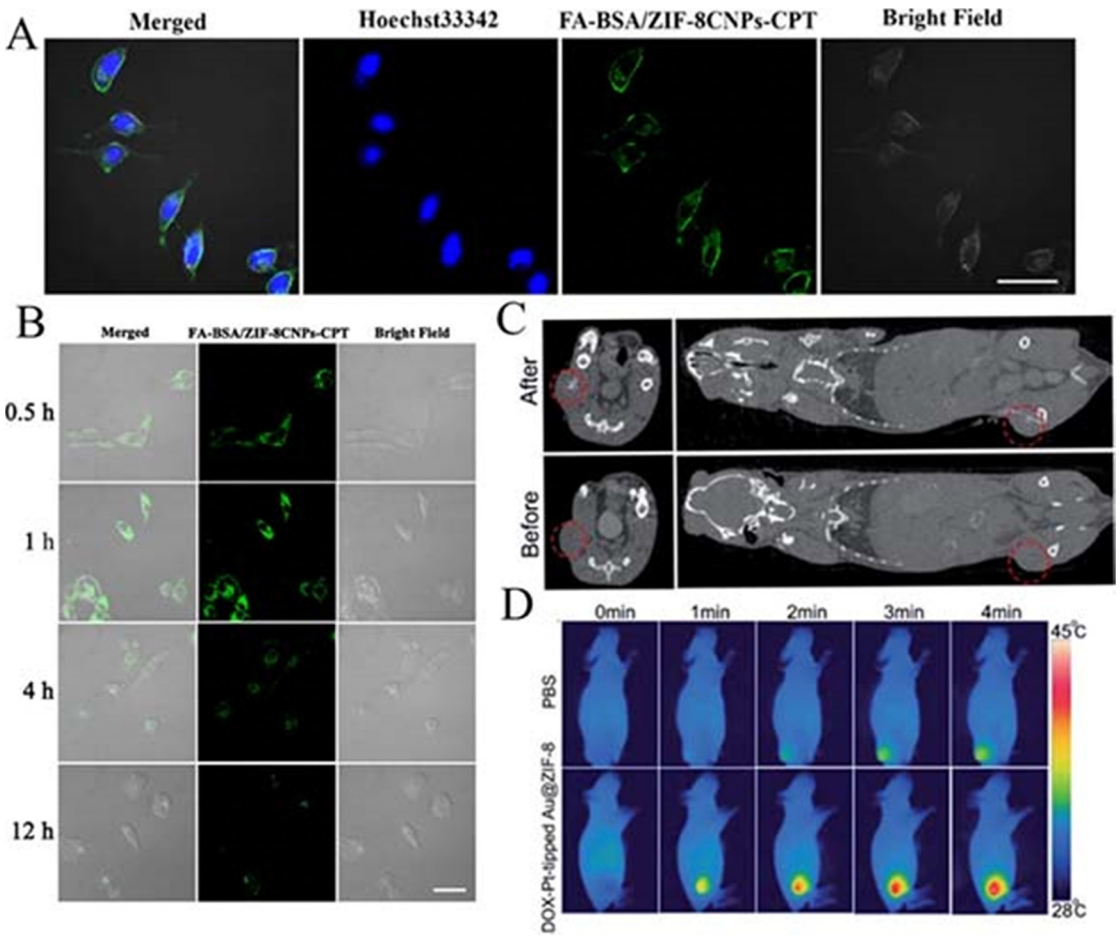

Fig. 16 (A) Confocal scanning microscopy (CLSM) images of HepG2 cells after co-culture with FA-BSA/ZIF-8CNPs (nuclei were then stained with Hoechst3342); (B) HepG2 cells were co-cultured with FA-BSA/ZIF-8CNPs for different times. Reproduced from ref. 88 with permission from American Chemical Society, copyright 2023. (C) Left: CT images of mouse tumor tissue Au@ZIF-8 (10 mg kg^{-1}) before and after intra-tumor injection of DOX Pt tips. Right panel: 3D reconstructed CT images of tumor-bearing mice Au@ZIF-8 (10 mg kg^{-1}) before and after intra-tumor injection of DOX Pt tip. (D) *In vivo* thermography of 4T1 tumor-bearing mice Au@ZIF-8 after PBS or DOX-Pt injection with various irradiation times under NIR laser irradiation at 1064 nm (1 W cm^{-2}). Reproduced from ref. 92 with permission from Royal Society of Chemistry, copyright 2023.

rapid warming after 10 min of 808 nm laser irradiation and they exhibited good photothermal stability and photothermal conversion efficiency. Compared with the therapeutic effects of other control groups, the PDA/DOX/ZIF-8+NIR treatment group was more capable of inducing apoptosis in tumour cells. The development of Zn-MOF sensors for synergistic chemo-photothermal treatments will undoubtedly provide a new combined multifunctional solution for the precise diagnosis and treatment of cancer.

12.2 CT/PDT

Combined CT/PDT offers multiple advantages in improving the efficiency of cancer treatment compared to monotherapy. Photodynamic therapy (PDT) is an oxygen-dependent therapeutic strategy and the response to the PDT process consumes large amounts of oxygen, exacerbating hypoxia in the tumour microenvironment. Yet, it can significantly promote the induction of cytotoxicity by tirazamine (TPZ) prodrugs to improve therapeutic efficiency. Thus Chao *et al.* envisioned the combination of PDT and TPZ-activated chemotherapy to improve the efficacy of cancer combination therapy. They found that inhibition of catalase (CAT), which is highly expressed in cancer cells, could alleviate hypoxia, while potentially converting toxic substances produced by TPZ into non-toxic substances. Thus, they designed to introduce zinc sulphide to produce H_2S *in situ* in cancer cells to regulate CAT expression. They prepared ZnS@ZIF-8 nanoparticles (ZSZ) at room temperature. During the coating process, ICG molecules were bound to the ZIF-8 shell to form ZnS@ZIF-8/ICG (ZSZI) and subsequently TPZ was grafted onto the surface of ZSZI to form ZnS@ZIF-8/ICG/TPZ (ZSZIT). Under 808 nm NIR radiation, ZSZIT-delivered ICG, effectively induced ROS, while depleting *in situ* oxygen. At the same time, zinc sulphide degraded in acidic TME to produce H_2S gas. H_2S not only exhibited some cytotoxicity, but also down-regulated the expression of CAT to further amplify the cancer cell-killing effect of TPZ.[90] The combined therapeutic effect of ROS, H_2S and hypoxia-activated TPZ achieved by ZSZIT nanocomposites resulted in significant tumour suppression in both *in vitro* and *in vivo* experiments. As shown in Fig. 17A and B, the injected ZSZIT+NIR irradiation group showed significantly enhanced

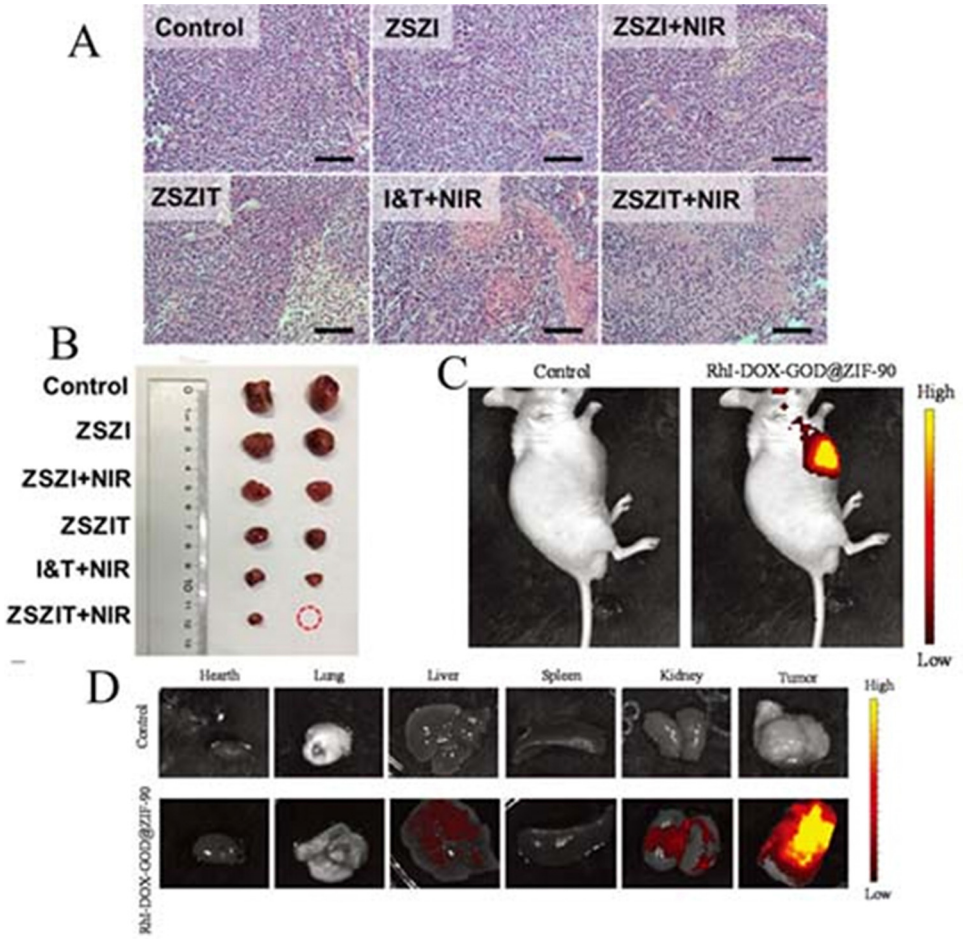

Fig. 17 (A) Slices of H&E stained tumor from different groups (scale bar: 50 μm). (B) Typical tumor photographs from other mouse groups on day 14. Reproduced from ref. 90 with permission from Ivyspring International Publisher, copyright 2023. (C) RhI-DOX-GOD@ZIF-90 NP fluorescence imaging in tumor-bearing mice. Control: the untreated mice. RhI-DOX@ZIF-90 group: the RhI-DOX@ZIF-90 treated mice. RhI-DOX-GOD@ZIF-90 group: the treated RhI-DOX-GOD@ZIF-90 mice. (D) The major organs' fluorescence imaging: heart, lungs, liver, spleen, and kidneys and tumors. Reproduced from ref. 26 with permission from Royal Society of Chemistry, copyright 2023.

tumour suppression, with tumours in group 6 having the lowest tumour weight and the smallest size and better suppression than those in mice directly injected with free ICG and TPZ (group 5), further suggesting that H_2S-sensitised PDT/chemotherapy nanoplatforms are effective in suppressing tumours in the *in vivo* setting. In addition, combined imaging-guided nanoscale therapeutic platforms can improve diagnostic and therapeutic accuracy, and multimodal imaging has been a focus of attention. Combining fluorescence imaging (FL) and magnetic resonance imaging (MRI) can address the shortcomings of limited fluorescence imaging penetration and low sensitivity of MRI images to improve imaging accuracy. In 2019, Qin *et al.* inspired by the excellent fluorescence and magnetic resonance properties of Si–Gd nanoparticles, rationally designed FZIF-8/DOX-PD-FA for CT/PDT co-imaging studies.[22] PEG-FA modified on the surface of the composite and the pH-responsive polymer HOOC-PDMAEMA-SH were solubilised in the tumour microacidic environment, which resulted in a precisely controlled pH-sensitive DOX release by FFZIF-8/DOX-PD-FA with almost no release of DOX at pH 7.4 and up to 57% release of DOX at pH 6.0 (tumour microenvironment). As observed by confocal microscopy imaging, MCF-7 cells (with high expression of FRs) showed stronger fluorescence intensity (*i.e.*, were able to phagocytose more FZIF-8/DOX-PD-FA) than A549 cells (with low expression of FRs). FZIF-8/DOX-PD-FA efficiently avoids the side effects caused by the leakage of the drug under physiological environmental conditions and exhibits excellent drug delivery capability. As expected, the FZIF-8/DOX-PD-FA nanocomposites successfully aggregated at the tumour site and showed fluorescence and magnetic resonance dual-peak imaging, confirming the targeting of the nanocomposites. In addition, fluorescence and magnetic resonance bimodal imaging-guided pH-responsive drug release chemo-/photodynamic combination therapy was validated in *in vivo* loaded mouse experiments, and the tumour volume of loaded mice was reduced to 0.22 times of the original one. The design of FZIF-8/DOX-PD-FA not only broadens the range of biological applications of Zn-MOF nanoparticles, but also opens up new possibilities.

However, the NDDS of ZIF-8 may also suffer from premature drug release and lack of most chemically active groups, limiting the development of Zn-MOFs in cancer. Thus, Shen *et al.*

envisioned the development of a robust trifunctional polymer coating strategy using ZIF-90. Specifically, ZIF-90 was used to encapsulate DOX during particle synthesis to form DOX@ZIF. Subsequently, acetylated dextran (SAD) shells modified with spermine were coated to form a new DOX-loaded NDDSDOX@-ZIF-D. At the same time, hydrophobic IR780 was then encapsulated *in situ* into the SAD shells (*i.e.* IR780/DOX@ZIF-D). The experimental results showed that the loading capacity of IR780 was 10 times higher than that of the conventional ZIF-90, which greatly increased the drug loading capacity. The ZIF-90 equipped with the SAD shell significantly improved the pH responsiveness of ZIF-90 and effectively prevented the premature release of the drug. In addition, this drug-loaded ZIF-D nanocomplex was then further chemically coupled with hyaluronic acid (HA) through amidation, which enabled precise drug delivery by targeting the drug to cancer cells overexpressing the HA receptor (CD44). In an *in vivo* evaluation IR780/DOX@ZIF-DH+laser therapy showed the highest tumour inhibition rate (86.5%) and the best biocompatibility among all treatment groups.[91] This simple strategy could offer fresh hope for overcoming the limitations of MOF-only-based DDS in cancer treatment and greatly expand the flexibility of Zn-MOFs for biomedical applications.

12.3 CT/PTT/PDT

CT/PTT/PDT has achieved excellent results in many refractory cases. The combination of CT/PTT/PDT can enhance the effect of photodynamic therapy in eliminating local tumours and inhibiting distant metastasis. The local high temperature generated by PTT inactivates the active substances in cancer cells, clearing the way for CT and PDT. However, off-target drug effects and treatment tolerance remain challenges in treating cancer. Meanwhile the development of effective synergistic therapies by combining different therapeutic modalities by individual vectors in combination therapy is very important for cancer treatment. In 2021, Chen *et al.* designed a biocompatible and multifunctional nanomaterial DOX-Pt-tipped Au@ZIF-8. Pt adsorbed on the ends of Au NRs to form anisotropic bimetallic nanostructures. Under single near-infrared II (1064 nm) laser irradiation, it can undergo more electron–hole spatial separation than a single metal, showing excellent photothermal and photodynamic properties. In addition, it can continuously generate oxygen to overcome tumour hypoxia. Meanwhile, platinum NRs are contrast agents for *ex vivo* imaging. Platinum NRs can be applied to computed tomography and photothermal imaging. As shown in Fig. 16C, it exhibits excellent CT signals in tumour tissue. The researchers recorded their photothermal properties within 4T1 tumour mice by infrared photothermal imaging. As shown in Fig. 16D, its temperature increased to 44.8 °C in 4 minutes compared to the others, indicating that its photothermal imaging is very effective. The ZIF-8 shell also encapsulates Pt-tipped NRs and DOX. With or without 1064 nm laser irradiation, their release of therapeutic agents under mild stimulation in the acidic environment of the tumour (pH = 5.2) was higher than in a solution at pH 7.4, significantly improving the efficacy of chemotherapy. DOX-Pt-tipped Au@ZIF-8 demonstrated significant anticancer effects with synergistic chemo-phototherapy under 1064 nm laser irradiation, with cell survival reduced to 21.5% and complete destruction of cultured cancer cells. DOX-Pt-tipped Au@ZIF-8 achieved complete inhibition of tumour growth both *in vivo* and *ex vivo* with minimal side-effects, which implies that the great potential of the Zn-MOF in tumour therapy.[92] However, scientists are not satisfied with exploiting this combination and they expect to work on developing additional materials to address the shortcomings in cancer combination therapy on the basis of combination therapy. In order to maximise the CT/PTT/PDT effect of Zn-MOF-based nanoplatforms, there is also a need to increase their ability to target specific tumours and evade immune clearance to address the off-target effects of drugs. Sun *et al.* focused on the fact that decorating nanoplatforms with homologous cancer cell membranes could evade a certain degree of immune clearance and target tumours. They prepared hollow porphyrin metal–organic framework (H-PMOF) nanoparticles with mesoporous spherical shells by a self-sacrificial ZIF-8 nanoparticle template strategy. This H-PMOF not only has inherent photodynamic activity, but also can form high drug loading. They can encapsulate adriamycin (DOX) and indocyanine green (ICG) to obtain (DOX and ICG)@H-PMOF NPs (referred to as DIHP). Finally, bionic combinatorial nanoplatforms (*i.e.*, DIHPm) were obtained by coating murine breast cancer (4T1) cell membranes on the surface of DIHP NPs.[93] The experimental results showed that DIHPm measured much stronger fluorescence in homozygous 4T1 cells than other cell lines, exhibiting excellent homologous tumour targeting and immune escape. Interestingly, DIHPm showed pH-controlled and NIR laser-triggered DOX release. DOX release was significantly increased to 65% after pH 5.0 + 808 nm laser irradiation. DIHPm killed tumour cells at very low doses in *in vitro* experiments and exhibited excellent efficiency in inhibiting tumour growth and metastasis *in vivo*, demonstrating good imaging-guided synergistic photodynamic/photothermal/chemotherapeutic anti-cancer activity with negligible systemic toxicity. The development of this high-performance H-PMOF nanoplatform provides a new idea to address the off-target effects of drugs.

However, CT/PTT/PDT also faces the challenge of treatment tolerance. In overcoming the constraints of anticancer drugs subject to multidrug resistance, Ouyang *et al.* made a new discovery. They designed a HA-SS@CuS@ZIF-8@TPZ& TB macn (HSCZTT) nanosystem, which breaks through the detoxification barrier of tirazamine (TPZ) delivery and combines the enhanced efficacy of HCT/PTT/AIE-PSs-PDT. HSCZTT targets cancer cells *via* hyaluronic acid (HA), plus the large number of disulfide bonds carried by HA on HSCZTT depletes glutathione (GSH) overexpressed in cancer cells, reducing the clearance of reactive oxygen species (ROS) and TPZ by GSH. They showed experimentally that HSCZTT dissociates to release CuS NPs, TPZ and TBMACN (consisting of a triphenylamine fragment, a thiophene fragment and two cyano units) in a slightly acidic tumour environment. Under 808 nm laser irradiation, AIE-disodium alginate enhanced the efficacy of photodynamic therapy and PTT and PDT effectively promoted cancer cell death. HSCZTT uses local high temperature to inactivate bioactive substances and aggravate the hypoxic microenvironment of

the tumour. The aggravated hypoxic environment further activates the toxicity of the chemotherapeutic drug TPZ (TPZ can exhibit great toxicity in the tumour's hypoxic microenvironment to kill cancer cells, but low toxicity in oxygen-rich normal tissues) and synergises with cellular mechanisms inactivated by local high temperatures, the anti-cancer effects of both enhance each other to further kill cancer cells.[95] The introduction of HSCZTT is expected to promote the development and advancement of anticancer drugs by solving the problem of multidrug resistance and greatly reducing the side effects of treatment. It also suggests that we can achieve the therapeutic effect of tumours not only by supplementing what they lack, but also by other means. However, HSCZTT studies are not comprehensive enough and lack further exploration *in vivo*, *etc.* In overcoming the difficulties of drug transporter protein-mediated chemotherapy resistance and heat shock proteins (HSPs)-mediated phototherapy resistance, Lu *et al.* had new insights. They designed a chondroitin sulfate (CS)-functionalized ZIF-8 nanoplatform (CS/ZIF-8@A780/DOX NPs) loaded with the photosensitizer iodide (IR 780)-spliced ATO (A780) and the chemotherapeutic agent Adriamycin (DOX). In the platform CS/ZIF-8@A780/DOX NPs, CS was used to achieve CD44-mediated cancer-specific targeting. The pH-responsive delivery behaviour of ZIF-8 endowed the nanoparticles with satisfactory release characteristics in acidic tumour microenvironments. At pH 7.4 and pH 5.5, the release of Zn^{2+} in CS/NPs was ~17.1% and 97.42%, respectively. Atovaquone (ATO) and Zn^{2+} released in the acidic tumour microenvironment can lead to a decrease in intracellular ATP levels by interfering with mitochondrial electron transport and glycolytic processes. Low levels of ATP inhibit the activities of P-glycoprotein (P-gp) and heat shock protein 70 (HSP70), respectively, thereby overcoming P-gp-mediated chemoresistance and HSP70-induced phototherapy tolerance. Reduced ATP content and expression of glucose transporter protein 1 (GLUT1), HSP70 and P-gp in tumour tissues under *in vivo* CS/NP tumour treatment showed a mechanism for overcoming treatment resistance *in vivo*. In *in vitro* experiments, CS/NP treatment reversed P-gp-induced resistance and enhanced DOX retention in MCF-7Adr cells. It also promoted the efficiency of PTT and PDT in inducing apoptosis in tumour cells and showed significant anti-tumour capacity in breast cancer cells.[94] The research done by CS/ZIF-8@A780/DOX NPs is also more comprehensive and provides a rational and effective strategy to combat drug resistance in cancer treatment.

As can be seen from the above examples, Zn-MOFs play a great role in CT, PDT and PTT synergistic therapy. In the synergy of CT and PTT, the photothermite released by Zn-MOFs generates a large amount of heat under the irradiation of near-infrared light, which can make the tumours more sensitive to the chemotherapeutic drugs and at the same time, the high heat can cause the cancer cells to absorb more drug carriers. And the released chemotherapeutic drugs can alleviate the heat shock reaction caused by high temperature and achieve CT/PTT synergistic treatment. In the synergy of CT and PDT, the more prominent strategy is to turn a disadvantage into an advantage through hypoxia-activated chemotherapy (HCT). The photosensitiser released by Zn-MOFs initiates PDT, and the continuous consumption of oxygen in PDT exacerbates the hypoxic environment of the tumour, which further activates the chemotherapeutic agents (*e.g.*, TPZ) released in the acidic microenvironment of the tumour to achieve the death of tumour cells. In the synergy of CT, PDT and PTT, photothermal agents and photosensitisers released by Zn-MOFs can effectively promote cancer cell death by using local high temperature to inactivate active substances in cancer cells, generating aggressive ROS to attack organelles and aggravate the hypoxic microenvironment of the tumour. And the hypoxia activates the toxicity of the chemotherapeutic drugs and synergises with a large number of cellular mechanisms inactivated by the local high temperature to further kill the cancer cells. From simply acting as a carrier to combine these three therapies to becoming a multifunctional CT/PDT/PTT cancer diagnostic carrier, Zn-MOFs show great potential. They are not only expected to overcome the tolerance of cancer treatment but also improve the accuracy of cancer diagnosis and treatment in conjunction with imaging-guided nanoscale therapeutic platforms.

13. CT/starvation therapy

Glucose oxidase (GOx)-based starvation therapy is a therapy that depletes glucose and produces toxic H_2O_2/gluconic acid in the presence of oxygen, which produces H_2O_2 that not only significantly enhances oxidative stress in tumours, but also converts into OH radicals to kill cancer cells. However, due to the diversity and heterogeneity of tumours, a single starvation therapy alone is not sufficient to overcome tumours. Thus, scientists have developed many synergistic strategies of chemotherapy/starvation therapy. However, most of them suffer from non-degradability of nanocarriers *in vivo* and off-target effects of drugs. Therefore, there is an urgent need for a degradable smart nanocarrier to solve this problem. In 2020, Guo *et al.* prepared a biomimetic, degradable smart nanoreactor consisting of glucose oxidase (GOx)-encapsulated ZIF-8 nanoparticles and MBN-modified Ag NPs (ZIF-8@GOx-AgNPs@MBN) for catalytic cascade-enhanced chemo-starvation synergistic therapy of tumours. The nanoreactor can sense glucose and GOx activities during treatment *via* surface-enhanced Raman scattering (SERS) feedback for immediate feedback of treatment progress. After the nanoreactor enters the cancer cells, the GOx in the nanoreactor can be gradually released according to the changes in the intercellular microenvironment of the cancer cells, triggering an *in vivo* catalytic cascade reaction to degrade ZIF-8, consume glucose, etch AgNPs@MBN, and generate toxic H_2O_2, Zn^{2+}, and Ag^+ ions for chemo-starvation synergistic treatment of cancer cells.[96] The nanoreactor (0.08 mg mL^{-1}) inhibited cervical cancer cells (HeLa) *in vitro* by about 95% after 6 h, while the nanoreactor (200 μg mL^{-1}) inhibited tumours in mice *in vivo* by 96.8% after 14 days of treatment. More importantly, this biodegradable nanoreactor could be effectively cleared from cervical cancer tumours in mice (it had been completely degraded after 14 days of treatment and almost no SERS signals

were observed in cancer tissues), solving the common problem of long-term accumulation of most nanocarriers or nanomedicines *in vivo* and endowing them with many *in vivo* application potentials. In 2022, inspired by the fact that ATP can be used as a cancer marker, Chen *et al.* constructed biocompatible RhI-DOX-GOD@ZIF-90 nanoparticles with good biocompatibility for near-infrared (NIR) fluorescence and synergistic chemo-starvation therapy. The composite particles were synthesised by encapsulating RhI (a NIR fluorescent dye), DOX (an anti-cancer drug) and GOD (glucose oxidase) in ZIF-90.[26] RhI-DOX-GOD@ZIF-90 nanoparticles can be activated and destroyed at high concentrations of ATP. It is well known that ATP levels in cancer cells are abnormally higher than in normal cells. Thus the composites were able to achieve controlled drug delivery by sensing changes in ATP levels in normal and tumour cells in mice through the prominent NIR emission of RhI. RhI-DOX-GOD@ZIF-90 took full advantage of the NIR emission, as shown in Fig. 17C, where the RhI-DOX-GOD@ZIF-90 group showed strong fluorescence in hormonal mice. As in Fig. 17D, RhI-DOX-GOD@ZIF-90 fluoresces much stronger in tumours than in major organs and it should be noted that there is also partial retention in the liver and kidneys.

However, it cannot be denied that the composite nanoparticles have *in vivo* ATP imaging and good drug delivery controllability in loaded mice. However, insufficiently targeted nanomedicine carriers will affect the effectiveness of cancer therapy. Some specific recognition molecules are overexpressed on different types of tumour cells leading to the inability of nanomedicine materials to accurately attack the targeted tumour cells. Thus, it is important to construct a targeted nanoparticle with higher accuracy. Targeting tumours with biomimetic nanoparticles camouflaged with cancer cell membranes caught the attention of Shao *et al.* In 2021, they meticulously constructed a biomimetic nanoreactor camouflaged with cancer cell membranes for synergistic cancer starvation therapy and cascade amplification of hypoxia-activated chemotherapy. Specifically, GOx and the hypoxia-activated prodrug barnosanoid (AQ4N) were loaded onto ZIF-8 nanocarriers to generate a nanoreactor AQ4N/GOx@ZIF-8 by accelerating the formation of nucleation preclusters around the proteins *via* protein/polyvinylpyrrolidone (PVP)/cysteine (Cys) self-assembly and permeabilisation methods. The surface of the nanoreactor was then camouflaged with natural tumour cell membranes to form a bionic nanoreactor AQ4N/GOx@ZIF-8@CM.[97] This nanoreactor possesses homotypic targeting, immune escape and prolonged blood circulation properties that greatly improve the precision of targeting tumours. When AQ4N/GOx@ZIF-8@CM targeting accumulates at the tumour site, the acidic environment triggers ZIF-8 degradation to release encapsulated GOx and AQ4N. GOx cuts off the energy supply to tumour cells for starvation therapy. In addition, GOx consumed oxygen, while exacerbating the hypoxic environment in tumour cells further activated the cytotoxicity of AQ4N to chemotherapy. The results of *in vitro* and *in vivo* experiments also confirmed that the combined application group of starvation therapy and cascade amplification of hypoxia-activated chemotherapy inhibited tumour growth most significantly. Both tumour growth and metastasis are highly dependent on tumour angiogenesis and thus tumour angiogenesis is considered an attractive anti-cancer target. The C-type lectin desialylate glycoprotein receptor (ASGPR) can be abundantly expressed on mammalian hepatocyte membranes.[126] And ASGPR is considered an ideal target for hepatic delivery due to its ability to bind and internalise galactose- or GalNAc-terminated glycoproteins.[127,128] Inspired by this, in 2022, Hu *et al.* encapsulated ZIF-8 with the anti-angiogenic drug sorafenib (Sor) and glucose oxidase (GOx), and further prepared SG@GR-ZIF-8 by stacking with *n*-acetylgalactosamine from π–π (GalNAc) and rhodamine B (RhB). Hepatocellular carcinoma cells highly express on their surface the asialoglycoprotein (ASGPR), SG@GR-ZIF-8 could enter hepatocellular carcinoma cells *via* specific lectin-ligand and specifically transfer Sor and GOx into hepatocellular carcinoma cells. Then Sor directly reduces tumour angiogenesis by decreasing VEGF expression. GOx rapidly consumes glucose and disrupts cancer cell metabolism, thus accelerating cell death. At the same time, the overproduction of ROS by Sor and GOx caused lethal oxidative stress in cancer cells, inducing apoptosis with cell loss. Sor and GOx exerted reciprocal therapeutic effects and inhibited the growth and metastasis of liver tumour cells, thus achieving targeted dual-mode therapy with chemotherapy and starvation therapy for hepatocellular carcinoma (HCC).[98] In an *in vitro* assay, SG@GR-ZIF-8 showed significant anti-metastatic HCC activity against hepatocellular carcinoma stem cell-like cell line C5WN1 cells. In a mouse model carrying c5wn 1-tumours subcutaneously, SG@GR-ZIF-8 inhibited tumour growth by 89%. In addition, the SG@GR-ZIF-8 treatment group significantly inhibited HCC growth and lung metastasis in *in situ* C5WN1-loaded mice. This strategy of targeting energy supply combined with first-line therapy could bring new hope for Zn-MOF applications in the future treatment of tumours.

14. CT/CDT

In the combination of chemotherapy and CDT, chemodynamic therapy (CDT) destroys cancer cells by converting endogenous H_2O_2 into lethal –OH, while the generated ROS induce mitochondrial dysfunction and down-regulation of P-gp protein expression to sensitise cancer cells to chemotherapeutic agents to enhance chemotherapeutic effects. Some chemotherapeutic agents (*e.g.*, cisplatin) can promote intracellular H_2O_2 production and H_2O_2 can be converted into more OH to address the limitation of insufficient H_2O_2 levels in CDT treatment. However, overexpression of glutathione (GSH) at the tumour site accelerates drug efflux and scavenging of ROS, greatly reducing the efficacy of chemotherapy and CDT. Given the extensive research on nanoenzymes in oxidising GSH, Dong *et al.* found that the combination of gold nanoclusters and copper ions could not only oxidise GSH but also solve the problem of low signal-to-noise ratio of conventional fluorescence imaging. They fabricated copper ion-doped ZIF-8 (denoted as ACD, A: gold nanoclusters, C: copper ions, and D: DOX) containing gold nano-enzymes and doxorubicin hydrochloride (DOX), and used it for fluorescence imaging-assisted studies of chemotherapy and CDT synergistic treatment of tumours. The

Cu^{2+}-doped ZIF-8 shell layer responded to the gradual degradation of the acidic TME by enhancing the release of Cu^{2+}, DOX and gold nanoclusters. Acidic pH and overexpressed GSH in the tumour microenvironment activate the quenching of fluorescence of ACD to achieve local fluorescence imaging of the tumour. Cu^{2+} consumes GSH through a redox reaction and the resulting Cu^{+} converts *in vivo* H_2O_2 to OH for tumour CDT. DOX, on the other hand, enhances chemotherapy by depleting glutathione and hydroxyl radicals to inhibit the drug flux and increase the sensitivity of the drug. At the same time, DOX also enhances CDT by increasing H_2O_2 levels *in vivo*. In addition, fluorescent Au NCs not only convert H_2O_2 to OH but also act as oxidases to deplete GSH, thereby amplifying the effects of chemotherapy and CDT.[25] The ACD showed optimal experimental results in both *ex vivo* and *in vivo* experiments in this work, providing an innovative strategy for Zn-MOF applications in synergistic CDT and chemotherapy. However, the pH-responsive drug release of ACD was only 41.97% at pH = 5 for 36 h, which still needs to be improved.

H_2O_2 concentrations in TME (100 μM to 1 mM) are not sufficient to induce cell death, which greatly limits the efficiency of chemokinetic therapy. Increasing the H_2O_2 concentration can be achieved by introducing sufficient H_2O_2 or H_2O_2-generating agents, but is very challenging. In 2021, Cui *et al.* designed a new platform, which was used to meet the H_2O_2 requirement for chemokinetics by introducing calcium peroxide (CaO_2) into copper-doped ZIF-8 (Cu/ZIF-8). It provides H_2O_2 for chemokinetic treatment in TME via a Cu-like-Fenton reaction. They reported a CaO_2/DOX@Cu/ZIF-8@HA (CDZH) drug delivery system. The CDZH was mainly obtained by preparing biodegradable copper-doped ZIF-8 (Cu/ZIF-8) shell-encapsulated CaO_2 nanoparticles loaded with the chemotherapeutic drug adriamycin to confer chemotherapeutic and imaging capabilities and coated with hyaluronic acid shells to provide targeting functionality and to improve the circulatory stability, which ultimately resulted in CDZH.[99] CDZH nanostructures target tumours in an acidic tumour microenvironment, where ZIF-8 is degraded to release adriamycin, Cu^{2+} and CaO_2. Adriamycin affects chemotherapy and bioimaging, and CaO_2 is used for chemokinetic therapy. The researchers confirmed the excellent ability of CDZH nanostructures to synergise chemokinetic therapy to inhibit tumour growth through cytotoxicity assays and tumour suppression experiments in tumour-bearing mice. In the same year, Li *et al.* also increased the amount of H_2O_2 in the tumour site to satisfy the need for H_2O_2 for chemokinetics by introducing glucose oxidase (GOD) on the basis of Cu-doped ZIF-8 (Cu/ZIF-8) as well as outsourcing MnO_2 nanostructures. Specifically, they constructed Cu/ZIF-8@DSF-GOD@MnO_2 (*i.e.*, CZ-DG-M) by loading disulfiram (DSF) into Cu/ZIF-8, followed by encapsulating GOD by physical adsorption, and finally encapsulating MnO_2 nanoshells on the surface. After systemic injection, the outer layer of MnO_2 consumed GSH and alleviated tumour hypoxia in TME, while the released paramagnetic Mn^{2+} initiated T1-MRI for *in vivo* tracking imaging and the oxygen produced in the reaction could enhance the catalytic efficiency of GOD for burst H_2O_2. The inner layer of Cu/ZIF-8@DSF can be rapidly biodegraded in the acidic environment co-caused by gluconic acid and tumour tissue to release Cu^{2+} and DSF, which are chelated *in situ* and converted into toxic DTC–Cu complexes (CuETs) to kill a large number of tumour cells. The researchers confirmed the high efficiency of DSF synergistic CDT by *in vitro* cellular analysis and *in vivo* experiments in a U14 subcutaneous hormonal mouse model, demonstrating the potential for an effective synergistic strategy of chemodynamic and chemotherapeutic treatments.[100]

These three works demonstrate that the combination of chemotherapy and CDT based on Zn-MOFs can enhance the anti-cancer efficacy and also provide an advanced paradigm for designing nanocatalysts with dual-enhanced CDT by trying to increase the amount of H_2O_2 or depleting GSH in Cu-doped ZIF-8. In addition, this approach can also prompt us to think about introducing another treatment to enhance the therapeutic effect of chemotherapy/CDT or exploring more multifunctional Zn-MOF applications for cancer therapy.

15. Conclusions

In conclusion, the modification strategy of Zn-based MOF nanomaterials represents a way to improve the limitations of various cancer therapies. Zn-MOFs play an important role both in monotherapy and in combination therapy. Meanwhile, many studies have shown that synergistic therapies are more effective than monotherapies. Synergistic therapies can not only overcome the limitations of various therapies, but also achieve the therapeutic effect of "1 + 1 > 2". Despite the rapid progress of Zn-MOFs in recent years, they still have limitations. Therefore, there is an urgent need to further investigate the potential of Zn-MOFs.

Firstly, zinc, as one of the endogenous elements, and its associated zinc-based MOFs have low toxicity and can be adapted to the needs of drug delivery systems. However, it still causes more serious cellular damage at high doses, and the cytotoxicity of Zn-MOFs is also related to the type of organic linkers. There are many studies cited in this review that have used components from endogenous sources to improve the biocompatibility of Zn-MOFs, such as haemoglobin,[66] *etc.*; but most of these studies lacked a specific exploration of the degree of cytotoxicity and the varying degrees of damage that the accumulated amount of materials can cause to normal cells. It is crucial to understand that nanomaterials must be metabolised quickly and safely once they enter the body. Otherwise, they can cause unwanted problems (*e.g.*, organ damage). Secondly, although some of the structures investigated suggest that Zn-MOFs are harmless to normal cells and mice, the sample size of mice studied *in vivo* is not large enough and the physiology of nude mice is different from that of humans; so the results obtained do not fully reflect the therapeutic efficacy of the nanoreactors and their safety for humans. Therefore, it is necessary to further consider better methods to study the long-term safety of Zn-MOFs in humans. Finally, the mechanism by which most Zn-MOFs are non-toxic and biodegradable in biomedical applications is still unclear; the introduction of heavy metal ions may harm human health, and some introduced biomaterials are poorly biodegradable in the human body, with

too many unknown effects on the human body due to long-term accumulation.

Although they still have some obstacles, we believe that their applications can be diversified by refining their synthesis methods and that the combined therapeutic effects of Zn-MOFs can be improved by introducing various monitorable tumour targets, biodegradable materials, and various bioenzymes that have minimal impact on the normal physiological environment. In addition, we need to increase our efforts to study the basic relationship between Zn-MOFs and linkers to identify future gaps in cancer research.[16] At the same time, we can develop more new biocompatible materials in combination with Zn-MOFs and find more effective ways to explore the transport, absorption, metabolism, and excretion pathways of Zn-MOFs in the human body. We can also study the life cycle of Zn-MOFs in tissues in greater depth to maximise the effectiveness of cancer treatment. It is evident that Zn-MOFs have great potential for clinical cancer therapy. We believe that it will not be long before Zn-MOFs and their complexes can be successfully applied in clinical treatment for the benefit of mankind.

Conflicts of interest

There are no conflicts to declare.

References

1 K. Bukowski, M. Kciuk and R. Kontek, *Int. J. Mol. Sci.*, 2020, **21**, 3233.
2 S. Wilhelm, A. J. Tavares, Q. Dai, S. Ohta, J. Audet, H. F. Dvorak and W. C. W. Chan, *Nat. Rev. Mater.*, 2016, **1**, 16014.
3 (*a*) Y.-M. Jo, Y. K. Jo, J.-H. Lee, H. W. Jang, I.-S. Hwang and D. J. Yoo, *Adv. Mater.*, 2022, 2206842; (*b*) X. Y. Dong, D. Q. C. Li, Y. Y. Li, H. Sakiyama, M. Muddassir, Y. Pan and D. Srivastava, *CrystEngComm*, 2022, **24**, 7157–7165; (*c*) G. J. Tan, S. Y. Wang, J. L. Yu, J. H. Chen, D. H. Liao, M. Liu, A. Nezamzadeh-Ejhieh, Y. Pan and J. Q. Liu, *Food. Chem.*, 2024, **430**, 136934; (*d*) X. R. Guo, L. Y. Zhou, X. Z. Liu, G. J. Tan, F. Yuan, A. Nezamzadeh-Ejhieh, N. Qi, J. Q. Liu and Y. Q. Peng, *Colloids Surf., B*, 2023, **229**, 113455; (*e*) D. W. Luo, J. F. Huang, Y. H. Jian, A. Singh, A. Kumar, J. Q. Liu, Y. Pan and Q. Ouyang, *J. Mater. Chem. B*, 2023, **11**, 6802–6822.
4 (*a*) Q. Wang and D. Astruc, *Chem. Rev.*, 2020, **120**, 1438–1511; (*b*) Q. Ding, Y. Pan, Y. Luo, M. Zhou, Y. Guan, B. Li, M. Trivedi, A. Kumar and J. Liu, *ACS Omega*, 2019, **4**, 10775–10783; (*c*) Y. Pan, Q. Ding, H. Xu, C. Shi, A. Singh, A. Kumar and J. Liu, *CrystEngComm*, 2019, **21**, 4578–4585; (*d*) J.-Q. Liu, Z.-D. Luo, Y. Pan, A. K. Singh, M. Trivedi and A. Kumar, *Coord. Chem. Rev.*, 2020, **406**, 213145; (*e*) J.-C. Jin, J. Wu, W.-C. Liu, A.-Q. Ma, J.-Q. Liu, A. Singh and A. Kumar, *New J. Chem.*, 2018, **42**, 2767–2775; (*f*) J.-C. Jin, J. Wu, Y.-X. He, B.-H. Li, J.-Q. Liu, R. Prasad, A. Kumar and S. R. Batten, *CrystEngComm*, 2017, **19**, 6464–6472; (*g*) J. J. Zhao, Z. Y. Dang, M. Muddassir, S. Raza, A. G. Zhong, X. X. Wang and J. C. Jin, *Molecules*, 2023, **28**, 6848.
5 (*a*) X. Y. Zhang, W. J. Zhang, R. F. Xiang, L. Lan, X. Y. Dong, H. Sakiyma and M. Muddassir, *Polyhedron*, 2023, **244**, 116625; (*b*) T. R. Qin, X. Y. Zhang, D. C. Li, X. Y. Dong, N. Qi, Y. J. Shang, H. Sakiyamad, M. Afzal and A. Alarifi, *J. Mol. Struct.*, 2023, **1291**, 136074; (*c*) J. Wang, B.-H. Li, L. Lu, J.-Q. Liu, H. Sakiyama and A. Kumar, *Dalton Trans.*, 2017, **46**, 15178–15180.
6 (*a*) D. Y. Ma, Z. Li, J. X. Zhu, Y. P. Zhou, L. L. Chen, X. F. Mai, M. L. Liufu, Y. B. Wu and Y. W. Li, *J. Mater. Chem. A*, 2000, **8**, 11933–11937; (*b*) J. Liu, G. Liu, C. Gu, W. Liu, J. Xu, B. Li and W. Wang, *J. Mater. Chem. A*, 2016, **4**, 11630–11634; (*c*) J.-Q. Liu, G.-P. Li, W.-C. Liu, Q.-L. Li, B.-H. Li, R. W. Gable, L. Hou and S. R. Batten, *ChemPlusChem*, 2016, **81**, 1299–1304.
7 (*a*) Z. Wang, Q. Sun, B. Liu, Y. Kuang, A. Gulzar, F. He, S. Gai, P. Yang and J. Lin, *Coord. Chem. Rev.*, 2021, **439**, 213945; (*b*) Y. Zeng, G. Xu, X. Kong, G. Ye, J. Guo, C. Lu, A. Nezamzadeh-Ejhieh, M. Shahnawaz Khan, J. Liu and Y. Peng, *Int. J. Pharm.*, 2022, 122228; (*c*) H. Li, K. Wang, Y. Sun, C. T. Lollar, J. Li and H.-C. Zhou, *Mater. Today*, 2018, **21**, 108–121; (*d*) L. Qin, F. Liang, Y. Li, J. Wu, M. Wu, S. Xie, M. Luo and D. Ma, *Inorganics*, 2002, **10**, 202; (*e*) W. B. Hu, S. Y. Wang, C. J. Jiang, M. B. Zheng, Z. Bai, D. Srivastava, A. Kumar and J. Q. Liu, *Dyes Pigm.*, 2003, **219**, 111596; (*f*) Y. Y. Zhong, Z. X. Peng, Y. Q. Peng, B. Li, Y. Pan, Q. Ouyang, H. Sakiyama, M. Muddassir and J. Q. Liu, *J. Mater. Chem. B*, 2023, **11**, 6335–6345; (*g*) X. L. Chen, M. M. Li, M. Z. Lin, C. Y. Lu, A. Kumar, Y. Pan, J. Q. Liu and Y. Q. Peng, *J. Mater. Chem. B*, 2023, **11**, 5693–5714.
8 S. Bahrani, S. A. Hashemi, S. M. Mousavi and R. Azhdari, *Drug Metab. Rev.*, 2019, **51**, 356–377.
9 H. Li, M. Eddaoudi, T. L. Groy and O. M. Yaghi, *J. Am. Chem. Soc.*, 1998, **120**, 8571–8572.
10 N. L. Rosi, J. Kim, M. Eddaoudi, B. Chen, M. O'Keeffe and O. M. Yaghi, *J. Am. Chem. Soc.*, 2005, **127**, 1504–1518.
11 H. Li, M. Eddaoudi, M. O'Keeffe and O. M. Yaghi, *Nature*, 1999, **402**, 276–279.
12 K. S. Park, Z. Ni, A. P. Cote′, J. Y. Choi, R. Huang, F. J. Uribe-Romo, H. K. Chae, M. O'Keeffe and O. M. Yaghi, *Proc. Natl. Acad. Sci. U. S. A.*, 2006, **103**, 10186–10191.
13 C. Gao, H. Zheng, L. Xing, M. Shu and S. Che, *Chem. Mater.*, 2010, **22**, 5437–5444.
14 Y. Wang, L. Shi, D. Ma, S. Xu, W. Wu, L. Xu, M. Panahandeh-Fard, X. Zhu, B. Wang and B. Liu, *ACS Nano*, 2020, **14**, 13056–13068.
15 W. Liu, Y. Pan, W. I. Xiao, H. Xu, D. Liu, F. Ren, X. Peng and J. Liu, *RSC Med. Chem.*, 2019, **10**, 2038.
16 R. S. Ali, H. Meng and Z. Li, *Molecules*, 2022, **27**, 100.
17 Q. Sun, H. Bi, Z. Wang, C. Li, C. Wang, J. Xu, D. Yang, F. He, S. Gai and P. Yang, *ACS Appl. Mater. Interfaces*, 2019, **11**, 36347–36358.

18 J. Zhang, M. He, C. Nie, M. He, Q. Pan, C. Liu, Y. Hu, T. Chen and X. Chu, *Chem. Sci.*, 2020, **11**, 7092–7101.
19 M. Yuan, S. Liang, Y. Zhou, X. Xiao, B. Liu, C. Yang, P. Ma, Z. Cheng and J. Lin, *Nano Lett.*, 2021, **21**, 6042–6050.
20 W. Zhang, Y. Zhou, Y. Fan, R. Cao, Y. Xu, Z. Weng, J. Ye, C. He, Y. Zhu and X. Wang, *Adv. Mater.*, 2022, **34**, e2105738.
21 S. Wu, K. Zhang, Y. Liang, Y. Wei, J. An, Y. Wang, J. Yang, H. Zhang, Z. Zhang, J. Liu and J. Shi, *Adv. Sci.*, 2022, **9**, e2103534.
22 Y.-T. Qin, H. Peng, X.-W. He, W.-Y. Li and Y. Zhang, *ACS Appl. Mater. Interfaces*, 2019, **11**, 34268–34281.
23 J. Feng, W. Yu, Z. Xua and F. Wang, *Chem. Sci.*, 2020, **11**, 1649–1656.
24 L. Zhang, Y. Fan, Z. Yang, M. Yang and C. Y. Wong, *J. Nanobiotechnol.*, 2021, **19**, 1–16.
25 D.-H. Zhao, C.-Q. Li, X.-L. Hou, X.-T. Xie, B. Zhang, G.-Y. Wu, F. Jin, Y.-D. Zhao and B. Liu, *ACS Appl. Mater. Interfaces*, 2021, **13**, 55780–55789.
26 X.-X. Chen, M.-J. Hou, W.-X. Wang, M. Tan, Z.-K. Tan, G.-J. Mao, B. Yang, Y. Li and C.-Y. Li, *Nanoscale*, 2022, **14**, 3808.
27 S. Abd Al-Jabbar, V. Atiroğlu, R. M. Hameed, G. Guney Eskiler, A. Atiroğlu, A. D. Ozkan and M. Özacar, *Bioorg. Chem.*, 2022, **118**, 105467.
28 K. Dong, Y. Zhang, L. Zhang, Z. Wang, J. Ren and X. Qu, *Talanta*, 2019, **194**, 703–708.
29 S. Javanbakht, A. Hemmati, H. Namazi and A. Heydari, *Int. J. Biol. Macromol.*, 2020, **155**, 876–882.
30 W. Pan, B. Cui, K. Wang, M. Shi, F. Lu, N. Li and B. Tang, *Theranostics*, 2021, **11**, 7869–7878.
31 X. Liu, Z. Liu, K. Dong, S. Wu, Y. Sang, T. Cui, Y. Zhou, J. Ren and X. Qu, *Biomaterials*, 2020, **258**, 120263.
32 P. Y. Siboro, V. K. T. Nguyen, Y. B. Miao, A. K. Sharma, F. L. Mi, H. L. Chen, K. H. Chen, Y. T. Yu, Y. Chang and H. W. Sung, *ACS Nano*, 2022, **16**, 12403–12414.
33 H. Zhang, Q. Zhang, Z. Guo, K. Liang, C. Boyer, J. Liu, Z. Zheng, R. Amal, S. L. J. Yun and Z. Gu, *J. Colloid Interface Sci.*, 2022, **615**, 517–526.
34 Z. Jiang, Y. Li, Z. Wei, B. Yuan, Y. Wang, O. U. Akakuru, Y. Li, J. Li and A. Wu, *Bioact. Mater.*, 2020, **6**, 740–748.
35 X. Zhong, Y. Zhang, L. Tan, T. Zheng, Y. Hou, X. Hong, G. Du, X. Chen, Y. Zhang and X. Sun, *J. Controlled Release*, 2019, **300**, 81–92.
36 P. Jiang, Y. Hu and G. Li, *Talanta*, 2019, **200**, 212–217.
37 Z. Jiang, Y. Wang, L. Sun, B. Yuan, Y. Tian, L. Xiang, Y. Li, Y. Li, J. Li and A. Wu, *Biomaterials*, 2019, **197**, 41–50.
38 L. Lu, G. Liu, C. Lin, K. Li, T. He, J. Zhang, Z. Luo and K. Cai, *Adv. Healthcare Mater.*, 2021, **10**, e2100978.
39 L. F. Hang, T. Zhang, H. Wen, L. B. Liang, W. M. Li, X. F. Ma and G. H. Jiang, *Nano Res.*, 2021, **14**, 660–666.
40 D. Xu, Y. You, F. Zeng, Y. Wang, C. Liang, H. Feng and X. Ma, *ACS Appl. Mater. Interfaces*, 2018, **10**, 15517–15523.
41 P. Yang, Y. Chang, J. Zhang, F. Gao, X. Liu, Q. Wei, X. Ma and Y. Guo, *J. Colloid Interface Sci.*, 2023, **629**, 522–533.
42 Y. Wang, L. Shi, D. Ma, S. Xu, W. Wu, L. Xu, M. Panahandeh-Fard, X. Zhu, B. Wang and B. Liu, *ACS Nano*, 2020, **14**, 13056–13068.
43 K. Tan, Q. Zhang, Q. Wang, X. Gong, S. Yu, R. Li, X. Liu and F. Wang, *Small*, 2022, **18**, e2204858.
44 X. Zheng, L. Zhang, M. Ju, L. Liu, C. Ma, Y. Huang, B. Wang, W. Ding, X. Luan and B. Shen, *ACS Appl. Mater. Interfaces*, 2022, **14**, 46262–46272.
45 C. Yang, K. Wang, S. Tian, L. Mo and W. Lin, *Anal. Chim. Acta*, 2023, **1239**, 340689.
46 P. Zhang, A. Fischer, Y. Ouyang, J. Wang, Y. S. Sohn, R. Nechushtai, E. Pikarsky, C. Fan and I. Willner, *Chem. Sci.*, 2021, **12**, 14473–14483.
47 Y. Liu, C. S. Gong, L. Lin, Z. Zhou, Y. Liu, Z. Yang, Z. Shen, G. Yu, Z. Wang, S. Wang, Y. Ma, W. Fan, L. He, G. Niu, Y. Dai and X. Chen, *Theranostics*, 2019, **9**, 2791–2799.
48 D. Yang, G. Yang, S. Gai, F. He, C. Li and P. Yang, *ACS Appl. Mater. Interfaces*, 2017, **9**, 6829–6838.
49 Q. Wu, M. Niu, X. Chen, L. Tan, C. Fu, X. Ren, J. Ren, L. Li, K. Xu, H. Zhong and X. Meng, *Biomaterials*, 2018, **162**, 132–143.
50 Y. Wang, H. Wang, Y. Song, M. Lv, Y. Mao, H. Song, Y. Wang, G. Nie, X. Liu, J. Cui and X. Zou, *J. Nanobiotechnol.*, 2022, **20**, 96.
51 Y. Li, N. Xu, J. Zhou, W. Zhu, L. Li, M. Dong, H. Yu, L. Wang, W. Liu and Z. Xie, *Biomater. Sci.*, 2018, **6**, 2918–2924.
52 T. Wang, S. Li, Z. Zou, L. Hai, X. Yang, X. Jia, A. Zhang, D. He, X. He and K. Wang, *J. Mater. Chem. B*, 2018, **6**, 3914–3921.
53 J. Li, D. Zhu, W. Ma, Y. Yang, G. Wang, X. Wu, K. Wang, Y. Chen, F. Wang, W. Liu and Y. Yuan, *Nanoscale*, 2020, **12**, 17064–17073.
54 B. Shao, Y. Zhu, Y. Du, D. Yang, S. Gai, F. He and P. Yang, *J. Colloid Interface Sci.*, 2022, **62**, 419–434.
55 Y. Shen, Y. Zou, B. Bie, C. Dong and Y. Lv, *Acta Biomater.*, 2023, **157**, 578–592.
56 L. An, M. Cao, X. Zhang, J. Lin, Q. Tian and S. Yang, *ACS Appl. Mater. Interfaces*, 2020, **12**, 8050–8061.
57 B. K. Kaang, L. Ha, J. U. Joo and D. P. Kim, *Nanoscale*, 2022, **14**, 10835–10843.
58 T. Li, J. Sun, Y. Yin, Q. Zhang, C. Wang and S. Wang, *Nanoscale*, 2022, **14**, 16193–16207.
59 S. Jin, L. Weng, Z. Li, Z. Yang, L. Zhu, J. Shi, W. Tang, W. Ma, H. Zong and W. Jiang, *J. Mater. Chem. B*, 2020, **8**, 4620–4626.
60 Q. Wang, Z. Gao, Q. Z. Zhong, N. Wang, H. Mei, Q. Dai, J. Cui and J. Hao, *Langmuir*, 2021, **37**, 11292–11300.
61 W. Wang, X. Pan, H. Yang, H. Wang, Q. Wu, L. Zheng, B. Xu, J. Wang, X. Shi, F. Bai and H. Liu, *ACS Nano*, 2021, **15**, 20003–20012.
62 W. Zhu, Q. Chen, Q. Jin, Y. Chao and Z. Liu, *Nano Res.*, 2021, **14**, 212–221.
63 W. Wang, B. Xu, X. Pan, J. Zhang and H. Liu, *Angew. Chem., Int. Ed.*, 2021, **60**, 7802–7808.
64 F. Li, T. Chen, F. Wang, J. Chen, Y. Zhang, D. Song, N. Li, X. H. Lin, L. Lin and J. Zhuang, *ACS Appl. Mater. Interfaces*, 2022, **14**, 21860–21871.
65 X. Meng, Z. Lu, Q. Lv, Y. Jiang, L. Zhang and Z. Wang, *Acta Biomater.*, 2022, **145**, 222–234.

66 H. Ranji-Burachaloo, A. Reyhani, P. A. Gurr, D. E. Dunstan and G. G. Qiao, *Nanoscale*, 2019, **11**, 5705–5716.
67 J. Yu, Z. Wei, Q. Li, F. Wan, Z. Chao, X. Zhang, L. Lin, H. Meng and L. Tian, *Adv. Sci.*, 2021, **8**, e2101467.
68 X. Wang, X. Li, X. Liang, J. Liang, C. Zhang, J. Yang, C. Wang, D. Kong and H. Sun, *J. Mater. Chem. B*, 2018, **6**, 1000–1010.
69 L. Yang, Y. Lin, J. Zhang, J. Huang, A. Qin, Y. Miao, P. Wang, X. Yu, L. Wang and L. Zhang, *J. Colloid Interface Sci.*, 2022, **625**, 532–543.
70 J. Liu, Q. Wen, B. Zhou, C. Yuan, S. Du, L. Li, L. Jiang, S. Q. Yao and J. Ge, *ACS Chem. Biol.*, 2022, **17**, 32–38.
71 J. Jiang, Y. Pan, J. Li and L. Xia, *Molecules*, 2022, **27**, 4364.
72 X. Zhao, Y. Wang, W. Jiang, Q. Wang, J. Li, Z. Wen, A. Li, K. Zhang, Z. Zhang, J. Shi and J. Liu, *Adv. Mater.*, 2022, **34**, e2204585.
73 Z. Li, H. Cai, Z. Li, L. Ren, X. Ma, H. Zhu, Q. Gong, H. Zhang, Z. Gu and K. Luo, *Bioact. Mater.*, 2022, **21**, 299–312.
74 C. Jiang, L. Zhang, X. Xu, M. Qi, J. Zhang, S. He, Q. Tian and S. Song, *Adv. Sci.*, 2021, **8**, e210250.
75 Y. X. Ge, T. W. Zhang, L. Zhou, W. Ding, H. F. Liang, Z. C. Hu, Q. Chen, J. Dong, F. F. Xue, X. F. Yin and L. B. Jiang, *Biomaterials*, 2022, **282**, 121407.
76 Z. Dai, Q. Wang, J. Tang, M. Wu, H. Li, Y. Yang, X. Zhen and C. Yu, *Biomaterials*, 2022, **280**, 121261.
77 S. Zhou, Q. Shang, J. Ji and Y. Luan, *ACS Appl. Mater. Interfaces*, 2021, **13**, 47407–47417.
78 P. Yang, Y. Tian, Y. Men, R. Guo, H. Peng, Q. Jiang and W. Yang, *ACS Appl. Mater. Interfaces*, 2018, **10**, 42039–42049.
79 X. Deng, R. Zhao, Q. Song, Y. Zhang, H. Zhao, H. Hu, Z. Zhang, W. Liu, W. Lin and G. Wang, *Drug Delivery*, 2022, **29**, 3142–3154.
80 Z. Xie, S. Liang, X. Cai, B. Ding, S. Huang, Z. Hou, P. Ma, Z. Cheng and J. Lin, *ACS Appl. Mater. Interfaces*, 2019, **11**, 31671–31680.
81 M.-J. Dong, W. Li, Q. Xiang, Y. Tan, X. Xing, C. Wu, H. Dong and X. Zhang, *ACS Appl. Mater. Interfaces*, 2022, **14**, 29599–29612.
82 F. Jiang, Y. Zhao, C. Yang, Z. Cheng, M. Liu, B. Xing, B. Ding, P. Ma and J. Lin, *Dalton Trans.*, 2022, **51**, 2798–2804.
83 C. Li, J. Ye, X. Yang, S. Liu, Z. Zhang, J. Wang, K. Zhang, J. Xu, Y. Fu and P. Yang, *ACS Nano*, 2022, **16**, 18143–18156.
84 P. An, F. Fan, D. Gu, Z. Gaoa, A. M. S. Hossain and B. Sun, *J. Controlled Release*, 2020, **321**, 734–743.
85 B. Zou, Z. Xiong, L. He and T. Chen, *Biomaterials*, 2022, **285**, 121549.
86 C. Sui, R. Tan, Y. Chen, G. Yin, Z. Wang, W. Xu and X. Li, *Bioconjugate Chem.*, 2021, **32**, 318–327.
87 J. Huang, Z. Xu, Y. jiang, W. Law, B. Dong, X. Zeng, M. Ma, G. Xu, J. Zou and C. Yang, *J. Nanobiotechnol.*, 2021, **19**, 1–13.
88 W. Liu, F. Semcheddine, H. Jiang and X. Wang, *Bioconjugate Chem.*, 2022, **33**, 1405–1414.
89 K. Tang, W. Wang, Z. Song and X. Luo, *Anal. Chim. Acta*, 2021, **1176**, 338779.
90 C. Fang, D. Cen, Y. Wang, Y. Wu, X. Cai, X. Li and G. Han, *Theranostics*, 2020, **10**, 7671–7682.
91 J. Shen, M. Ma, H. Zhang, H. Yu, F. Xue, N. Hao and H. Chen, *ACS Appl. Mater. Interfaces*, 2020, **12**, 45838–45849.
92 M.-M. Chen, H.-L. Hao, W. Zhao, X. Zhao, H.-Y. Chen and J.-J. Xu, *Chem. Sci.*, 2021, **12**, 10848–10854.
93 X. Sun, G. He, C. Xiong, C. Wang, X. Lian, L. Hu, Z. Li, S. J. Dalgarno, Y.-W. Yang and J. Tian, *ACS Appl. Mater. Interfaces*, 2021, **13**, 3679–3693.
94 S. Lu, H. Tian, L. Li, B. Li, M. Yang, L. Zhou, H. Jiang., Q. Li, W. Wang, E. C. Nice, N. Xie, C. Huang and L. Liu, *Small*, 2022, **18**, 2204926.
95 F. Ouyang, X. Zhang, L. Zhang, Y. Liu and Q. Shuai, *J. Photochem. Photobiol., B*, 2022, **234**, 112535.
96 D. Sun, G. Qi, K. Ma, X. Qu, W. Xu, S. Xu and Y. Jin, *iScience*, 2020, **23**, 101274.
97 F. Shao, Y. Wu, Z. Tian and S. Liu, *Biomaterials*, 2021, **274**, 120869.
98 J. Hua, J. Hub, W. Wu, Y. Qinc, J. Fu, J. Zhou, C. Liu and J. Yin, *Acta Biomater.*, 2022, **151**, 588–599.
99 W. Li, X. Zhou, S. Liu, J. Zhou, H. Ding, S. Gai, R. Li, L. Zhong, H. Jiang and P. Yang, *ACS Appl. Mater. Interfaces*, 2021, **13**, 50760–50773.
100 R. Cui, J. Shi and Z. Liu, *Dalton Trans.*, 2021, **50**, 15780.
101 B. Faraji Dizaji, M. Hasani Azerbaijan, N. Sheisi, P. Goleij, T. Mirmajidi, F. Chogan, M. Irani and F. Sharafian, *Int. J. Biol. Macromol.*, 2020, **164**, 1461–1474.
102 J. Zhuang, C. H. Kuo, L. Y. Chou, D. Y. Liu, E. Weerapana and C. K. Tsung, *ACS Nano*, 2014, **8**, 2812–2819.
103 S. Kulkarni, A. Pandey, A. N. Nikam, S. H. Nannuri, S. D. George, S. M. A. Fayaz, A. P. Vincent and S. Mutalik, *Int. J. Biol. Macromol.*, 2021, **178**, 444–463.
104 P. Zhang, Y. Ouyang, Y. S. Sohn, M. Fadeev, O. Karmi, R. Nechushtai, I. Stein, E. Pikarsky and I. Willner, *ACS Nano*, 2022, **16**, 1791–1801.
105 H. Wang, Y. Chen, J. Shang, H. Wang, M. Pan, X. Liu, X. Zhou and F. Wang, *ACS Appl. Mater. Interfaces*, 2020, **12**, 34588–34598.
106 Y. Liang, M. Li, Y. Huang and B. Guo, *Small*, 2021, **S17**, e2101356.
107 X. Gao, Z. Jia, Y. Cheng, M. Ouyang, L. Feng, Y. Wang, B. Tang and K. Xu, *Chem. Commun.*, 2022, **58**, 12090–12093.
108 J. Bai, C. Peng, L. Guo and M. Zhou, *ACS Biomater. Sci. Eng.*, 2019, **5**, 6207–6215.
109 L. Hang, T. Zhang, H. Wen, M. Li, L. Liang, X. Tang, C. Zhou, J. Tian, X. Ma and G. Jiang, *Theranostics*, 2021, **11**, 10001–10011.
110 Y. Zhang, X. Huang, L. Wang, C. Cao, H. Zhang, P. Wei, H. Ding, Y. Song, Z. Chen, J. Qian, S. Zhong, Z. Liu, M. Wang, W. Zhang, W. Jiang, J. Zeng, G. Yao and L. P. Wen, *Biomaterials*, 2021, **271**, 120720.
111 M. Wang, Z. Yang, Y. Song, P. Wei, N. Ishiwme, L. Wang, H. Zhang, M. Jing, M. Gao, L. Wen and Y. Zhang, *Acta Biomater.*, 2022, **150**, 402–412.

112 Z. Wang, J. Niu, C. Zhao, X. Wang, J. Ren and X. Qu, *Angew. Chem., Int. Ed.*, 2021, **60**, 12431–12437.
113 J. Zhao, Z. Tian, S. Zhao, D. Feng, Z. Guo, L. Wen, Y. Zhu, F. Xu, J. Zhu, S. Ma, J. Hu, T. Jiang, Y. Qu, D. Chen and L. Liu, *Adv. Sci.*, 2023, **10**, e2204808.
114 X. Xiao, S. Liang, Y. Zhao, M. Pang, P. Ma, Z. Cheng and J. Lin, *Biomaterials*, 2021, **277**, 121120.
115 H. Wu, Q. Jiang, K. Luo, C. Zhu, M. Xie, S. Wang, Z. Fei and J. Zhao, *J. Nanobiotechnol.*, 2021, **19**, 1–14.
116 X. Yuan, J. Cen, X. Chen, Z. Jia, X. Zhu, Y. Huang, G. Yuan and J. Liu, *J. Colloid Interface Sci.*, 2022, **605**, 851–862.
117 K. S. Park, Z. Ni, A. P. Côté, J. Y. Choi, R. Huang, F. J. Uribe-Romo, H. K. Chae, M. O'Keeffe and O. M. Yaghi, *Proc. Natl. Acad. Sci. U. S. A.*, 2006, **103**, 10186–10191.
118 Y. Shi, J. Zhang, H. Huang, C. Cao, J. Yin, W. Xu, W. Wang, X. Song, Y. Zhang and X. Dong, *Adv. Healthcare Mater.*, 2020, **9**, e2000005.
119 Q. Li, Y. Zhang, X. Huang, D. Yang, L. Weng, C. Ou, X. Song and X. Dong, *Chem. Eng. J.*, 2021, **407**, 127200.
120 K. W. Lee, Y. Wan, X. Li, X. Cui, S. Li and C. S. Lee, *Adv. Healthcare Mater.*, 2021, **10**, 2100055.
121 S. Wang, L. Li, Y. Yu, C. Chi, K. Wang, J. Zhang, R. Shi, H. Shen and G. I. Waterhouse, *Adv. Mater.*, 2016, **28**, 8379–8387.
122 F. Yin, C. Yang, Q. Wang, S. Zeng, R. Hu, G. Lin, J. Tian, S. Hu, R. F. Lan, H. S. Yoon, F. Lu, K. Wang and K.-T. Yong, *Theranostics*, 2015, **5**, 818–833.
123 J. W. Fisher, S. Sarkar, C. F. Buchanan, C. S. Szot, J. Whitney, H. C. Hatcher, S. V. Torti and C. G. Rylander, *Cancer Res.*, 2010, **70**, 9855–9864.
124 J. Feng, Z. Xu, P. Dong, W. Yu, F. Liu, Q. Jiang, F. Wang and X. Liu, *J. Mater. Chem. B*, 2019, **7**, 994–1004.
125 M. Ren, J. Zhou, Z. Song, H. Mei, M. Zhou, Z. F. Fu, H. Han and L. Zhao, *Chem. Eng. J.*, 2021, **411**, 128557.
126 R. J. Stockert and A. G. Morell, *Hepatology*, 1983, **3**, 750–757.
127 D. A. Wall, G. Wilson and A. L. Hubbard, *Cell*, 1980, **21**, 79–93.
128 A. D. Springer and S. F. Dowdy, *Nucleic Acid Ther.*, 2018, **28**, 109–118.
129 V. F. Yusuf, N. I. Malek and S. K. Kailasa, *ACS Omega*, 2022, **7**, 44507–44531.
130 Y.-Z. Chen, C. Wang, Z.-Y. Wu, Y. Xiong, Q. Xu, S.-H. Yu and H.-L. Jiang, *Adv. Mater.*, 2015, **27**, 5010–5016.
131 C. Wang, X. Jia, W. Zhen, M. Zhang and X. Jiang, *ACS Biomater. Sci. Eng.*, 2019, **5**(9), 4435–4441.
132 V. Nejadshafiee, H. Naeimi, B. Goliaei, B. Bigdeli, A. Sadighi, S. Dehghani, A. Lotfabadi, M. Hosseini, M. S. Nezamtaheri, M. Amanlou, M. Sharifzadeh and M. Khoobi, *Mater. Sci. Eng., C*, 2019, **99**, 805–815.
133 Y. Yang, Q. Chen, J. P. Wu, T. B. Kirk, J. K. Xu, Z. H. Liu and W. Xue, *ACS Appl. Mater. Interfaces*, 2018, **10**, 12463–12473.
134 W. Shang, L. Peng, P. Guo, H. Hui, X. Yang and J. Tian, *ACS Biomater. Sci. Eng.*, 2020, **6**, 1008–1016.
135 N.-M. Parinaz, A. Nasser, J. Siamak and S. B. Ahmad, *J. Drug Delivery Sci. Technol.*, 2019, **50**, 174–180.
136 Y. T. Li, J. L. Zhou, L. Wang and Z. G. Xie, *ACS Appl. Mater. Interfaces*, 2020, **12**, 30213–30220.
137 Y. Wang, W. Wu, J. Liu, P. N. Manghnani, F. Hu, D. Ma, C. Teh, B. Wang and B. Liu, *ACS Nano*, 2019, **13**, 6879–6890.
138 K. Zhang, Z. Yu, X. Meng, W. Zhao, Z. Shi, Z. Yang, H. Dong and X. Zhang, *Adv. Sci.*, 2019, **6**, 1900530.
139 T. Luo, Y. Fan, J. Mao, E. Yuan, Z. You, Z. Xu and W. Lin, *J. Am. Chem. Soc.*, 2022, **144**, 5241–5246.
140 X. Zheng, L. Wang, Y. Guan, Q. Pei, J. Jiang and Z. Xie, *Biomaterials*, 2020, **235**, 119792.
141 M. Liu, L. Wang, X. Zheng, S. Liu and Z. Xie, *ACS Appl. Mater. Interfaces*, 2018, **10**, 24638–24647.